Silica nanoparticles as gene delivery systems for skin tissue repair

Xiaolin Wang

Université Pierre et Marie Curie

ED 397 Physique et Chimie des Matériaux

Laboratoire de Chimie de la Matière Condensée de Paris, UMR 7574

Nanoparticules de silice comme systèmes de délivrance de gènes pour la réparation tissulaire de la peau

Par Xiaolin Wang

Thèse de doctorat de Chimie des Matériaux

Présentée et soutenue publiquement le 21 septembre 2015

Devant un jury composé de :

DURAND Jean-Olivier	DR CNRS, ICGM (Montpellier)	Rapporteur
WEISS Pierre	PU-PH Université de Nantes	Rapporteur
GUEGAN Philippe	PR Université Pierre et Marie Curie	Examinateur
MIDOUX Patrick	DR INSERM, CBM (Orléans)	Examinateur
PANDIT Abhay	PR University of Galway	Examinateur
CORADIN Thibaud	DR CNRS, LCMCP (Paris)	Directeur de thèse
HELARY Christophe	IR CNRS, LCMCP (Paris)	Co-encadrant

Sommaire

INTRODUCTION

Skin is the barrier that protects the body against infection and dehydration. After a skin injury, wound healing process rapidly occurs to restore the skin integrity. Healing requires a well-orchestrated integration of biological events that lead to tissue repair. Wound healing is characterized by four overlapping phases: coagulation, inflammation, migration/proliferation and remodeling. In tissues with preexisting pathophysiological abnormalities such as chronic wounds, parts of the wound can be stuck in different phases as their progression does not occur in synchrony.[1]

Cutaneous chronic wounds are characterized by the absence of healing six weeks after the injury. More than 6 million persons in the United States are affected by these pathologies; in France they are 1.5 million.[2] The most prevalent cutaneous chronic wounds are venous, diabetic foot ulcers (**Figure 1**) and bedsores. The number of affected persons is expected to increase in the next years as the European population ages and more people develop diabetes related to overweight and obesity.[3]

Figure 1. Diabetic foot ulcers are characterized by impaired wound healing of skin. This sometimes leads to infection and leg amputation. It is a major complication of diabetes mellitus because they occur in 15% of all patients with diabetes.

To correct impaired wound healing, it is necessary to treat the underlying disease. Meanwhile, the local treatment of the wound is crucial to prevent infection, to control the removal of exudates and to create the right environment to allow for skin wound healing. The classical treatment is the debridement of the wound bed to remove necrotic tissue.[4] This procedure is followed by the wound compression with sterile gauze.[5] Another technique is the negative wound pressure therapy. Sometimes, these techniques are not effective enough and require the application of a wound dressing.

Initially wound dressings had a passive and protective role in the healing process. Further on, bioactive dressings consisting of cellularized scaffolds were designed as skin substitutes. A typical example is the Apligraf® dressing, consisting of **collagen** matrices associated with living fibroblasts and keratinocytes (**Figure 2**).[6] These cells produce a panel of growth factors that can promote tissue repair. Nowadays research orientation is towards **medicated dressings** based on the integration of active biomolecules within scaffolds in order to tune cell phenotype towards migration, differentiation or modulation of inflammation. First efforts in this direction were done using proteins as therapeutic molecules.[7] However, despite the effort in the development of drug delivery systems, protein therapies suffer from high cost, rapid diffusion and degradation of biomolecules. **Gene therapy** represents a promising alternative as it overcomes the concerns about the protein stability and affords a sustained delivery of biomolecules.[8] Gene delivery into cells makes them produce therapeutics molecules that can act locally, limiting possible side effects.[9]

Figure 2: The Apligraf® skin substitute used in the treatment of diabetic foot ulcers associate a matrix, made of collagen with fibroblasts and keratinocytes cells.

Success of gene delivery depends on the development of an efficient delivery vector that permits the penetration of genes into the cells as well as their protection against endosomal degradation. Viruses are the most efficient vectors to transfect cells but they suffer from safety concerns such as immunogenicity or oncogenicity.[10] Among the non-viral vectors, **polyethyleneimine** (PEI) has attracted a lot of interest as it is able to compact large DNA sequences, permits DNA penetration into cells thanks to its positive charge and is able to escape from the endosome.[11] However, as its transfection efficiency and cytotoxicity are strongly correlated, efforts have been made to explore the possibility of tuning PEI properties by chemical modification[12] or complexation with nanoparticles[13] to shield its positive charge.

In this context, **silica nanoparticles** (SiNPs) possess several attractive characteristics such as suitable cytocompatibility, large surface area, tunable size/shape and versatile bioconjugation chemistry[14] making them ideal drug delivery vehicles[15] and gene transfection agents.[16] Nevertheless, bare SiNPs, being plain or mesoporous, cannot be used alone as gene carriers as they bear a negative charge near neutral pH and are unable to compact DNA, thereby preventing its internalization. Hence conjugation of these particles with PEI appears as a promising method to design nanoscale hybrid gene carriers.[17]

In this context, the present work aimed at designing novel medicated dressings allowing for the production of biomolecules favoring cutaneous wound repair within collagen scaffolds. Our strategy has relied on the use of PEI-conjugated silica nanoparticles as gene carriers to transfect fibroblasts cells immobilized with the scaffolds (Figure 3).

Figure 3: Schematic overview of the project

In the following pages, we first provide a literature survey of the biomedical and biological contexts of our work, introduce the main concepts and strategies of gene therapy and give the reader an overview of the past and current developments related to silica nanoparticles as drug delivery systems (**Chapter I**).

We then describe our study of PEI-coated silica particles as vectors of a model plasmid to transfect 3T3 fibroblast cells first in 2D cultures and then in various 3D configurations (**Chapter II**).

The encouraging outcome of this study led to us to explore further the transfection properties of PEI-SiNPs systems, by modifying the conjugation mode of the polymer on the silica surface. The ability of these hybrid nanocarriers to transfect human primary fibroblast and keratinocytes was also studied (**Chapter III**).

Finally, first attempts were made to use PEI-coated silica nanoparticles for the expression of the anti-inflammatory interleukin-10 protein by 3T3 cells and the inhibition of TNF-α[a] expression in macrophages (**Chapter IV**)

A **conclusion** section gathers our main results, enlightening our contribution to the understanding of the mechanisms of gene transfection as mediated by silica nanoparticles, and provides some perspectives in the different fields relevant to this work.

References

1. Falanga V. *Lancet* **2005**, *366*, 1736-43.

2. Menke, N.B. ; Ward, K.R. ; Witten, T.M. ; Bonchev, D.G. ; Diegelmann, R.F. *Clin. Dermatol*. **2007**, *25*, 19-25

3. Greer, N.; Ward, K.R.; Witten, T.M. *Ann. Inter. Med*. 2013, *159*, 532-42

4. Eming, S. A.; Krieg, T.; Davidson, J. M. *J. Invest. Dermatol.* **2007**, *127*, 514-525.

5. Vasconcelos, A. ; Cavaco-Paulo, A. Appl. Microbiol. Biotechnol. 2011, 90, 445-60

6. Wilkins, L.M.; Watson, S.R.; Prosky, S.J. ; Meunier, S.F. ; Parenteau, N.L. *Biotechnol Bioeng*. 1994, *43*, 747-756

7. Cam, C.; Segura, T. *Curr. Opin. Biotechnol.* **2013**, *24*, 855-863.

8. Conwell, C. C.; Huang, L. *Adv. Genet.* **2005**, *53*, 1-18.

9. Eming, S. A.; Krieg, T.; Davidson, J. M. *Clin. Dermatol.* **2007**, *25*, 79-92.

10. Sun, J. Y.; Anand-Jawa, V.; Chatterjee, S.; Wong, K. K. *Gene Ther.* **2003**, *10*, 964-976.

11. Remy, J. S.; Abdallah, B.; Zanta, M. A.; Boussif, O.; Behr, J. P.; Demeneix, B. *Adv. Drug Delivery Rev.* **1998**, *30*, 85-95.

12. Petersen, H.; Fechner, P. M.; Martin, A. L.; Kunath, K.; Stolnik, S.; Roberts, C. J.; Fischer, D.; Davies, M. C.; Kissel, T. *Bioconjugate Chem.* **2002**, *13*, 845-854.

13. Hu, C.; Peng, Q.; Chen, F.; Zhong, Z.; Zhuo, R. *Bioconjugate Chem.* **2010**, *21*, 836-843.

14. Mamaeva, V.; Sahlgren, C.; Linden, M. *Adv. Drug Delivery Rev.* **2013**, *65*, 689-702.

15. Kim, T.-W.; Slowing, I. I.; Chung, P.-W.; Lin, V. S.-Y. *ACS Nano* **2010**, *4*, 360-366

16. Kim, M.-H.; Na, H.-K.; Kim, Y.-K.; Ryoo, S.-R.; Cho, H. S.; Lee, K. E.; Jeon, H.; Ryoo, R.; Min, D.-H. *ACS Nano* **2011**, *5*, 3568-3576.

17. Buchman, Y. K.; Lellouche, E.; Zigdon, S.; Bechor, M.; Michaeli, S.; Lellouche, J.-P. *Bioconjugate Chem.* **2013**, *24*, 2076-2087.

[a]A list of abbreviations used in this manuscript is provided on pages 169-170.

CHAPITRE I

Rappels bibliographiques

CHAPITRE I

Rappels bibliographiques

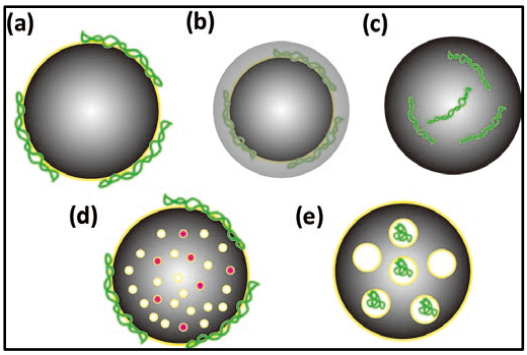

Résumé

Cette introduction bibliographique vise à rassembler l'état de l'art dans les trois grands domaines couverts par ce travail de thèse : les plaies chroniques de peau, la thérapie génique et les nanoparticules de silice comme vecteurs thérapeutiques. Dans une première partie, nous rappelons les évènements impliqués dans la cicatrisation des plaies cutanées et décrivons les phénomènes à l'origine des plaies chroniques. Le rôle particulier joué par les macrophages d'une part, et l'interleukin-10 (IL-10) d'autre part dans les processus de réparation cutanée est souligné. Les différents traitements actuellement utilisés ou à l'étude pour favoriser la cicatrisation sont ensuite présentés, mettant en lumière l'intérêt du développement actuel de pansements médicamenteux. Une deuxième partie est consacrée à la thérapie génique. Après une présentation des différentes formes de gènes thérapeutiques, la distinction entre vecteurs viraux et non-viraux est introduite et les défis rencontrés dans l'utilisation de ces derniers sont présentés. Le principe de matrices tri-dimensionnelles promouvant la transfection est enfin exposé. La dernière partie de ce chapitre offre un panorama des progrès réalisés ces dernières années dans la synthèse et la fonctionalisation de nanoparticules de silice à visée médicale, avec une attention particulière à leur application dans la délivrance de gène. La possibilité d'associer ces particules avec un polymère naturel biocompatible, le collagène, pour obtenir des biomatériaux nanocomposites est finalement présentée.

I-1. CHRONIC WOUNDS - A FAILURE TO HEAL

I-1-1. Structure of human skin

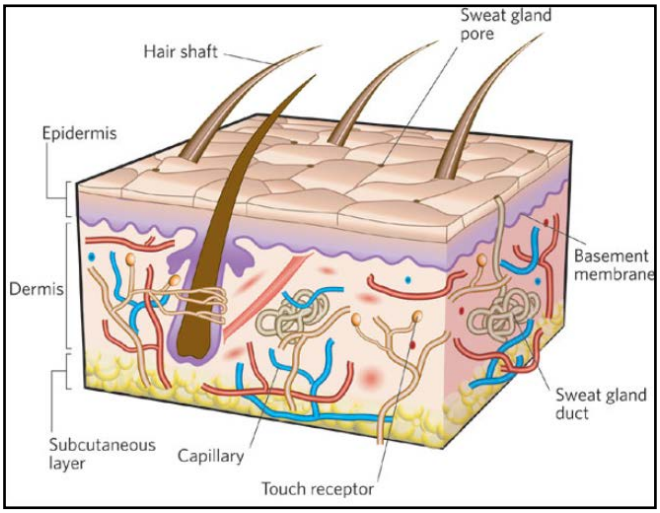

Figure I-1: Structure of the skin[2]

The skin constitutes the largest organ in the body and possesses multiple functions in daily life. It not only acts as the barrier to hazardous substances but also plays indispensible roles in physical protection, temperature regulating, immune response, and sensory detection.

Skin is composed with three layers: the epidermis, dermis and subcutaneous layer (**Figure I-1**). The epidermal barrier layer is ~ 0.1–0.2 mm in depth and tightly attached to the underlying dermis by a specialized basement membrane zone, consisting of several different types of collagen and laminin 5. This tissue is a stratified epithelium composed of several layers of keratinocytes (at least four). Some epidermal stem cells are present in the basal layer located on the basement membrane. They are responsible for the renewal of the epidermis by the generation of a differentiated cell and another stem cell. New cells continually move towards the surface while they are differentiating. They gradually die and become flattened and then die. Dead cells form the stratum corneum, an impermeable squamous epithelium. This layer gives properties of resistance against bacterial infection and prevents fluid and electrolyte loss.[3] Other types of cells are found in the epidermis such as Langerhans cells or melanocytes. Langerhans cells belong to the immune system and act as antigen-presenting cells. Melanocytes synthesize melanin, molecule involved in the cutaneous photoprotection

The dermis is a dense connective tissue which gives skin resistance and elasticity. This well-vascularized tissue feeds the epidermis by nutrient diffusion. Those blood vessels provide nourishment and waste removal for both dermal and epidermal cells. Some epidermal annexes are inserted dermis such as hair follicles, sweat glands and sebaceous glands. The

dermis also contains receptors for touch, temperature and pain. It varies in thickness depending on its site in the body (1-4 mm). The dermis consists of an extracellular matrix (ECM) in which several kinds of cells are encapsulated. Structural components of the extracellular matrix are collagen (type I, III and V), elastin, fibronectin, hyaluronic acid and proteoglycans. Furthermore, the ECM also mediates cell-matrix adhesion and transducer signals into cells.[4] In addition, hair follicles, sweat glands, sebaceous glands, apocrine glands, lymphatic vessels and blood vessels are present in the dermis. Those blood vessels provide nourishment and waste removal for both dermal and epidermal cells. The dermis is composed of three major types of cells: fibroblasts, macrophages, and adipocytes (energy storing cells). Fibroblasts are the main type of cells of this tissue because they synthesize the whole macromolecules forming ECM and they continuously communicate with epidermis *via* soluble factors. Together with macrophages, they play important roles in wound healing, which will be described in detail in the following subsection.

I-1-2. Process of wound healing

I-1-2-1. Acute wounds

Wound healing is a complex process that involves the simultaneous actuation of soluble mediators (i.e. growth factors and cytokines/chemokines), blood cells, ECM and parenchymal cells (**Figure I-2**). This process can be divided into several phases: homeostasis/inflammation, proliferation, and remodeling.[6] These phases are not associated with specific period of time and may overlap:

(i) Haemostasis and Inflammatory Phase (day 1-3)

Immediately after an injury, the inflammatory and haemostasis phase occur to stop bleeding and combat the infection. First, a fibrin clot is formed around aggregated platelets in order to reestablish haemostasis (**Figure I-2a**). This clot serves as a temporary shield protecting the injured tissue and provides a matrix over and through which cells can migrate. Meanwhile, aggregated platelets secrete a wide range of mediators such as platelet-derived growth factor (PDGF) and TNF-β that recruit neutrophils and monocytes to the wound site, which then secrete proteinases and reactive oxygen species (ROS) to kill microorganism and clean up cell debris by phagocytosis. Other cells such as mastocytes migrate to the wound site, secrete histamine, thereby promoting inflammation. Two days after the injury neutrophils are progressively replaced by macrophages. These cells activated from monocytes, act as

biological bins as they digest cellular debris. They play a part in the early stage of wound healing by the expression of colony-stimulating factor (CSF), VEGF, TGF-β and PDGF. These mediators moderate the transition between the initial phase of inflammation and tissue repair. These cytokines play a role in cell migration, proliferation and ECM production.

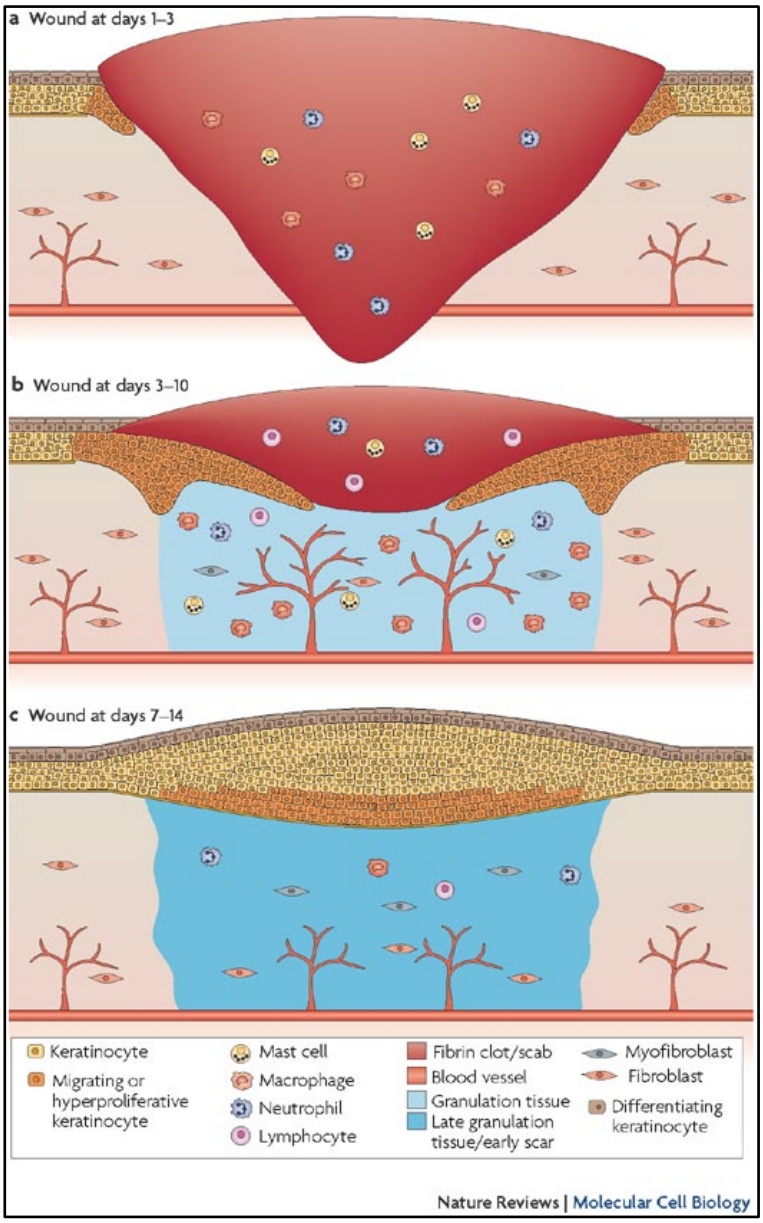

Figure I-2: The different phases of skin wound repair[5]

(ii) Proliferation Phase (day 2-10)

This phase consists of neoangiogenesis, granulation tissue formation, ECM deposition and re-epithelialisation (**Figure I-2b**).[139] After the destruction of the cutaneous tissue, the initial migration of keratinocytes operates from the wound borders and the hair follicles. They migrate on the fibrin clot made of fibrin and fibronectin and then proliferate, differentiate to form a novel epidermis.[140] Re-epithelialization is favoured by the secretion of fibroblastic growth factors such as Keratinocyte Growth Factors (KGF) and Fibroblasts Growth Factor – 10 (FGF-10).

Fibroblasts begin to migrate into the wound by around day 3 after the injury, marking the start proliferation phase. The angiogenic factors, such as fibroblast growth factor (FGF), VEGF and PDGF induce angiogenesis by stimulating the production of basic fibroblast. The neovascularization arises in the wound by the end of the first week, and continue to grow until the wound is healed. In addition, growth factors released by platelets and secreted by macrophages during the first phase of healing have been sequestered in the provisional matrix. Thus these growth factors stimulate cells as they move into the wound. Fibroblasts start proliferating and secrete ECM macromolecules in the fibrin clot to form the granulation tissue. They mainly synthesize collagen III at this stage. After their migration, fibroblasts progressively differentiate into myofibroblasts. With this pro-fibrotic phenotype, they acquire contractile capabilities and biosynthetic activities with the aim of replacing the damaged tissue. At the end of the proliferative phase, the wound is closed thanks to the contraction by myofibroblasts. When the wound area is completely filled with new granulation tissue, angiogenesis stops and the apoptosis of many new vessels is then started.

(iii) Remodelling Phase (several months)

The last phase is characterized by the degradation of the previously formed granulation tissue and by dermis regeneration (**Figure I-2c**). Matrix formation requires the removal of granulation tissue with revascularization. A framework of collagen and elastin fibers replaces the granulation tissue. This framework is then saturated with proteoglycans and glycoproteins. This is followed by tissue remodeling involving the synthesis of new collagen mediated by TGF-β. Collagen remodeling during the transition from granulation tissue to scar is dependent on continued synthesis and catabolism of collagen. The degradation of collagen in the wound is controlled by several matrix metalloproteinases secreted by macrophages, epidermal cells, and endothelial cells, as well as fibroblasts. The final product of this phase is scar tissue.

Main sources and functions of cytokines and growth factors involved in wound healing are summarized in **Table I-1**.

Name	Sources	Target	Function
EGF	Platelets, Macrophages Fibroblasts	Keratinocytes	Re-epithelialization
FGF-2	Keratinocytes Mast Cells, Fibroblasts Endothelial cells Smooth muscle cells Chondrocytes	Keratinocytes Fibroblasts Endothelial cell	Granulation tissue formation Re-epithelialization Matrix formation and remodeling
TGF-β	Platelets, Keratinocytes Macrophages, Lymphocytes Fibroblasts	Platelets, Keratinocytes Macrophages, Fibroblasts, Leukocytes, Endothelial cells, ECM	Inflammation Granulation tissue formation Re-epithelialization Matrix formation and remodeling
TNF-α	Neutrophils Macrophages	Epidermal, mesenchymal cells	Inflammation Re-epithelialization
PDGF	Platelets, Keratinocytes Macrophages, Fibroblasts Endothelial cells	Leukocytes, Macrophages, Fibroblasts	Inflammation Granulation tissue formation Reepithelialization Matrix formation and remodeling
VEGF	Platelets, Neutrophils Macrophages, Fibroblast Endothelial cells Smooth muscle cells	Endothelial cells, macrophages	Granulation tissue formation
IL-1	Neutrophils Monocytes Macrophages Keratinocytes	Endothelial cells, Macrophages, Leukocytes, Fibroblasts Keratinocytes,	Inflammation Reepithelialization
IL-6	Neutrophils Macrophages	Endothelial cells, Macrophages, Kerotinocytes,Leukocytes	Inflammation Reepithelialization
IL-10	Leukocytes	Leukocytes	Anti-inflamamtion

Table I-1: Cytokines and growth factors involved in wound healing[7]

I-1-2-2. Chronic wounds

Chronic skin ulcers are wounds that have failed to progress through the normal healing stages and enter a state of chronic and pathological inflammation.[141] While acute wounds usually progress linearly through the different healing phases, chronic wounds do not follow this timeline, but are locked in one of the above-mentioned healing phases (**Figure I-3**)[8].

The most prevalent chronic wounds in the developed world are venous leg ulcers and diabetic foot ulcers. Venous leg ulcers (VLUs) result from hypertension or sustained ambulatory venous pressures as a consequence of a chronic venous insufficiency.[142,143] Hypertension leads to an infiltration of leukocytes into the dermis, which is responsible for inflammation.[144] Diabetic foot ulcers are consequences of neuropathy or/and vascular disease related to diabetes.[145] The major complications of chronic ulcers are microbiological

contamination and malignant transformation.[146,147] In the case of FDUs, bacteriological infection can lead to gangrene and eventually leg amputation.[148] Indeed, bacteria colonizing the wound produce a biofilm composed of a wide variety of polysaccharides, which is impervious to phagocytic cells and impermeable to antibiotics.[10] Frustrated phagocytes release a plethora of proteases and toxic oxygen radials into the wound milieu making a bad situation worse as these agents destroy tissue cells, extracellular matrix, and growth factors in the wound.

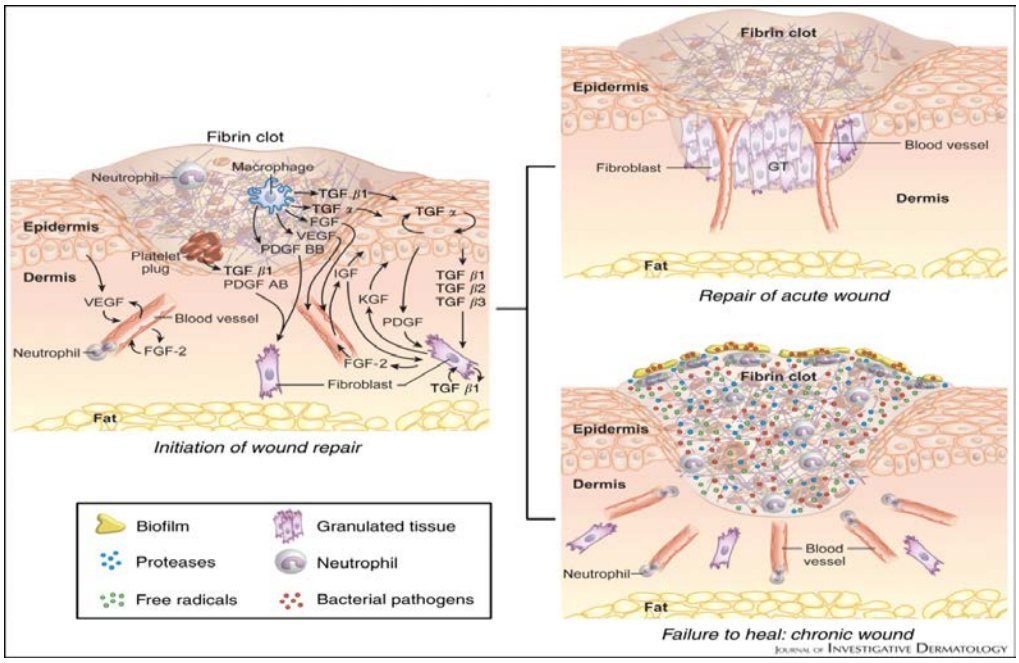

Figure 1-3: Acute wound and chronic wound undergoes different processes[8]

The large amount of proteases and presence of reactive oxygen species, both produced by inflammatory cells is the main characteristic of chronic wounds. The presence of proteases in dermis leads to fibroblast senescence, poor vascularization and keratinocytes apoptosis. As a consequence, the protective barrier constituted by the epidermis is disrupted. As keratinocytes at the wound edge are unable to migrate into the wound bed, re-epithelialization is inhibited and wound closure impossible. Lastly, non-healing skin wounds are characterized by poor vascularization, with disturbance in blood vessel formation within the wound.[149] Not surprisingly, such chronic wounds lack ingrowth of granulation tissue

I-1-3. Macrophages, target cells for chronic wounds treatment

I-1-3-1. Role of macrophages in cutaneous wounds

The macrophage is a prominent inflammatory cell in wounds, but its role in healing remains incompletely understood.[11] Macrophages have various functions in wounds, including host defense, promotion/ resolution of inflammation, removal of apoptotic cells and necrotic tissues, support of cell proliferation and tissue restoration. The specific activities of macrophages concerning these functions in wound healing are summarized in **Table 1-2**.

Although macrophages are beneficial for the repair of normal wounds, this pleotropic cell type may promote excessive inflammation or fibrosis under certain circumstances. Emerging evidence suggests that macrophage dysfunction is a component of the pathogenesis of non-healing and poorly healing wounds.[12] Consequently, the macrophage is widely deemed as an attractive therapeutic target, both to reduce fibrosis and scarring, and to improve healing of chronic wounds.

Wound healing process	**Activities of Macrophages**
Phagocytosis	ROS, NO
Debridement	Collagenase, elastase
Cell recruitment and activation	Growth factors: PDGF, TGF, EGF, IGF Cytokines: TNF-α, IL-1, IL-6 Fibronectin
Matrix synthesis	Growth factors: TGF, EGF, PDGF Cytokines: TNF-α, IL-1, IFN Enzymes: arginase, collagenase Prostaglandins NO
Angiogenesis	Growth factors: FGF, VEGF Cytokines: TNF NO

Table I-2: Activities of macrophages in wound healing processes

I-1-3-2. Recruitment and residence of macrophages

Leukocytes (including monocytes, neutrophils, mast cells, etc) are present during each of the phases of wound repair, represented in **Figure I-4**, as haemostasis (yellow panel), early inflammation (light pink panel), late inflammation (dark pink panel) and resolution/ remodelling (blue panel). Specially, macrophages differentiated from monocytes, are first recruited by factors such as split products from coagulation cascade (e.g. degredaded ECM molecules), factors released from platelet degranulation and activated complement components. Later, much more macrophages infiltrate in response to chemotactic gradients in

the wound during inflammation phase.[13] Finally, low numbers of resident macrophages are present during the lengthy remodeling phase whereas neutrophils and lymphocytes disappear.

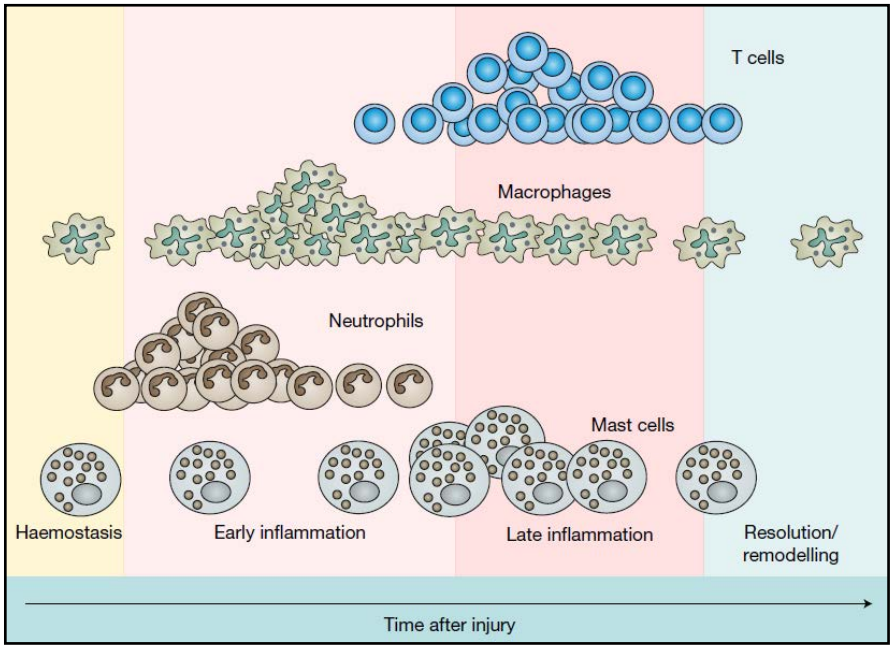

Figure I-4: Pattern of leukocyte infiltration into wounds[11]

I-1-3-3. Plasticity of macrophages in wound healing

Macrophages exist in different phenotypic states during wound healing process and can change their phenotype in response to environmental cues (**Figure 1-5**). Recent studies suggest the influence of these cells on each stage of repair varies with the specific phenotype. Macrophages are considered to have two phenotypes, namely M1 and M2 type. Recently, Mosser *et al.* came up a third phenotype- wound healing macrophages, which arise in response to IL-4.[12]

(i) Classically activated macrophages (M1 type) arise in response to interferon-γ (IFNγ), which can be produced T helper 1 (TH1) cells, CD8+ T cells (not shown) and natural killer (NK) cells. In addition, TNF, produced by antigen-presenting cells (APCs) can also activate macrophages to M1. Moreover, in wound site, PDGF (released by platelets due to tissue damage) and bacteria (main component LPS shown in **Figure 1-5B**) will also lead to the transformation of tissue macrophages to M1 phenotype.[150]

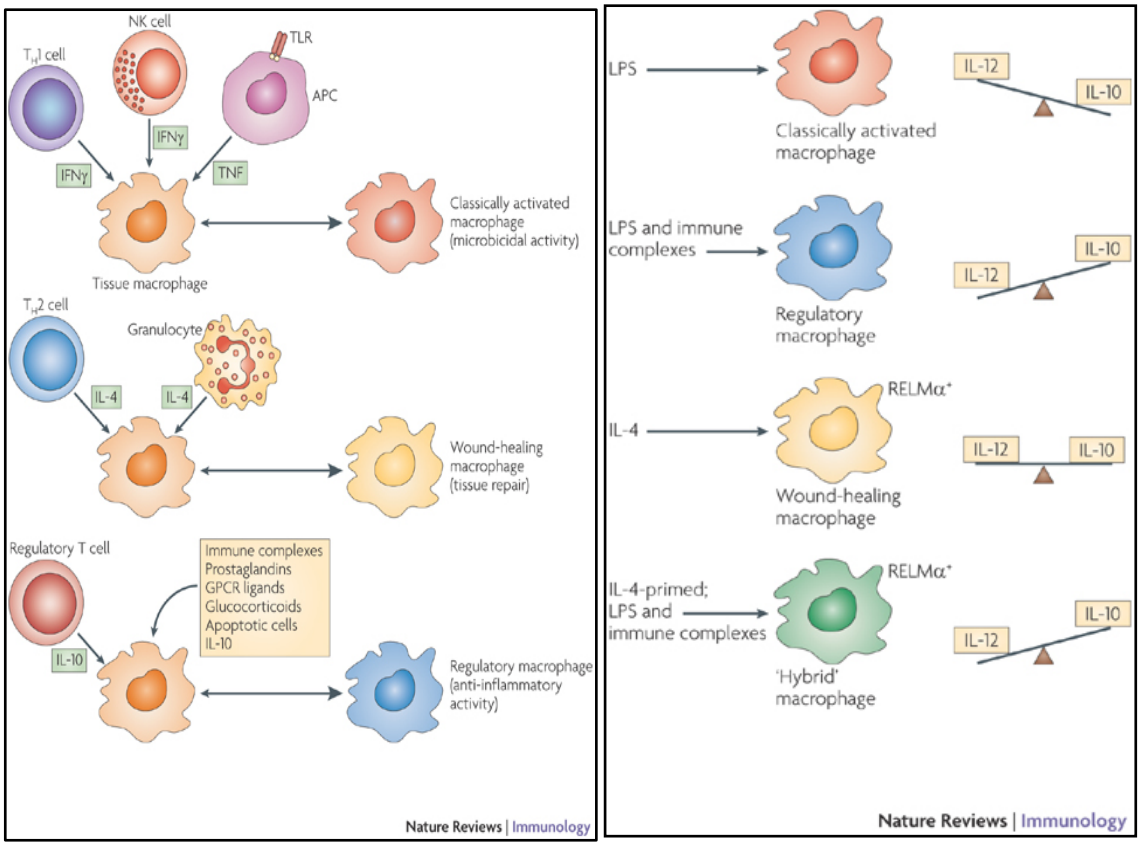

Figure I-5: The macrophages activated by endogeneous factors (A) and exogeneous factors (B) [12]

(ii) Wound-healing (alternatively activated) macrophages arise in response to interleukin-4 (IL-4) or interleukin-13 (IL-13), which can be produced during an adaptive immune response by TH2 cells or during an innate immune response by granulocytes.

(iii) Regulatory macrophages (namely M2 type) are generated in response to various stimulis, including immune complexes, prostaglandins, G-protein coupled receptor (GPCR) ligands,glucocorticoids, apoptotic cells or IL-10. Their hallmark is the production of large quantities of IL-10, which inhibits the inflammatory hallmark is the production of large quantities of IL-10, which inhibits the inflammatory response.

Each of these three populations has a distinct physiology. Classically activated macrophages have microbicidal activity, whereas regulatory macrophages produce high levels of IL-10 to suppress immune responses.

I-1-4. The IL-10 anti-inflammatory cytokine

I-1-4-1. Production and function of IL-10

As introduced above, macrophages play a key role in wound healing and they can be damaging if the response is excessive. Interleukin 10 (IL-10) is a cytokine that promotes macrophages toward an anti-inflammatory state (M2 phenotype) and therefore promotes wound healing.[14] A good understanding in its molecular event about its production and functions will help better design of new strategies of wound treatment.

IL-10 is produced by many cells of the innate and adaptive immune response, including macrophages, dendritic cells, B cells, and T cells.[15] It plays a crucial role in preventing inflammatory and autoimmune pathologies. More specifically, it regulates and represses the expression of pro-inflammatory cytokines produced by innate cells such as macrophages and dendritic cells during the recovery phase of infections and reduces the tissue damage caused by these cytokines. Specially, IL-10 has multiple modulating effects on the macrophage population including the suppression of pro-inflammatory cytokines, and the promotion of macrophages towards the wound healing M2 phenotype. As demonstrated before, the shift in the balance from M1 to M2 populations is postulated to be essential since it occurs in tissues that undergo wound healing.

IL-10 stimulation promotes arginase-1 expression in macrophages that suppresses pro-inflammatory mediators by shunting metabolic pathways away from the production of nitric oxide (NO). Arginase-1 expressing macrophages have also been shown to suppress T-cell responses causing inflammation and fibrosis as well as producing components of the ECM. In addition to arginase-1 expression, M2 macrophages also express the mannose receptor, CD206, which has been used in conjunction with arginase-1 as a marker to identify M2 macrophage subtypes. The mannose receptor facilitates phagocytosis of mannose N-linked glycoproteins that are found on a variety of microorganisms. Promoting IL-10 following tissue injury at strategically defined locations may therefore offer targeted therapeutic benefits by capitalizing on its inflammatory suppressing/ wound healing potential.

I-1-4-2. IL-10 delivery as an anti-inflammation therapeutic strategy

The bioactive half-life of IL-10 is dependent on the cellular microenvironment and ranges from minutes to hours in vivo. To date, investigations of IL-10 have been carried out using direct administration of the IL-10 protein or peptide fragmentswhich remains biologically

active for a restricted period of up to 2.5 h in vivo. Efforts have been devoted to extending the bioavailability and bioactivity of IL-10.

One strategy is to immobilize IL-10 to polymeric scaffolds for sustained release to neighboring tissues. In some cases, IL-10 is covalent bonded to the matrix to manipulate a cell population towards a wound healing (M2) phenotype in spatially confined regions and therefore offer novel and practical therapeutic approaches to promote wound healing. [16] Gene therapy represents an alternative to protein therapy as "fresh IL-10" could be continuously produced via cell transfection. Studies combing gene delivery and polymeric scaffold to improve efficacy[17] and achieve long-term release[18] of IL-10 to modulate inflammation have also been recently reported.

I-1-5. Cutaneous wound treatment

I-1-5-1. Treatment strategies

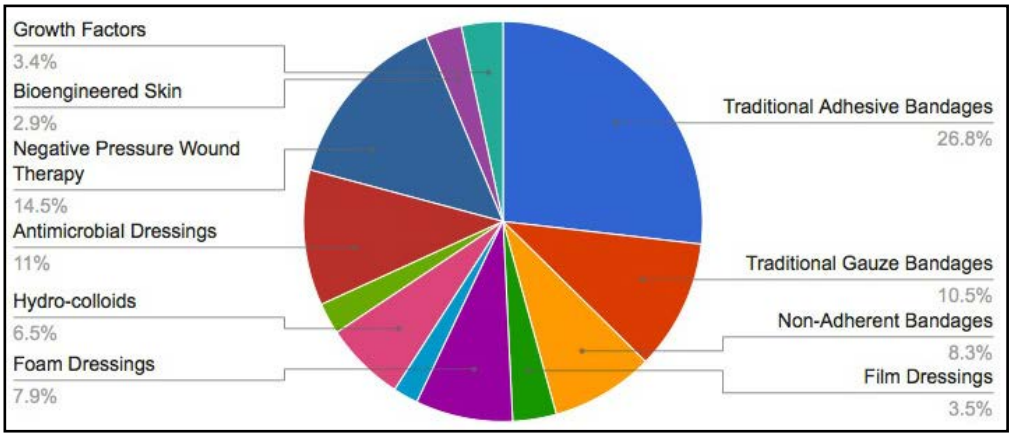

Figure I-7: Global cutaneous wound care market in 2013 (http://www.mediligence.com)

The classical treatment of chronic skin ulcers consists at first in a surgical debridment to remove necrotic tissue and exudates followed by a bandaging method to compress the wound. As shown in **Figure I-7**, this type of treatment accounts for almost half of current wound care market (45.6%). When wound healing is unsuccessful, different strategies have been evaluated to enhance and speed up wound closure. Protein therapy based on growth factors such as PDGF (Platelet Derived Growth Factor) and TGF-β1 (Transforming Growth Factor) takes up only 3.4% due to their instability in vitro and short half-life in vivo. Cell therapy is another effective treatment, however, the preparation and storage are challenging to current technological conditions.

New and recent alternatives to conventional dressings have been developed to guarantee an optimal wound environment. In the following part, these dressings are introduced as non-

medicated dressing and medicated dressing. As impaired wound healing such as Diabetic Foot Ulcers (DFU) involves multiple biochemical deficiencies[19], a singular treatment modality is unlikely to be effective. Combination of different strategies is thus urgent to address the complex underlying pathology.

I-1-5-2. Protein therapy

As introduced before, the process of wound healing is driven by numerous cellular mediators, including eicosanoids, cytokines, nitric oxide, and various growth factors. The field of biologic wound products aims to accelerate healing by modulating these inflammatory mediators. So far, Granulocyte/macrophage colony-stimulating factor (GM-SCF), PDGF-BB, VEGF and bFGF are the most extensively studied proteins for wound treatment, especially for non-healing wounds.[20]

Cytokines include chemokines, lymphokines, monokines, interleukins, colony-stimulating factors, and interferons. These molecules regulate inflammation by influencing hematopoietic cells. GM-CSF has been most extensively studied, which can stimulate neutrophils, macrophages, keratinocytes, and fibroblasts and increase VEGF production, rendering it a very promising molecule in wound healing. There have been encouraging results in a prospective randomized control study involving patients with venous ulcers[21], as well as studies on diabetic-foot ulcers[22]. Interleukins are still in preliminary studies, yet they have displayed positive effects in wound healing. For example, IL-19 has been found to be effective for wound closure by increasing fibroblast keratinocyte growth factor expression[23]. IL-10 has been intensively studied as a strong general inhibitor of immune response and inflammation.[14]

Growth factors stimulate mainly fibroblasts and keratinocytes via transmembrane glycoproteins and are so far the most intensive studied and applied protein product in wound treatment. They are divided into five superfamilies, the most known being PDGF. Recombinant PDGF was studied in a series of 118 patients with DFUs by Steed and co-workers.[24] Patients were treated with rhPDGF or placebo for up to 20 weeks in randomized double-blind study. The rhPDGF group showed a significantly higher percentage of patients that achieved wound healing, 48% versus 25%, as well as a greater reduction in wound size. This study has led to FDA approval of rhPDGF for diabetic ulcers, which is now known as becaplermin (Regranex®). Additional studies have confirmed increased odds of wound

healing and decreased rates of amputation in diabetic foot ulcers, as well as accelerated wound healing in abdominal wound separation and irradiated wounds.

Despite the effort in the development of drug delivery systems, protein therapies suffer from high cost, rapid diffusion, and degradation. For example, after intravenous injection, the half-life of basic fibroblast growth factor (bFGF) is 3 min and that of vascular endothelial growth factor (VEGF) is 50min. Instabilities of these proteins may also lead to the formation of immunogenic degradation products.[25] A more promising approach is based on the integration of the bioactive proteins within a scaffold for long-term delivery. Such medicated dressings are introduced in the next section.

I-1-5-3. Wound dressings

Wound dressings can be made from natural (chitosan, hyaluronic acid, cellulose, alginate, collagen, fibrin) or synthetic (PVA, PEG, PVP, PU, PHEMA, poly(esters)) materials and processed in the form of films, foams, hydrocolloids and hydrogels. In general, wound dressings should provide a moist microenvironment, offer protection from further infections, remove wound exudates and promote tissue regeneration. To have a better efficacy, it is promising to integrate of active biomolecules (e.g. antibiotics, growth factors, cytokines) within dressings to tune cell phenotype toward migration, differentiation, or modulation of inflammation. Recent studies and commercial products are summarized based on material resources in **Table I-3**.

(i) Non-medicated dressing:

Hydrocolloids: they are composed with a semi-permeable film (for water and oxygen) and a layer of hydrophilic particles that usually made of proteins or polysaccharides. Hydrocolloids can absorb wound exudates and provide a moisted environment. They can be applied to granulating, epithelializing, and necrotic wounds, but can't be used in case of severe infections because of macerates.

Hydrogels: they are composed with hydrated polymers (> 20 wt %) and water. Advantages of hydrogels lie in flexibility, non-antigenicity and permeability to water, oxygen and metabolites. Therefore, they can maintain high level of moisture and promote wound debridement. Poor mechanical behavior is the main drawback of hydrogel-based dressings.

Foams: foams are highly absorbent, cushioning, and protective to the wound site. As they don't promote tissue repair and can be only used in the first stages of wound healing.

Films: Films are durable, easy to manipulate, adhesive, semipermeable to oxygen and water and impermeable to liquid and bacterias. Therefore, they can only use as protective dressings when there are few exudates present.

(ii) Medicated dressings

Dressings loaded with antimicrobials/antibiotics (to challenge biofilm formation in the wound site), platelet-derived substances, growth factors and peptides act to balance the biochemical events of inflammation in the chronic wound and to improve healing. These medicated dressing have therapeutic effects on the wounds and therefore release profile should be well tuned to fit the application purposes. Stability and burst releases of bioactive molecules are the main obstacles and sustained release over one week is often desirable to avoid frequent administration. In some cases, novel drug delivery system at micro- or nano-scale, including liposomes, polymeric or inorganic nanoparticles are integrated into the dressing scaffold to improve drug stability and release kinetics.

The release of *antibiotics* can be controlled by swelling or degradable properties of the scaffold and in many cases the drug is released by diffusion. This problem of burst release is often solved by hydrophobic coatings on the dressing surface to inhibit drug diffusion. Fine tuning the physical (e.g. mechanical strength, porosity, degradation rate) and chemical (e.g. polymer modification, cross-linking) properties are proved to achieve desired drug release. Interestingly, pH-responsive polymers offer possibility for intelligent release due to the basic microenvironment of serious infections. More recently, the incorporation of nanoparticles into the scaffold has also emerged as a solution for sustained drug release.

As introduced before, direct injection of therapeutic proteins (*growth factors, cytokines*) suffers from short effective time in vivo. Sophisticated delivery systems allowing long-term stability, controlled release and even multiple deliveries of proteins with independent release profile have been developed to favor wound healing. Proteins can be covalent or non-covalent bonded to the scaffold for immobilization. Moreover, the incorporation of growth factors during scaffold fabrication was found to have more controlled delivery kinetics.

Novel methods for more efficient delivery involve micro- or nanotechnology in materials design. Proteins can be loaded in micro- or nanoparticles to improve stability and modify protein release profile. The incorporated micro- or nanoparticles also have the potential to improve mechanical strength of the scaffold.

Polymers	Undergoing research		Commercial dressing
	Matrix	**Bioactive components**	
Chitosan and derivatives	Chitosan-PEO nanofiber mat	Ciprofloxacin Hydrochloride Moxifloxacin hydrochloride[26]	Kytocel® Gelling fiber dressing
	Chitosan nanofibers	Honey[27]	
	Chitosan-crosslinked collagen	aFGF[28]	
	Chitosan, alginate and poly(r-glutamic acid) hydrogel	No therapeutics added[29]	
Hyaluronic acid(HA) and derivative	HA nanocapsule	Polyhexanide[30]	Bionect®
	HA scaffold	Autologous fibroblasts[31]	
	Crosslinked HA fibrous membrane	No therapeutics added[32]	
	Cross-linked high/low Mw of HA foam	Arginine and EGF[33]	
	HA gel (Vulcamin)	Mixture of amino acids[34]	
Cellulose and derivatives	Cellulose dressing	Silver nanoparticles[35]	Regranex®Gel Aquacel®
	Collagen-oxidized regenerated cellulose foam	No therapeutics added[36]	
	Microbial-derived cellulose hydrogel	Polyhexamethylasebiguanide[37]	
Alginate	Alginate hydrogel	$ZnCO_3$[38]	MediHoney® Sorbalgon® Koltostat® Tegaderm™ high gelling
	Alginate gel coated with chitosan	rhodamine B[39]	
	Alginate hydrogel	Phenytoin[40]	
Collagen/Gelatin	Gelatin microspheres	bFGF[41]	Unite®Biomatrix BGC Matrix® Promogran® Prisma®Dermocol /Ag™ Fibracol®
	Geltin-PLGA scaffold	EGF[42]	
	Concentrated collagen	Ampicillin[43]	
	Collagen sponge	Model plasmid encoding for luciferase[44]	
	Collagen matrix	Glucose oxidase[45]	
	Collagen-gelatin foam	bFGF[46]	
Fibrin	Fibrin scaffold	VEGF/bFGF-loaded PLGA nanoparticles [47]	Tisseel®
	PEGylated fibrin gel	Chitosan microspheres loaded with silver[48]	

	Fibrin gel	CD 34^+ cells[49]	
Silk fibroin	Fibroin film	Aloe vera extract[50]	
	Fibroin fiber	Silver[51]	
Dextran	Dextran fibers	Thrombin or antibiotics[52]	
	Dextran hydrogel	No therapeutics added[53]	
Elastin	Elastin film	silver[54]	
	Elastin-like peptides gel	KGF[55]	
	Elatin-silk fibroin scaffold	No therapeutics added[56]	
PVA	Aminated-PVA hydrogel	NO[57]	
	Aminophenylboronic acid with PVA	Ciprofloxacin[58]	
PEG	PCL-PEG copolymer	rhEGF[59]	
	PEG-PCL nanofibers	EGF and bFGF[60]	
	PEGylated fibers	Rha FGF[61]	
	PEG	PEI-Plasmid encoding bFGF [62]	
PVP	PVP fibers	Indomethacin[63]	
	Poly (Vinyl methyl ether co-maleic anhydride) and PVP	NO[64]	
PHEMA	PHEMA hydrogel	NO[65]	
Poly (α-esters)	PLGA film	TiO_2 nanoparticles[66]	
	PCL nanofibers	Curcumin[67]	
	PLGA nanoparticles	rhEGF[68]	
	PLA fibers	bFGF[69]	

Table 1-3: Wound dressings in lab research and in the market

I-1-5-4. Cell therapies

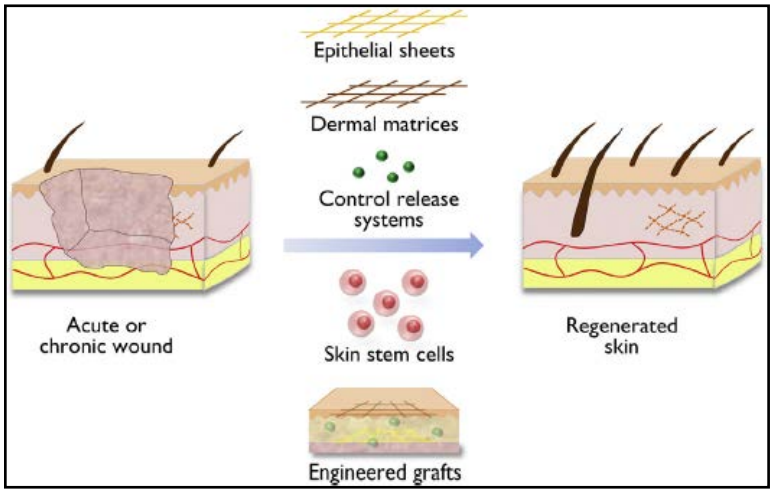

Figure 1-8: Current strategies of cell therapies for wound repair

Wound healing requires the integration of cell migration and proliferation as well as extracellular matrix deposition, angiogenesis, and remodeling. Therefore, cell therapies is also widely applied in wound treatment, particularly in cases where host cells, due to disease, age, or excessive trauma, are unable to repair the defect or deficiency alone. Direct injection and fusion cell suspension has been proved unsuccessful.[61] Current bioengineered skin substitutes, both biosynthetic skin substitutes and cultured autologous engineered skin, are available to provide temporary or permanent coverage, with the advantages of availability in large quantities and negligible risk of infection or immunologic issues. The main limitation of these products is high expense and storage conditions to preserve cell viability (generally at -80^{o}C in liquid nitrogen).

Apligraf® is composed of an epidermal layer of allogeneic neonatal keratinocytes and fibroblasts from neonatal foreskin. The cells are deposed on bilayered type I bovine collagen that is used as an adjunct covering to autograft, providing accelerated healing times. It is also used alone in chronic wound ulcers, showing decreased healing times when compared to controls. However, the chance of successful skin repair is less than 50%. In addition, Apligraf® has several drawbacks such as low resistance against degradation by proteases and weak persistence of fibroblasts within the normal collagen hydrogels. Recent studies on engineered hydrogels mimicking the extracellular matrix have provided significant insights into the designs of cell delivery systems. The matrix environment should provide directional cues to the transplanted cells in terms of adhesive ligands, integrin specificity, and a carefully engineered growth factor microenvironment. Future research is heading for dynamic or triggered changes in bioactivity, as well as multiple growth factor delivery for synergistic effects in directing cell fate for successful tissue repair.[70]

I-2. GENE THERAPY – AN ALTERNATIVE STRATEGY FOR TISSUE ENGINEERING

I-2-1. Introduction

Gene therapy is the intentional modulation of gene expression in specific cells to treat pathological conditions. The European Medicines Agency (EMA) defines that a gene therapy medicinal product is a biological product which fulfils the following two characteristics: (a) it contains an active substance which contains or consists of a recombinant nucleic acid used in or administered to human beings with a view to regulating, repairing, replacing, adding or

deleting a genetic sequence; (b) its therapeutic, prophylactic or diagnostic effect relates directly to the recombinant nucleic acid sequence it contains, or to the product of genetic expression of this sequence.

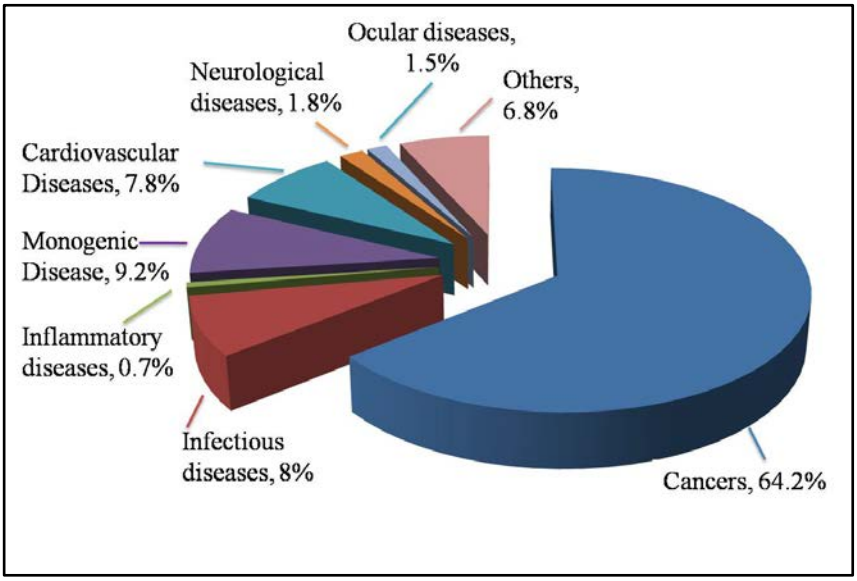

Figure I-9: Graphical presentation of different indications that have been addressed by gene therapy in clinical trials (n=2145), 2015, The Journal of Gene Medicine, Wiley and Sons (http://www.abedia.com/wiley/index.html)

Since the first gene therapy trials in 1970s, two decades has seen more than 1700 approved clinical trials worldwide. Although gene therapy was first conceived for genetic disorders, it has found broader applications for the treatment of severe diseases, with cancers being the major interest (64.2%), followed by infectious diseases (8%) and monogenic diseases (9.2%) (**Figure I-9**). Generally, gene therapy can be categorized into two categories- germ line gene therapy and somatic gene therapy. The difference between these two approaches is that in somatic gene therapy genetic material is inserted in some target cells, but the change is not passed along to the next generation, whereas in germ line gene therapy the therapeutic or modified gene will be passed on to the next generation. This difference is of importance, since current legislation allows gene therapy only on somatic cells[71], which will be also the focus of this section.

I-2-2.Therapeutic genes

The concept to use genes as drugs for the treatment of human diseases was fist conceived around 1970s, owing to the fast growing knowledge in gene function and advancement of technologies for DNA delivery into mammalian cells. Plasmid DNA is most commonly found

in bacteria as small (compared with chromosomal DNA), circular, double-stranded DNA molecules. When specific sequences encoding for therapeutic proteins (e.g. growth factors, cytokines) is inserted into the plasmid, this artificial plasmid can be used as vectors in molecular cloning, driving the expression of recombinant DNA sequences within host organisms. Progress in molecular biology has led to the availability of other therapeutic genes and shorter nucleic acid sequences, in particular anti-sense oligonucleotides (AS-ODN) and small interfering RNA (siRNA). Nevertheless, these molecules with relatively large size and negative charge can not penetrate the cell membrane efficiently and are also susceptible to degradation by nucleases, particularly the single stranded AS-ODN. Consequently, the delivery of these macromolecules should be mediated by carriers and vectors. DNA and oligonucleotides must be transported into the nucleus, while RNA (siRNA, miRNA and mRNA) act in the cytoplasm at the level of protein synthesis, as shown in **Figure I-10**.

New generation of therapeutic genes provides more precise way to repair disease-causing genes is needed.[1] mRNA and DNA encoding gene editing systems including sequence-specific zinc-finger nuclease (ZFPs), TALEs (transcription activator-like effector nuclease) and CRISPR–Cas (clustered regularly interspaced short palindromic repeat) systems can carry out precise gene correction and insertion in genome. Therefore, this strategy offers great potential for personalized medicine.

In brief, although substantial progress has been made in gene therapy over the past three decades (**Table I-4**), DNA-based drugs are faced with greater delivery and safety challenges than other nucleic acid therapeutics owing to their large molecular sizes, the difficulty crossing the nuclear barrier and the risk of mutagenesis. In this regard, further clinical progress is needed to bring insights into the key steps limiting effective delivery and structure–function relationships for vector design. Generally speaking, gene delivery vectors are classified into viral and non-viral vectors. Their applications in clinical trials are shown in **Figure I-11** and introduced in details in the following subsections.

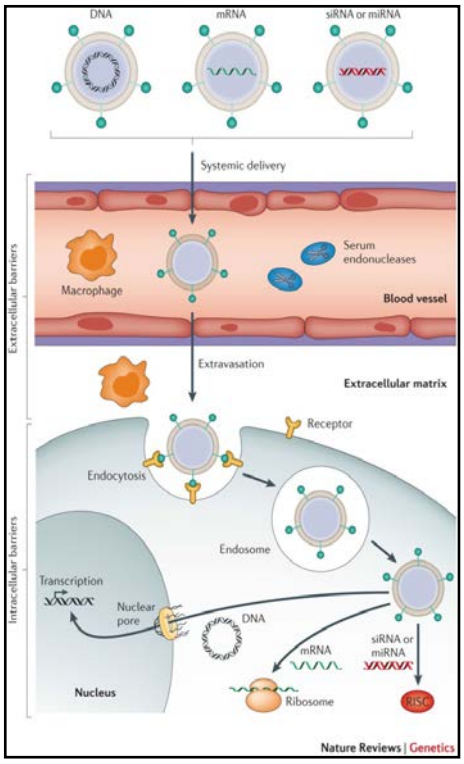

Types	Characteristics	Function site
DNA	Double stranded, Several kbps, Upgrade target protein expression	Nucleus
mRNA	Single-stranded, Alternative to DNA, Reduced immunogenicity	Cytoplasm, Ribosome
siRNA	Double-stranded, Chemically synthesized, 19–21 bp in length, Downgrade target protein expression	Cytoplasm, RNA-induced silencing complex
miRNA	Similar to siRNA, Endogenously synthesized, 18–25 nucleotides in length, Promote mRNA degradation and/or translational inhibition	Cytoplasm, RNA-induced silencing complex
AS-ODN	single-stranded DNA molecules, 13-25 nucleotides in length, Promote mRNA degradation and/or translational inhibition	Cytoplasm
Gene editing system	mRNA or DNA encoding ZFPs, TALEs, CRISPR-Cas	Nucleus

Figure I-10. Overview of the gene delivery process ; **Table I-4**. Different categories of therapeutic genes

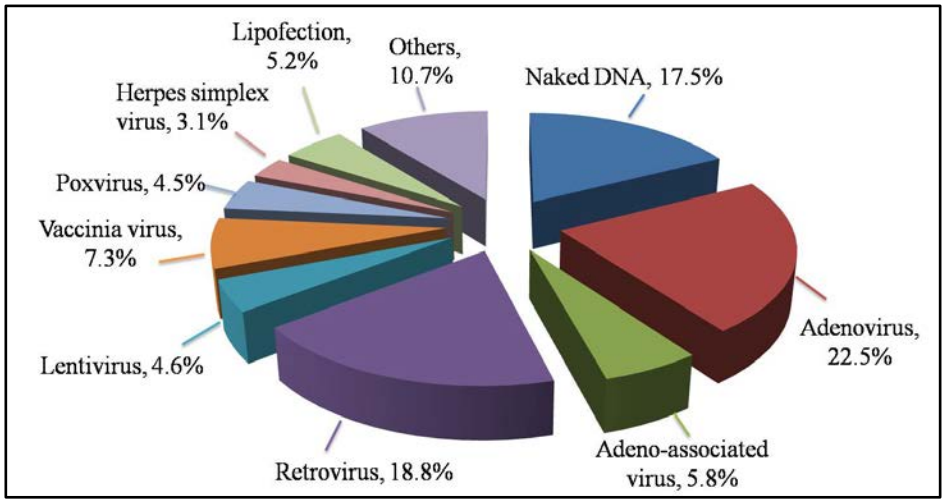

Figure I-11: Graphical presentation of different vectors that have been addressed by gene therapy in clinical trials (n=2206), 2015, The Journal of Gene Medicine, Wiley and Sons (http://www.abedia.com/wiley/index.html)

I-2-3. Viral vectors- a natural system

Viral vectors are so far the most efficient vectors for gene delivery, adopted by 66.6% of current clinical trials for gene therapy (Figure 1-11). Adenoviral (AV), retroviral/lentiviral (RV/LV), and adeno-associated viral (AAV) vectors are the major ones used in gene therapy (**Figure I-12**). They are generally below 100 nm and AAV with the size of 20 nm is the smallest viral vector. Despite their remarkable transduction efficiency, both clinical trials and laboratory experiments have suggested that viral vectors have inherent shortcomings for gene therapy, including limited loading capacity, immunogenicity, genotoxicity, and failure to support long-term adequate transgenic expression. In order to learn the mechanisms of high transfection from the natural system, this subsection will only cover the intracellular process of viral vectors and strategies to overcome the disadvantages mentioned above.

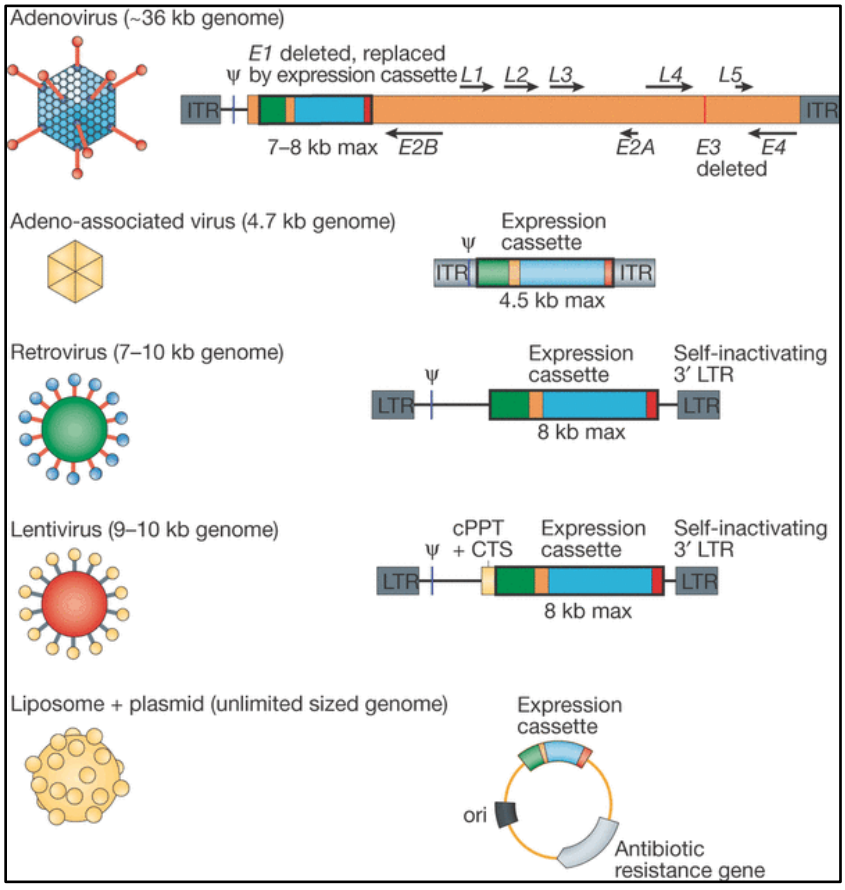

Figure I-12: Main viral vectors for gene delivery and their load capacity (liposome adopted here as typical non-viral vector for comparison) [72]

Viral vectors usually consist of viral capsids and viral genome. When considering for gene delivery, the virus have to undergo several modifications and meet some prerequisites.[73]

First, most genes encoding for viral proteins, especially pathogenic ones, should be removed from viral genome. Meanwhile, sequences of the viral genomes required for viral replication should be maintained. Expression of viral proteins required for viral replication within the virus-producing cells (called packaging cells) should also be kept. Finally, the therapeutic gene cassette could be inserted into the viral genome to replace the native genes by recombination or introduced into the viral vector as episomal genes.

In general, viral vectors fall into one of the main categories: integrating vectors (e.g. gamma-RV, LV), which insert themselves into the recipient's genome, while non-integrating vectors (e.g. AV, AAV) usually form an extra chromosomal genetic element. Integrating vectors, such as gamma-retroviral vectors and lentiviral vectors, are generally used to transfect actively dividing cells, as they are stably inherited. Non-integrating vectors, such as adenoviral vectors and adeno-associated virus (AAV) vectors, can be used to transfect quiescent or slowly dividing cells, but they are quickly lost from cells that divide rapidly. There are two mechanisms for cellular uptake of viral vectors. AV (binding with coxsackie and adenovirus receptor, CAR) and AAV (binding with heparansulphate proteoglycan, HSPG) can bind specific receptors on cell membrane and then enter the cellular cytoplasm via clathrin-mediated endocytosis. Genome is then transported to the nucleus through the nuclear pore, where the association of the AdV genome with nuclear matrix initiates the transcription. For RV/LV, membrane fusion is the main mechanism whereby enveloped viruses deliver their genomes into cells.

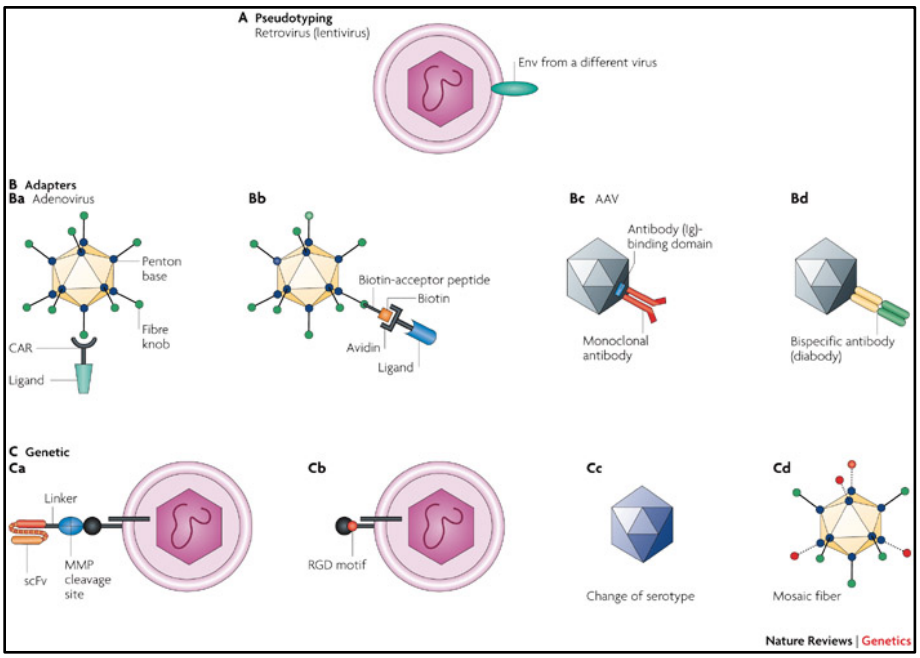

Figure I-13: Viral vectors engineering to reduce toxicity and immunogenicity[74]

Many modification strategies have been implemented for all three vector types as shown in Figure above (**Figure I-13**) with the goal to reduce the side effect of viral system. To start with, viral vector with high transfection as well as high toxicity can be pseudotyped with an envelope protein (EP) from a different virus with lower toxicity (**Figure I-13A**). More sophisticated hybrid viral vectors have recently been developed and reviewed in details by Huang *et al.*[75]

An alternative strategy relies on modification virus with target ligand. On the one hand, viral vectors can be coupled with a receptor-ligand fusion (Figure 1-13B). Adaptors are molecules with dual specificities: one end binds the viral attachment protein and the other binds the receptor on the target cell. The advantages of this approach are its great flexibility, as different adaptors can readily be coupled to the same vector, and the fact that it does not require changes in vector structure that could be detrimental to vector production or gene transfer. On the other hand, this could be achieved by genetic fusion of a targeting ligand (Figure 1-13C). Despite being more technically challenging than the use of adaptors, such single component systems provide homogenous retargeted vector particles, unlike adaptor-based approaches. Muench and co-workers modified the capsid of AAV with ligands specific for Her2/neu, EpCAM or CD4 receptors that are expressed on tumor cells.[76] Vector targeted to the tumour antigen Her2/neu was sufficient to track 75% of all tumour sites. CD4-targeted AAVs hit human CD4-positive cells present in spleen of a humanized mouse model, while other off-target organs remained unmodified. EpCAM-AAV detected single tumour cells in human blood opening the avenue for tumour stem cell tracking. Thus, ligand engineered viral vectors could deliver genes to target cell types of choice with high specificity.

To end with, the virus are naturally optimized in essential processes for gene delivery, including targeting of specific receptors (e.g. CAR for AV, HSPG for AAV), internalization, delivering of nucleic acids to nucleus and, in some cases, permanent modification of the host cell genome. Imitating some of these features will contribute to progress in the field towards broader and more successful gene therapy.

I-2-4. Non-viral vectors - learning from nature

To overcome the limitations of viral systems, namely limited load capacity and toxicity, a variety of vectors have been developed to deliver therapeutic nucleic acids to their site of actions, including lipids and liposomes, polymers (linear and branched polymers, dendrimers and polysaccharides), polymersomes, cell-penetrating peptides[77] and inorganic nanoparticles.

These synthetic vectors have lower immunogenicity, higher load capacity and easy fabrications. Specifically, nucleic acids can be delivered through physical encapsulation or electrostatic attraction. Among the non-viral systems, cationic vectors occupy the overwhelming percentage, taking advantage of the high charge density to compact and protect therapeutic genes.

I-2-4-1. Barriers to non-viral gene delivery

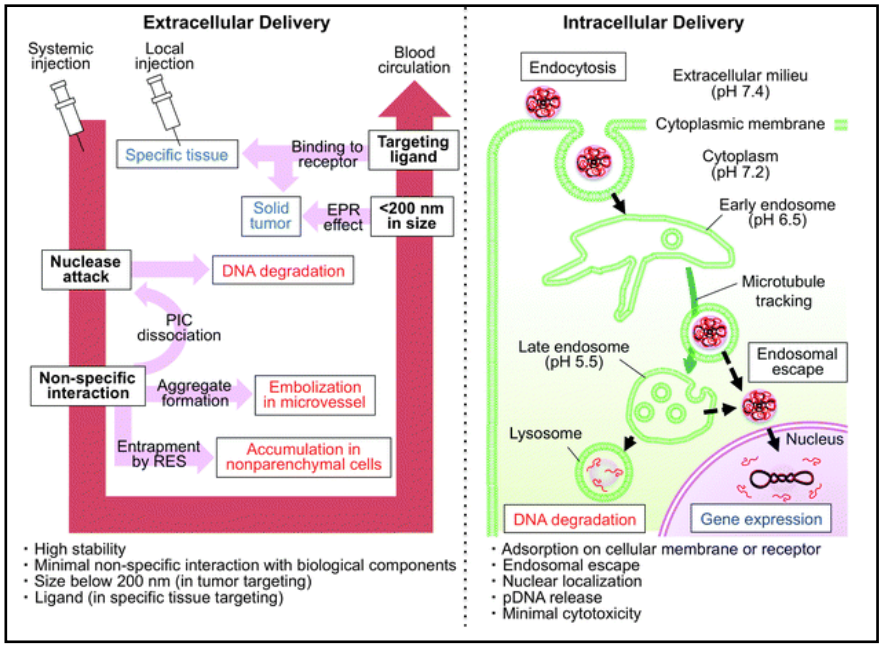

Figure I-14: Extracellular and intracellular barriers for non-viral gene delivery

(i) Stability

The presence of endo-nucleases in physiological fluids and extracellular space pose threat on the stability of therapeutic genes (**Figure I-14**). Thus, the vectors should allow the nucleic acids from degradation and elimination by RES system.

(ii) Cellular uptake

Cell internalization of DNA complexes is generally size-dependent. For exemple, polyplexes be internalized by cells via multiple mechanisms, including clathrin-mediated endocytosis (CME, for endocytic vesicles with a size of ~100–150 nm), caveolae-mediated endocytosis (~50–80 nm), micropinocytosis (~90 nm) and macropinocytosis (~500–2000 nm). Surface charge and ligand conjugation are another two factors affecting cellular uptake. Positive charge can strengthen the affinity DNA complexes with cell membrane and therefore

facilitate internalization. Modificaiton with ligand that can bind specific receptors on cell membrane can also lead to higher cellular uptake.

(iii) Endosomal escape

When DNA complexes are internalized by phagocytosis or endocytosis, they will be sequestered in a membrane-bound vacuole, which is subsequently acidified and fused with a lysosome containing acid hydrolases. Therefore, some mechanism must be included to allow the nucleic acid to escape from the endosome before it is degraded.

In case of lipoplexes, a model for local endosomal membrane destabilization was proposed for smooth escape from endosomes (**Figure I-15**, left panel). Specifically, electrostatic interactions between cationic lipids and endosomal membrane induce the replacement of anionic lipids from the cytoplasm–facing monolayer of the endosomal membrane, by means of the so-called flip-flop mechanism. The formation of a neutral ion pair between anionic lipids present in the endosomal membrane and the cationic lipids of the vector will then result in decomplexation of the DNA and its release into the cytoplasm. Moreover, the neutrally charged helper lipid will facilitate membrane fusion and help destabilize endosomal membrane.

The most popular although challenged hypothesis for endosomal escapes of polyplexes is the so-called “proton sponge” effect[78] (**Figure 1-15**, right panel). The core of this theory is that different amines on polymer chains can be further protonated inside endolysosomes, leading to an influx of counter ions (Cl^-) and an increase of osmotic pressure inside so that the endolysosomes are finally burst. Recently, conjugation of endosome disruptive peptides to polyplexes[79] and co-administration with week base (e.g. chloroquine) become other options for their capacity to induce endosomal escapes.

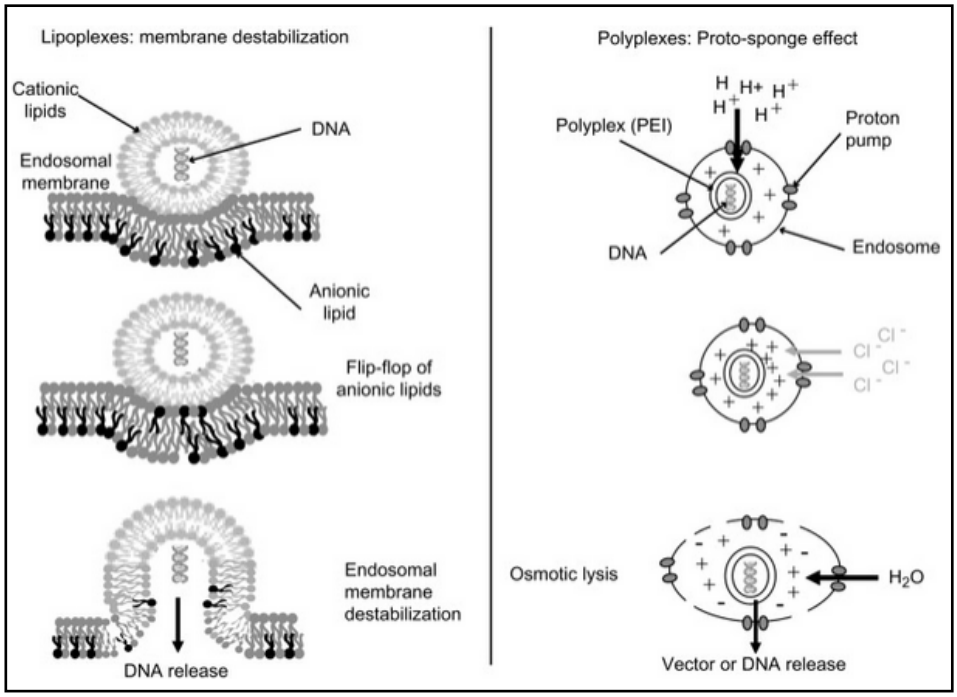

Figure I-15: Hypothesis of endosomal escape of lipoplexes and polyplexes gene delivery systems.[80]

(iv) Vector unpacking

This process is widely assumed to be indispensible for gene expression, but the extent and the timing effect on transfection efficiency remains unclear. In some studies, vectors have high capacity to complex DNA were found to have low transfection efficiency, indicating the unpacking is somewhere indispensible for gene expression.

I-2-4-2. Lipid-based systems

Lipid-based DNA vectors accounts for more than 1/3 of all non-viral vectors applied in clinical trials (**Figure I-11**). The concept of "lipofection" was advanced by Felgner *et al.*[81] Small liposomes, formed from DOPE and DOTMA (available as Lipofectamine®), were mixed with DNA and the resulting "lipoplexes" were able to condense the linear and plasmid DNA into a complex. Many other cationic lipids have been developed, including DOTAP, DOGS, DC-cholesterol (**Figure I-16a**). These lipids are usually mixed with a "helper" lipid, such as DOPE or cholesterol that improves their stability and overall transfection efficiency. The net positive charge of the complexes is probably responsible for their high toxicity and also promotes the adsorption of plasma protein that leads to their rapid elimination.

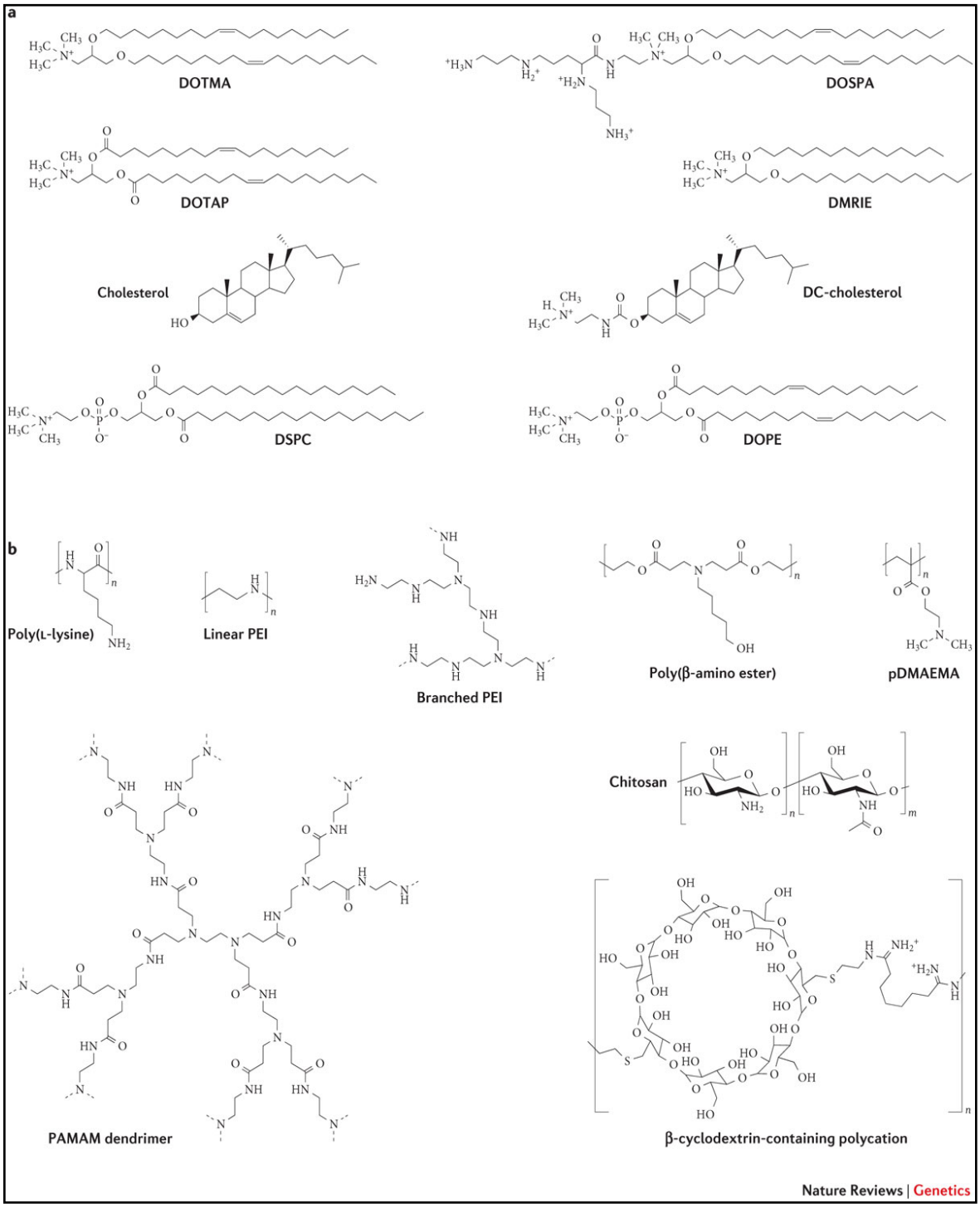

Figure 1-16. Chemical structures of cationic and neutral lipids (a) and selected polymeric vectors (b) that are commonly used in gene delivery studies and clinical trials.

The surface therefore is modified by the addition of anionic lipids or by the inclusion of PEGylated lipids.

To increase the circulation half-life of liposomal nucleic acids, they should have a near-neutral surface charge (**Figure I-17**) Two approaches have been used to achieve this: the formation of coated cationic liposomes (Figure D-F) and the use of ionizable lipids. Ligands are needed for specific binding and internalization (Figure G). Efficient endosomal release following internalization is needed for therapeutic activity, and this can be provided by ionizable cationic lipids with optimized bilayer destabilizing capacities and pKa. Lee and co-workers have newly reported a PCR-based nanofactory mediated with neutral lipid as a potential gene delivery system (Figure H).[82] Plasmid DNA can be amplified by PCR inside liposomes about 200 nm in diameter, and the quantity of loaded genes highly increased by more than 8.8-fold after PCR reation. Moreover, good biocompatibility was obtained owing to free of positive charge. Therefore, this novel system offers new possibility to address both efficiency and toxicity issues simultaneously.

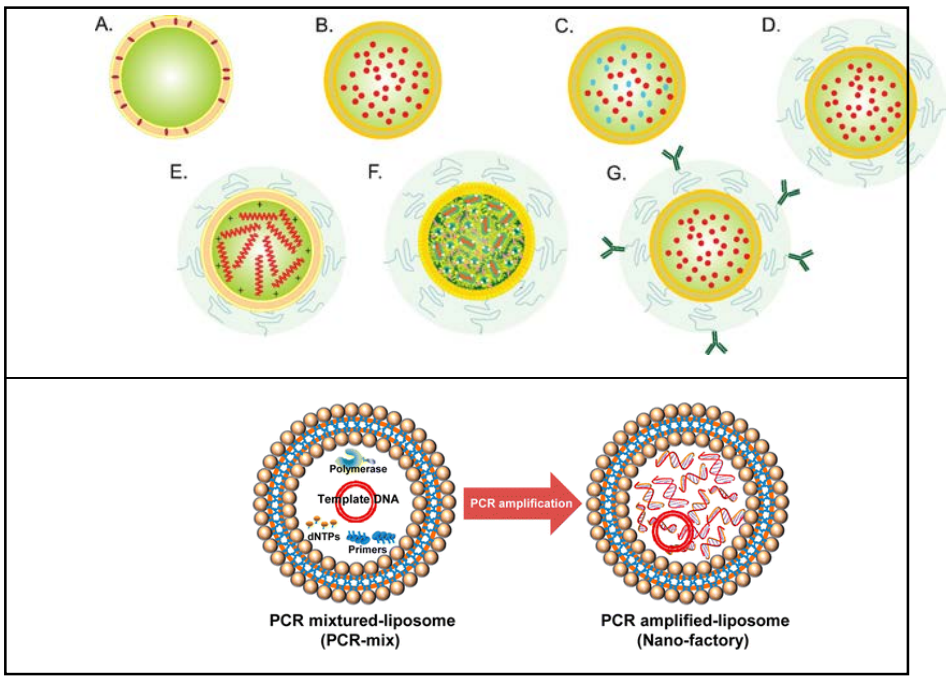

Figure I-17. Versatility of liposomes as drug/gene delivery carriers (A-G), symbols in different shapes and colours represent different therapeutics, e.g. drug, protein or nucleic acids. PCR-based nanofactory system mediated with neutral lipid (H).

I-2-4-3. Cationic polymer-based systems

Polymers are alternative competent candidates for gene delivery, largely due to the chemical diversity and functionality. They can be classified by surface charge at physiological pH (caitionic, neutral or ionic), or by resources (natural or synthetic). As cationic polymers play a predominant role in polymer-based gene delivery system, this subsection only covers their versatility as gene vectors.

Cationic polymers can bind DNA molecules to form nanometer-sized complexes known as polyplexes. Parameters including the amount and type of amine groups, charge density and hydrophilic and hydrophobic contents have been found to direct impact on the transfection efficiency of polyplexes.[78] Polyplexes have some advantages compared to lipoplexes such as small size, narrow distribution, etter protection against enzymatic degradation, higher stability, and easy control of the physical factors. However, like cationic lipid-based system, cationic vectors share the same challenge in balancing transfection efficiency and cytotoxicity due to the excessive positive charge.

Poly(L-lysine) (PLL) and polyethylenimine (PEI) are among the oldest and most commonly used polymeric gene vectors. To improve safety and efficacy, numerous other polymers have been studied for gene delivery, including methacrylate-based polymers such as poly[(2-dimethylamino) ethyl methacrylate] (pDMAEMA), carbohydrate-based polymers such as chitosan and β-cyclodextrin-containing polycations, polyamidoamine (PAMAM) dendrimers and degradable poly(β-amino ester) polymers.

(i) PLL (Poly-L-lysine)

PLL is a homopolypeptide of the basic amino acid lysine, and its ability to condense DNA has been recognized since the 1960s. The biodegradable nature of PLL is advantageous for in vivo applications. Pioneering studies in the late 1980s indicated that PLL conjugated to the asialoorosomucoid glycoprotein could potentially be applied in non-viral liver-targeted gene delivery. In general, in the absence of a lysosomal disruption agent such as chloroquine, PLL has fairly poor transfection activity, presumably due to low capacity for endosomal buffering and lysis. Numerous modified variants of PLL with enhanced gene delivery properties have been reported. One example includes PLL covered with the hydrophilic polymer PEG, which is designed to minimize nonspecific interaction with serum components and thereby increase circulation time. The clinical potential of PEGylated PLL was investigated as a vector to treat cystic fibrosis.[1]

(ii) Polyethylenimine (PEI)

PEI and its variants are among the most studied polymeric materials for gene delivery. PEI has a high charge density at a wide range of pH values with a nitrogen atom at every third position along the polymer chain. This attribute of PEI has been postulated to aid in condensation of DNA and endosomal escape. The ability of PEI to promote gene transfection *in vitro* and *in vivo* was first demonstrated in 1995.[83] Soon after, it was shown that the transfection efficiency and cytotoxicity of PEI strongly depend on its structural properties, especially with respect to molecular weight and the linear versus branched forms. Higher molecular weight and branched structures generally result in high transfection as well as high cytotoxicity. Examples to balance efficiency and safety include PEGylation, degradable disulphide-crosslinking, alkylation and ligand conjugation of PEI.[84] Adding low molecular weight PEIs onto biocompatible polymers (e.g. cyclodextrin, chistosan, dextrans) can significantly improve the biocompatibility of PEIs. Hydrophobic segments such as alkyl chains of fatty acids and cyclic hydrophobic molecules are also used for PEI modifications, based on the principles that acylation reduces the basicity and availability of free amine groups.

(iii) Dendrimers

They are three-dimensional polymers with spherical, highly branched structures. Frequently used dendrimers are polyamines, polyamides, or polyesters, among which polyamidoamine (PAMAM) is the most commonly used. The primary amine groups promote DNA cellular uptake because of their participation in DNA binding but the buried tertiary amino groups act as a proton-sponge break down the endosomes and facilitate the translocation of DNA into nucleus. Emanating from the core, dendrimer is constituted of repeat units having at least one branch junction, whose repetition is organized in a geometrical progression that results in a series of concentric layers called “generations”. It’s well defined that with the increase of generation number, transfection efficiency as well as toxicity increase in the same trend. Dendrimers displays a pH-dependant relase profile, and in low pH it adopts an extended conformation which facilitate the release of genes or drug.[85] Moreover, the presence of numerous peripheral functional groups on hyperbranched dendrimers affords efficient conjugation of targeting ligands and biomarkers that can recognize and bind to receptors overexpressed on specific cells for active targeting.

(iv) More intelligent polymeric systems have been proposed. Surface shielding with PEG and other moieties often leads to a dilemma. It's necessary for long circulating time and reduction of toxicity of cationic polymers wheras it often results in decreased transfecition. One possible solution will be PEGylation with different chain length, in which longer PEG chains are bonded with cleavable linkers (**Figure I-18A**). In this way, PEG detaches from polyplexes upon cellular uptake and polyplexes could maintain sponge effect for endosomal escape

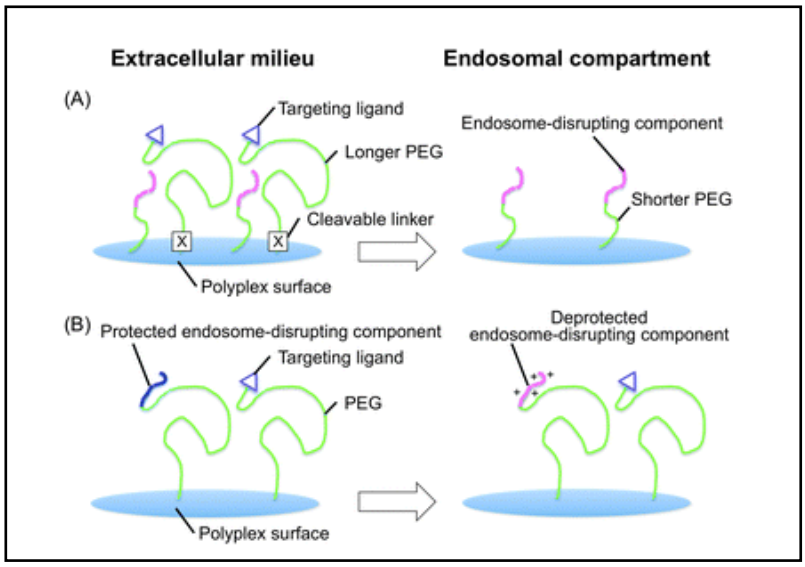

Figure 1-18: Schematic illustration showing the combined use of a targeting ligand and an endosome-disrupting component, providing dual functionality. (A) The system equipped with varying lengths of detachable poly(ethylene glycol) (PEG) chains with the detachability. (B) The system equipped with a protected endosome-disrupting component containing primary amines.[86]

Alternatively, the introduction of targeting ligand molecules can be adopted to facilitate selective accumulation of polyplexes in the target tissue/cells. So far, a variety of ligand molecules have been introduced onto the surface of nanoparticles including polyplexes. For instance, asia loorosomucoid, lactose, galactose, and their derivatives have been utilized for targeting the liver, while transferrins (Tfs) and folate have been used for targeting cancer cells. Furthermore, peptides and antibodies have been utilized for targeting specific tissues.

Moreover, fine-tuning of polycationic structures can substantially enhance their acidic pH sensitivity to induce endosome-selective destabilization without compromising cell viability and functions. Furthermore, degradable nature of polycations can reduce the cumulative toxicity of repeated transfection and also can allow the easier release of pDNA from polyplexes for effective transcription to mRNA in nucleus.

I-2-4-4. Solid nanoparticles-based system

(i) Organic nanoparticles

They are generally prepared from bio- (collagen, gelatin, elastin, fibronectin, silk, albumin, etc)[87] or synthetic (PEG, PCL, PLGA, etc) polymers[88]. As they are neutrally charged at physiological conditions, they are generally applied as "non-condensing vector". Consequently, therapeutic genes are generally incorporated in the polymer matrix by physical encapsulation, in which multiple genes could be loaded simultaneously. The as-formed particles can be further conjugated with moieties stimulating receptor-mediated endocytosis, the bioactivity of the encapsulated genes could be maintained by preventing digestion by nucleases. Synthetic polymers such as Poly (d,l-lactide-*co*-glycolide) (PLGA) have been extensively investigated for sustained and targeted/localized delivery plasmid DNA. Although this kind of system suffers from the low transfection efficiency and low encapsulation efficiency, higher transfection was observed in vivo compared with liposomes. Further, gene transfection was observed for up to 28 days, suggesting the application of nanoparticles for sustained gene expression.

(ii) Inorganic nanoparticles and hybrid nanosystems

Silica nanoparticles, carbon nanotubes (CNTs), magnetic nanoparticles, calcium phosphate nanoparticles, gold nanoparticles, and quantum dots (QDs) have been widely evaluated as gene delivery carriers. Compared with organic nanoparticles, they are not subjected to microbial attack and also show good storage stability. These nanoparticles possess many advantages in gene delivery such as facile fabrication and surface functionality. However, surface modification with cationic amine group is indispensible to compact the negatively charged nucleic acids. Consequently, a hybrid nano-system consisting both organic and inorganic moieties have emerged to maximize to advantages of the two components[89]. More specifically, the inorganic part in the core, with tunable size, shape, porosity, provides a variety of possibilities for gene loading. At the same time, organic part over the surface is responsible for charge tuning, biomolecules conjugating, surface shielding and targeting delivery. Specially, silica nanoparticles will be introduced in details in the following section as hybrid nanovectors for drug and gene delivery.

I-2-5. Scaffold-based gene delivery systems for tissue engineering

Local strategies evolved from repair and replacement tissues and organs, then to sustained delivery of recombinant cytokines and now reached an epoch for sustained delivery of plasmid. Local plasmid-based gene transfer technology is known as gene activated matrix (GAM). Studies over the past two decades suggest that GAM may serve as a platform for local gene delivery in the wound bed of various tissues and organs, such as acutely injured tendon, ligament, bone, muscle, skin and nerve. Fast catabolism of DNA in the blood stream avoids systematic toxicities. Additional advantage includes that plasmid DNA is stable and flexible compared with protein, thus more likely to be compatible with established sustained delivery systems.

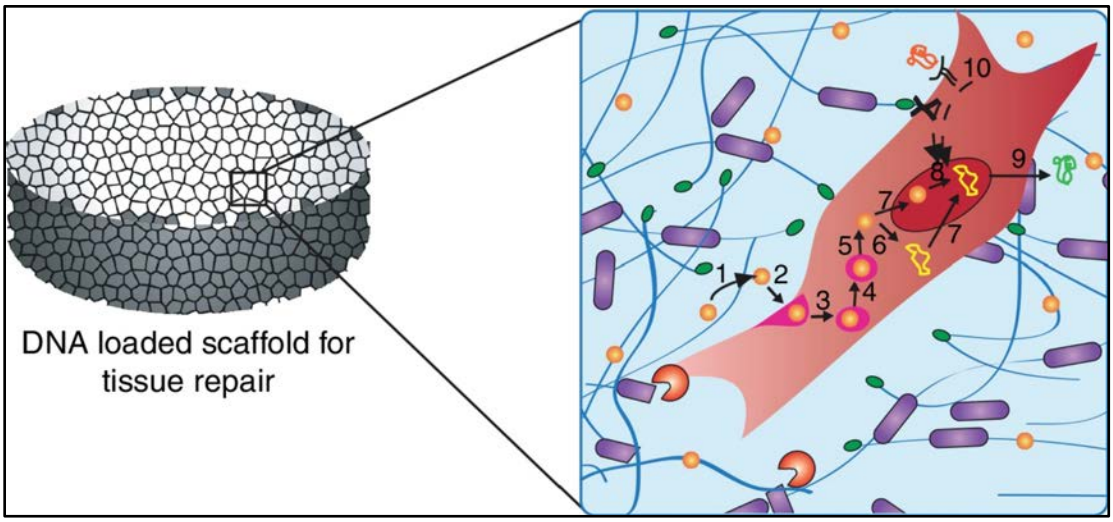

Figure I-19: Schematic overview of protein expression in scaffold based gene delivery[90]

An important assumption was that, following gene transfer, the recombinant cytokines will be expressed at more nearly physiological levels but for prolonged period of time by wound healing cells. As shown in the **Figure I-19**, nDNA (1) is released from the scaffold through either hydrolysis or cellular migration (2) and internalized into the endosome (3). The endosome matures changing its oxidation and acidity resulting in endosomal escape of nDNA (4 and 5). nDNA can enter the nucleus (7) to be unpacked (8) or be de-coupled in the cytosol (6) for nuclear entry (7), where transcription and translation occurs (9) for protein expression. Growth factors or other bioactive signals can be used to induce intracellular signaling pathways that prime cells for transfection (10).

Although naked DNA has been reported to achieve therapeutic effects, the research interest now is focused on the delivery of compacted DNA (nDNA) with the help of either viral or non-viral (mainly cationic lipid, polymer and inorganic nanoparticles) vectors, due to greater

potential for high transfection efficiency.[90] The release profile of vectors largely depends on the interactions between the matrix and DNA complexes. nDNA can be either encapsulated into the system either during matrix fabrication or deposited to the wall surface of the fabricated matrix by immersion in nDNA solutions or pipeting. The latter has the advantage to avoid the harsh preparation conditions and aggregation of DNA complexes. Yet, it may suffer from burst release due to the week interaction with the matrix. Consequently, covalent bonding is necessary to achieve stronger affinity and therefore more sustained release.

As scaffold-based gene delivery involves complex participation of matrix and DNA vector and cells, there are therefore different classifications for scaffold-based delivery systems. Herein, the systems are classified into 3 types based on the nature of matrix (degradability, pore size, stiffness), the source of cells (encapsulated or infiltrated), the presence of biochemical molecules (growth factors, cytokines, peptides, etc). In all cases, nDNA can be incorporated in the matrix by all the method mentioned above.

Type 1. Matrix-oriented delivery

This type of system is characterized by controlled release of DNA to neighbouring cells or tissues, with the belief that sustained release of the transfection vector achieves prolonged transgene expression over burst-released vectors. The release of DNA generally relies on the degrability of the matrix, and therefore, biodegradable polymers such as PLGA, PEG and PCL, are of first choice for the system design.

Type 2. Cells-oriented delivery

In this case, cells play a central role for the gene delivery. Therapeutic genes are generally immobilized in the system and thus difficult to be released out of the matrix. Therefore, cell transfection could only happen when cells infiltrated and colonized in the matrix. Hydrogel scaffold such as fibrin, collagen, peptide crosslinked hyaluronic acid and peptide crosslinked PEG are often chosen for matrix design.

Interestingly, this type of matrix can combine cell therapy and gene therapy for successful tissue engineering when cells encapsulated in the scaffold. On the one hand, the cells can act as bioreactors for the continuous production of therapeutic proteins. On the other hand, the cells introduced can help tissue regeneration when the host cells are unable to repair the defect or deficiency alone to disease, age, or excessive trauma.

Type 3. Biochemical cues meditated delivery

This type of system is aimed to prime cells for transfection by encapsulation of biochemical cues such as ECM components (e.g. fibronectin, glycosaminoglycan), growth factors (e.g. FGF), peptide (e.g. RGD). The presence of biochemical cues can influence proliferation, migration, internalization, intracellular trafficking and gene expression. For example, glycosaminoglycans (GAGs) in the native ECM are known to play an important role in sequestering biomolecules within the matrix based on their degree of sulfatation and structural variations in their carbohydrate backbone. Biomaterials incorporating GAGs have increasingly been explored as a strategy to transiently regulate growth factor availability[91].

A potential problem of single gene therapy is that simply increasing the concentration may not promote all phases of wound healing. A single growth factor cannot counteract all the deficiencies of a burn wound, nor control the complexities of chronic wound healing. Lynch et al. demonstrated in a partial thickness wound healing model that the combination of PDGF and IGF-I was more effective than either growth factor alone, while Sprugel *et al.* found that a combination of PDGF and FGF-2 increased the DNA content of wounds in the rat better than any single growth factor. The efficacy of KGF nDNA in combination with IGF-I nDNA was compared to the same genes individually. Noticeably, this combination accelerated re-epithelization, increased proliferation, and decreased skin cell apoptosis compared to the single construct alone. The re-epithelialization in the burn model was over twice that of the untreated control with a significant improvement in cell survival. Transfection of multiple growth factor genes at strategic time points of wound healing (sequential growth factor therapy) is therefore the next logical step in augmenting wound healing.

Slow-release matrices and gene-delivering gel matrices are used for prolonged transgenic expression. The concept of a genetic switch is another exciting development, where transgenic expression in target cells can be switched ‘on’ or ‘off’, depending on the presence of or absence of a stimulator such as tetracycline. Biotechnological refinements, such as wound chamber technique, may also improve the efficacy of gene delivery to wounds. These new techniques need further studies to define their efficacy and clinical applicability. More studies are also needed to define growth factor and cytokine levels in different phases of wound healing and to elucidate the timing of gene expression or down-regulation required for better wound healing.

I-3. SILICA NANOPARTICLES – VERSATILE DELIVERY PLATFORMS

I-3-1. The chemistry of silica nanoparticles

I-3-1-1. Non-porous silica nanoparticles

Plain silica particles have been developed at the industrial scale for many years. They are currently used as additives in a wide range of applications, including pharmaceutical formulations, foodstuff and toothpaste.

Three main methods exist for the preparation of silica nano- and microparticles (**Figure I-20**)

(i) the aqueous route:

This method uses water glass solutions. Water glass is obtained by the dissolution of siliceous sand in highly concentrated sodium (or potassium) hydroxide solutions. The resulting solutions have a $M_xSi_yO_z.nH_2O$ general formula (M = Na, K). They consist of silicate oligomers in very alkaline solutions (pH > 12). To obtain silica particles, these solutions are dropped down in an aqueous acidic solution (usually H_2SO_4). The size of the particles is controlled by the concentrations of the two reagents as well as other processing parameters (addition rate, stirring rate, temperature, etc…)

(ii) the sol-gel route:

In 1968, Stöber and Fink reported a simple synthesis of monodisperse spherical silica particles by means of hydrolysis/condensation of a dilute solution of tetraethyl orthosilicate (TEOS) in ethanol in the presence of ammonium hydroxide.[115] Uniform amorphous silica spheres whose sizes ranged from 10 nm to 2 μm were obtained simply by changing the concentrations of the reagents. This Stöber method was later improved by many others and appears to be the simplest and most effective route to monodispersed silica spheres.

(iii) the microemulsion route:

The emulsion route has been widely developed to design silica capsules for microencapsulation.[116] These particles can be prepared by water-in-oil W/O or oil-in-water O/W processes, mainly depending on the hydrophilic or hydrophobic character of the molecule to encapsulate (**Figure I-20**). If the molecule is hydrophilic, it is first dissolved in the water phase in the presence of the hydrolyzed silicon alkoxide and a surfactant. This aqueous phase is then dispersed in the oil phase (W/O). If the molecule is lipophilic, it is

dissolved in an organic solvent together with the un-hydrolyzed alkoxide. This oily phase is dispersed in the surfactant-containing water solution.

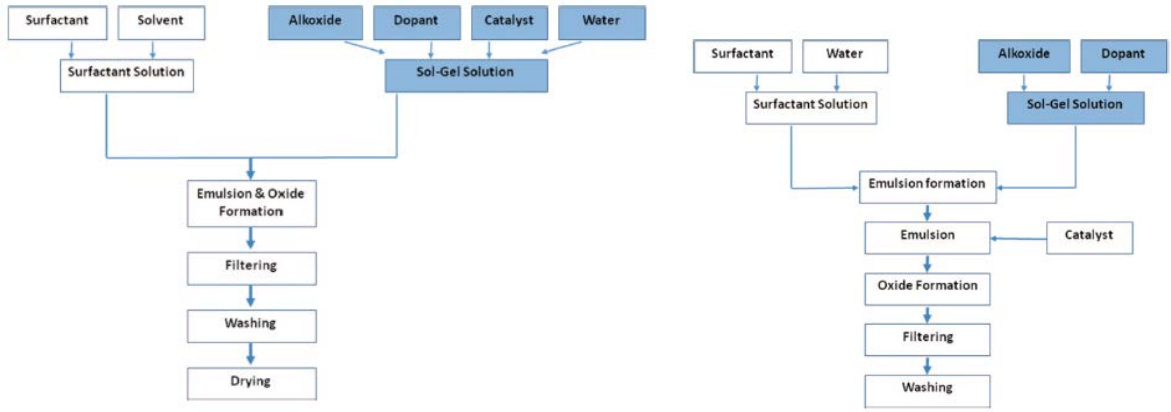

Figure I-20. Microemulsion route to doped silica particles: (left panel) water-in-oil W/O, (right panel) oil-in-water O/W.[116]

It must be noticed that the obtained particles have some porosity in the micropore range (a few angströms in diameter). However, these pores are too small to serve as host cavities for the loading of molecules by impregnation routes. This is the reason why they are usually termed as plain or non-porous, in contrast to the mesoporous particles described in the next section.

I-3-1-2. Mesoporous silica nanoparticles (MSN)

Since their discovery in 1992, mesoporous materials have attracted extensive attention due to the unique physical and chemical features including large specific surface area and pore volume, ordered pore channels and great potentials across a wide variety of fields such as catalysis, biomedicine, optics and so on.[117] The synthesis of MSNs is typically relying on co-operative self-assembly of supramolecular surfactant assemblies, acting as structure directing agents, and oligomeric silica species (**Figure I-21**). Furthermore, controlled nucleation and growth allows for tailoring of particle size (10–1000 nm). By tuning the synthesis conditions and/or by variation of the reactants elongated MSNs with tunable aspect ratios can be synthesized, providing yet another method for optimization of the particle technology for biological applications. Mesoporous nanoparticles are obtained after removal of the structure-directing agent leading to opening of the porosity. MSNs typically have a high specific

surface area (600–1000 $m^2.g^{-1}$) and a large pore volume (0.6–1.0 $cm^3.g^{-1}$) that allow for high levels of drug loadings to be achieved.

Typical pore dimensions of MSNs are 2–4 nm, but recent advances have made it possible to synthesize MSNs with pore dimensions as large as 50 nm, which are generally referred as large-pore MSNs (LPMSN).[118,119] Several synthetic methods have been proposed to enlarge the pore sizes of MSNs including post-enlargement by introducing a swelling agent (e.g., 1,3,5-trimethylbenzene) into the core part of micelles or using large molecular weight block copolymers (e.g., F127, P123, and PS-b-PEO) with long organic molecular chains as mesopore template. Although these approaches are effective in enlarging the pore sizes of MSNs, the obtained MSNs unfortunately usually suffer from the over large particle sizes (typically > 100–300 nm), irregular morphologies, and a severe tendency to aggregate.

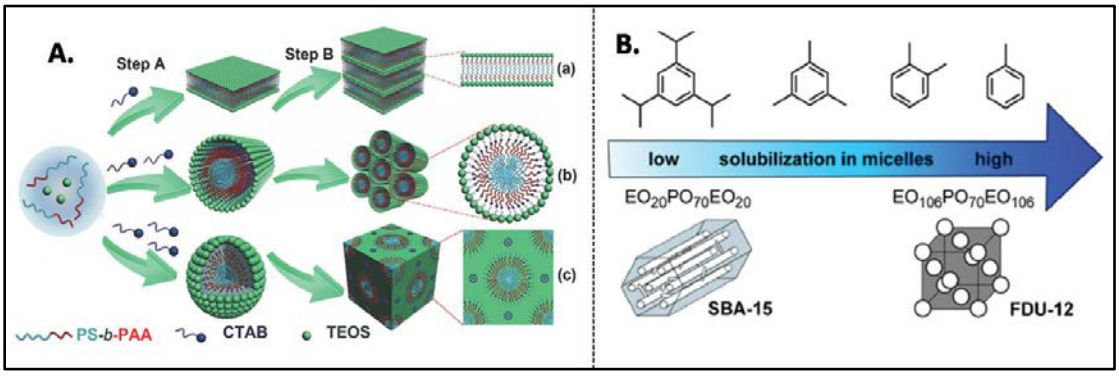

Figure I-21: Schematic illustration of the formation mechanism of ordered large-pore silica nanospheres. A. Pore structure tuning achieved by modifying surfactant concentration: (a) lamellar, (b) hexagonal and (c) cubic.[118] B. Pore expansion with benzene derivatives.[119]

For biomedical applications, precise control over particle size, shape, pore size, and pore geometry is very important. Totally, the pore size and its orientation are mainly determined by the nature of surfactant templates. The particle size and morphology can be controlled from sphere-, rod-, to wormlike structures by tailoring the molar ratio of silica precursors and surfactants, pH control using base catalysts, addition of co-solvents or organic swelling agents, and introduction of organoalkoxysilane precursors during the co-condensation reaction (**Figure I-22**).

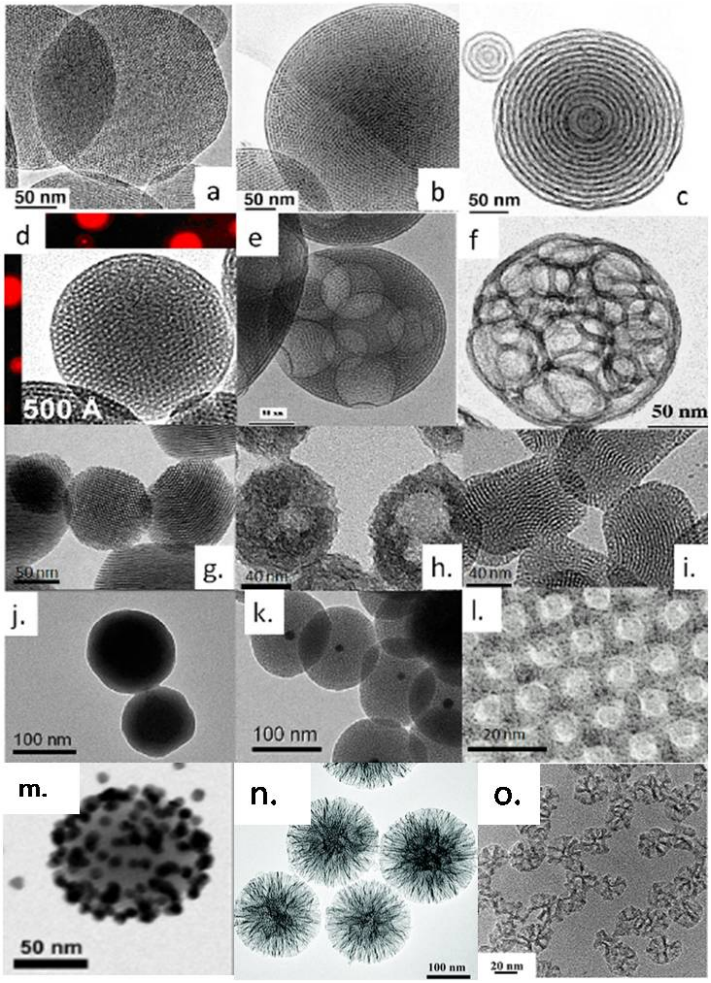

Figure I-22. Versatile structures of silica nanoparticles: a-l[92], m[93], n. dendrimer-like[120] and o. cone-shaped[121] pores silica nanoparticles

I-3-1-3. Surface functionalization

Three methods can be used to modify the external and, for MSN, internal surface of silica particles:

(i) Surface adsorption

The isoelectric point of amorphous silica is around pH 2-3, which means that in the absence of specific ion adsorption, the silica surface is negatively charged under biologically conditions. Therefore, electrostatic adsorption of positively-charged species is an attractive technique for simple surface modification of silica particles. This approach has been largely explored for the coating of SiNPs with biopolymers.[122] A major issue of this strategy is that the surface-sorbate interactions are highly dependent on the physico-chemical conditions of the medium (pH, ionic strength)

(ii) Post-grafting

The surface of silica particles exhibits 3-5 silanol groups per nm^2. This provides readily available moieties for surface modification via silanization reaction involving the condensation of trifunctional organosilanes ($SiR'(OR)_3$) in an organic solvent (**Figure I-23**). The organic group R' of the silane is usually selected so as to provide a reactive site for further interaction/binding with functional (bio)-molecules

To restrict or bias the deposition to the exterior surface of the MSN, the modification can be performed prior to extracting the templating agent. The templating agent can then be removed, and the protected, unreacted silanol groups in the pore interiors can be further modified.

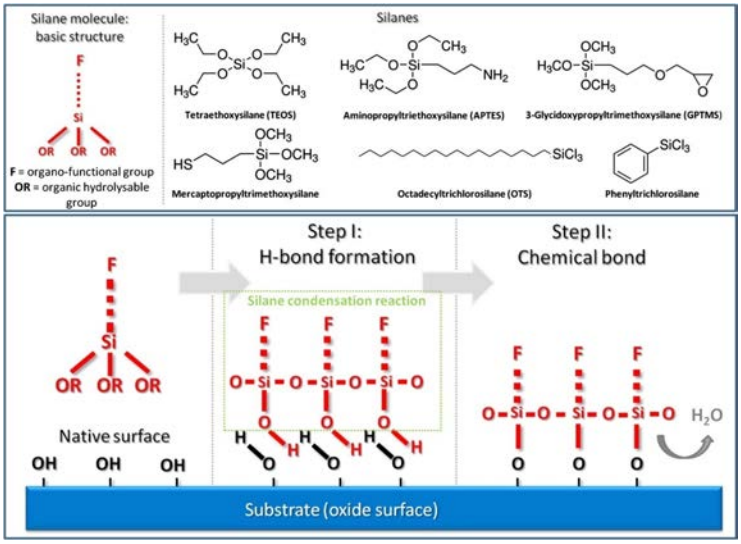

Figure 1-23: Silanization of ceramic surfaces. (A) Organo-functional silane molecule basic structure: an organic hydrolyzable group (OR) and an organo-functional group (F). (B) Chemical structures of mostly used silane precursors for surface functionalization of ceramic materials.[123]

(iii) Co-condensation

The co-condensation method relies on the formation of the particles from a mixture of hydrolyzed alkoxysilanes with organosilanes, resulting in an hybrid network. In this case, the amount of organic functions on the particle/pore surface should be the same as within the silica network. In order to favor the localization of these groups on the pore surface, it is possible to use amphiphilic organosilanes that serve as cosurfactants and are incorporated into

the templating micelle.[124] Here again, the principle is to introduce organic groups that may further interact with functional molecules.

I-3-2. Silica nanoparticles in drug delivery

I-3-2-1. Overview

There are two main methods by which drugs can be loaded in particles: encapsulation (i.e. incorporation of the drugs during particle synthesis) or adsorption/grafting on the external/internal surface. In the case of non-porous silica nanoparticles, only the two first methods are available. The microencapsulation method has been used successfully for the *in situ* incorporation of drugs.[125] Recent results from our group concerning antibiotics encapsulation within Stöber nanoparticles have shown that this approach allowed to achieve significant drug loadings but that the amount of incorporated drugs was highly dependent on their interactions with the silica precursors.[94]

When adsorption/grafting is considered, MSNs with high specific surface area are by far more advantageous. Consequently, the main research on drug delivery applications of silica nanoparticles are based on porous silica nanoparticles.[126] In 2001, Vallet-Regí firstly reported the application of MSNs as a drug delivery system for ibuprofen release.[127] Later, drugs of different hydrophobic/hydrophilic properties, molecule weights, and biomedical effects such as ibuprofen, doxorubicin, camptothecin, cisplatin have also been loaded in the mesopores to enhance high bioavailability or to balance efficacy and toxicity.[128] Moreover, MSNs systems allow the delivery of protein drugs, which are fragile structures of large molecular weight.[129] MSNs can well protect these biomacromolecules from premature degradation, thanks to their porous structure and stable nature.

More recently, Brinker and co-workers fused supported lipid bilayer onto MSNs to construct a “protocell”.[130] The organic-inorganic nanocomposites can synergistically combine the advantage of MSNs with extraordinarily high drug loading capacity, and liposome with enhanced lateral bilayer fluidity. They enable targeted delivery and controlled release of high concentrations of multicomponent cargos within the cytosol of cancer cells. The hybrid nanocomposites were used to deliver drugs and drug cocktails, siRNA cocktails and protein toxins. The killing effect of protocells on multidrug resistant cells of was 106 times higher over that of liposomes when delivering a cocktail of DOX, 5-fluorouracil and cisplatin. Nano-based drug co-delivery systems have been designed for targeting the ATP-dependent trans-

porters concurrently delivering chemo-drugs for increasing intracellular drug concentration. It is also possible to co-deliver cytotoxic drugs and genes targeting non-pump resistant related molecules including Bcl-2, transcription factor NF-κB and hypoxia-inducible factor alpha (HIF-1α).

"On-demand" release systems have also emerged as intelligent delivery platforms. They can respond to a range of endogenous or exogenous stimuli, including redox, pH or temperature, enzymes, competitive binding and photo-irradiation, thus more controllable release profiles can be achieved.[95] This kind of system requires stimuli-responsive caps over the mesopores, ranging from polymers (e.g. PEI, β-CD) to nanoparticles (e.g. Au, tiO_2)[96]. Moreover, multiple stimuli-responsive systems were also developed (one example is shown in **Figure I-24**). Nevertheless, very few studies of these systems are performed in vivo.

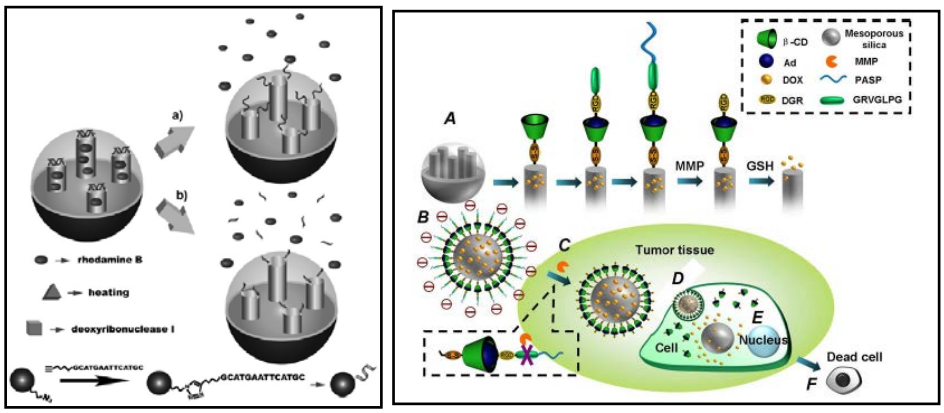

Figure I-24: (Left panel) Release of guest molecules from the pores of DNA-capped MSPs upon a) heating and b) treatment with DNase I.[95] (right panel) (A) Functionalization protocol of the MSN; (B) drugs loaded MEMSN under physiological condition; (C) removal of PASP protection layer in response to MMP at a tumor site; (D) cell uptake through RGD-mediated interaction; (E) glutathione-triggered drug release inside the cell; and (F) apoptosis of tumor cells.[131]

The current trend is this area is to incorporate more and more functions within a single particle to obtain multifunctional platforms. In particular, the association of magnetic, fluorescent and photothermal properties allows simultaneous bioimaging and drug delivery for nanotheranostics (**Figure I-25**).[132]

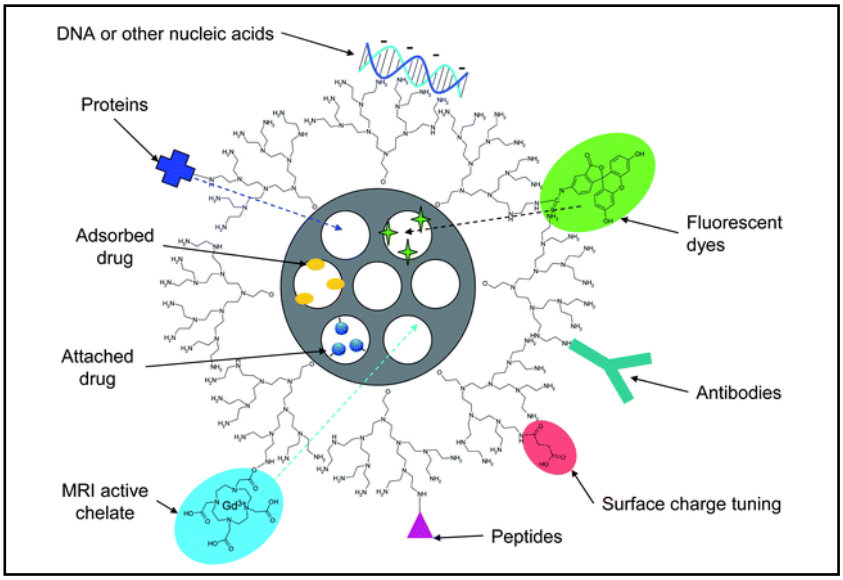

Figure I-25: Cargo loading possibilities of silica nanoparticles.[132]

I-3-2-2.Silica nanoparticles for gene delivery

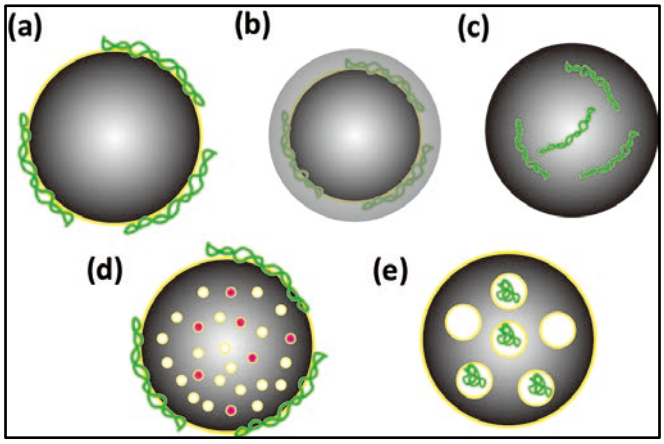

Figure I-26: The state-of-art of silica nanoparticle-based gene delivery system. Non-porous SiNP(a-c) and porous SiNP. Yellow layer represents fuctionalization of particle surface (d-e) and red dots indicate co-delivery with drugs (d).

Nonporous silica nanoparticles were used for the first time as inorganic nonviral gene delivery carriers by Kneuer et al., in 2000[97]. However, this study and most of the following ones focus on particle surface modification and adsorption of model plasmids by electrostatic interactions. Very recently, Paunescu et al., proposed a method for encapsulating DNA into amorphous silica spheres to mimic the protection of nucleic acids within ancient fossils[98]. DNA encapsulation was achieved by electrostatic adsorption and the following formation of

silica shell. This interesting work may not only be applied in medical field such as gene therapy and gene storage, but also in products tagging and tracing in the market.

Particle type	Gene location	Modification	Gene type	Results	
NSN	Outer surface	AH-APTES[a] AE-APTES[b]	pDNA	SiNP:DNA(w/w) of 30 was sufficient for complexation; absorbed DNA was protected from enzymatic degradation by DNase I.	101
	Interface between Core and shell	TMAPS[c]	DNA	Loaded DNA high temperature and radical oxygen species; DNA can be further extracted intact	98
MSN	Outer surface	APTES	pDNA	Optimal ratio for transfection is TEOS: APTES 1:10	102
	Pores (3 nm)	Outer surface with PEI cap and KALA peptide	short salmon DNA and siRNA	Successful downgrading of EGFP and VEGF in vitro; System loaded with VEGF-siRNA inhibited the growth of tumor over a month	103
	Outer surface	PEI, PEG and anti-HER2 antibody	siRNA	HER2 protein levels reduced by 60%; Multiple intravenous injections over 3 weeks significantly inhibits tumor growth	104
LPMSN	Pores (20 nm)	APTES, PLL	Oligo DNA-Cy3	PLL-modified MSN showed a higher reduction of cellular viability of cancer cells at 30%	105
	Pores (23 nm)	APTES	siRNA targeting EGFP and VEGF	GFP expression level decreased to 12% in vitro and 42% in vivo; tumor weight was 20% of control group	106
	Pores (20 nm)	PDMAEA	siRNA	Controlled release of siRNA mediated by self-catalyzed hydrolysis of PDMAEA	107
	Pores (inside 6 nm, opening ~10 nm)	PEI and TAT peptide	pDNA	Nucleus targeting, High transfection (36.5%) was obtained, substantially higher than that by LPMSN-PEI (13.5%) and MSN–PEI-TAT (4.97%)	121

[a] *N*-(2-aminoethyl)-3-aminopropyltrimethoxysilane(AE-APTES)

[b] *N*-(6-aminohexyl)-3-aminopropyltrimethoxysilane(AH-APTES)

[c] N-trimethoxysilylpropyl-N,N,Ntrimethylammoniumchloride (TMAPS)

Table I-5: Typical silica nanoparticles-based gene delivery systems

Mesoporous silica nanoparticles (MSNs) have extensive potential in gene delivery due to the large surface area, versatile functionality and excellent biocompatibility. However, the loading of DNAs or RNAs inside the mesopores of MSNs seems a challenging mission and in

most reports therapeutic genes were only adsorbed on the outer surface mainly due to poor availability of the mesopores. Therefore, optimization of loading conditions[99] and enlargement of mesopores were two most promising solutions to enhance the adsorption of genes inside the MSNs.

Considering the large size of nucleic acids, more promising gene delivery system will be SiNP with large pore size (10-50 nm), which will provide better protection for instable therapeutic genes and more functionality, such as targeting and stimuli-responsive moieties, for more intelligent delivery and release. Wu *et al.* has newly reported a LPMSN based targeting delivery system for transport of the therapeutic genes into the nucleus, where nucleic acids can be exactly and efficiently expressed.[100] High transfection was obtained due to the combined proton sponge effect of PEI grafted on the particle walls and the nuclear localization signal of TAT peptide on the surface. Small particle size (~30 nm) and large pore size (6-10 nm) was found to be responsible the readily uptaken and pDNA protection respectively. As summarized in **Table I-5**, positive charge generation is still the predominant strategy for the gene loading to SiNP.

I-3-3. Silica-collagen nanocomposites

I-3-3-1. Collagen

Collagens are the most abundant proteins in the mammalian body, accounting for 20–30% of the total protein. Collagens form a large family of triple helical molecules with about 28 different types described, with types I, II, III and IV being the most commons.[133] All collagens share the same triple-helical structure where three parallel polypeptides, α-chains, coil around each other forming a right handed triple helix chain (collagen type I as an example, **Figure I-27**). In animals these collagen triple helices are known as tropocollagen and its hierarchical organization into more complex structures generates the fibers and networks in tissues such as bone, skin and tendons (**Figure I-28**). The primary functions of type I collagen are to provide mechanical support and to control cell adhesion and migration.

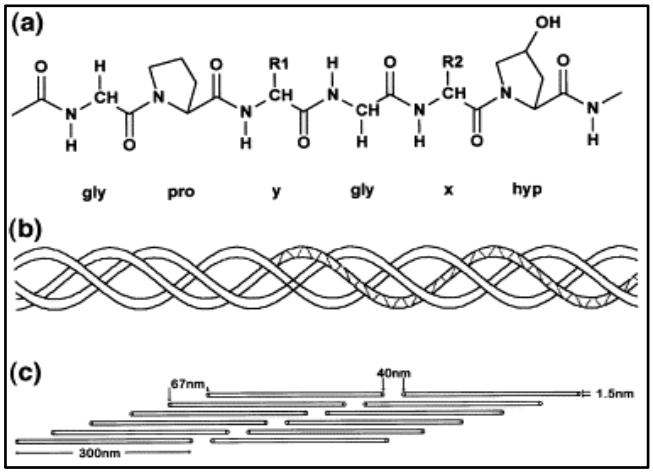

Figure 1-27: Chemical structure of collagen type I. (a) Primary amino acid sequence, (b) secondary left-handed helix and tertiary right-handed triple-helix structure and (c) staggered quaternary structure.[134]

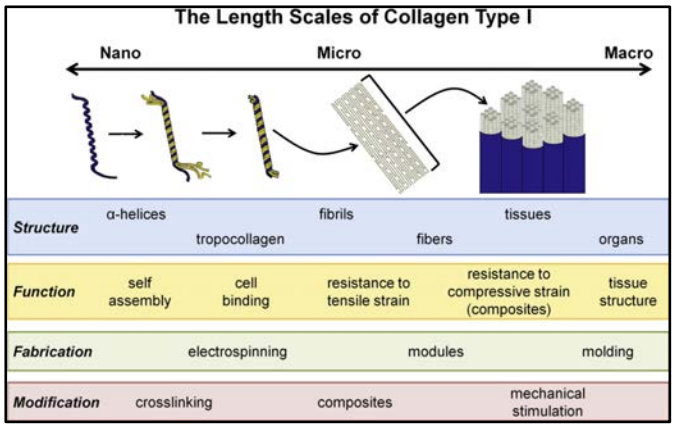

Figure I-28: Hierarchical structure of collagen type I leads to specific functions and characteristics across length scales.[109]

The abundance, non-antigenicity, biodegradability, biocompatibility and plasticity make collagen a promising biopolymer for medical applications. Collagen scaffolds have been extensively used for soft tissue repair, vascular and dermal tissue engineering, bone repair and as a carrier for the delivery of drugs and biologically active molecules.[135] Many of them are commercially available in diverse forms that include gels, pads, particles, pastes, powders, sheets or solutions.

Thanks to the above-mentioned characteristics, collagen is frequently used to prepare wound dressings. However, collagen-based materials suffer from uncontrolled degradation and low mechanical strength, which necessitate the chemical and physical modifications of the collagen. Composite collagen hydrogels obtained from introducing other natural (e.g. elastin, hyaluronan) or synthetic (e.g. PEG) polymers[109] and particulates (e.g. calcium phosphate particles, silica nanoparticles) have been widely used to add strength and functionality to the system. Another efficient approach is through chemical (e.g. carbodiimides, glutaraldehde) and physical (e.g. UV light, gamma radiation) modification.

Raftery et al. studied collagen-based scaffolds for localized gene delivery, where chitosan-DNA was loaded by surface adsorption.[44] The scaffolds used in the study include a collagen scaffold and collagen-hydroxyapatite (CHA) scaffold for bone repair, and a collagen-hyaluronicacid (CHyA) with properties optimized for cartilage regeneration. Sustained gene expression from MSCs seeded on the scaffolds was maintained for up to 28 days and interestingly the composition of the scaffold had an effect on transfection efficiency. These results demonstrate that by simply varying the scaffold composition and the gene chosen, the system has potential for a myriad of therapeutic applications.

I-3-3-2. Silica-collagen nanocomposites

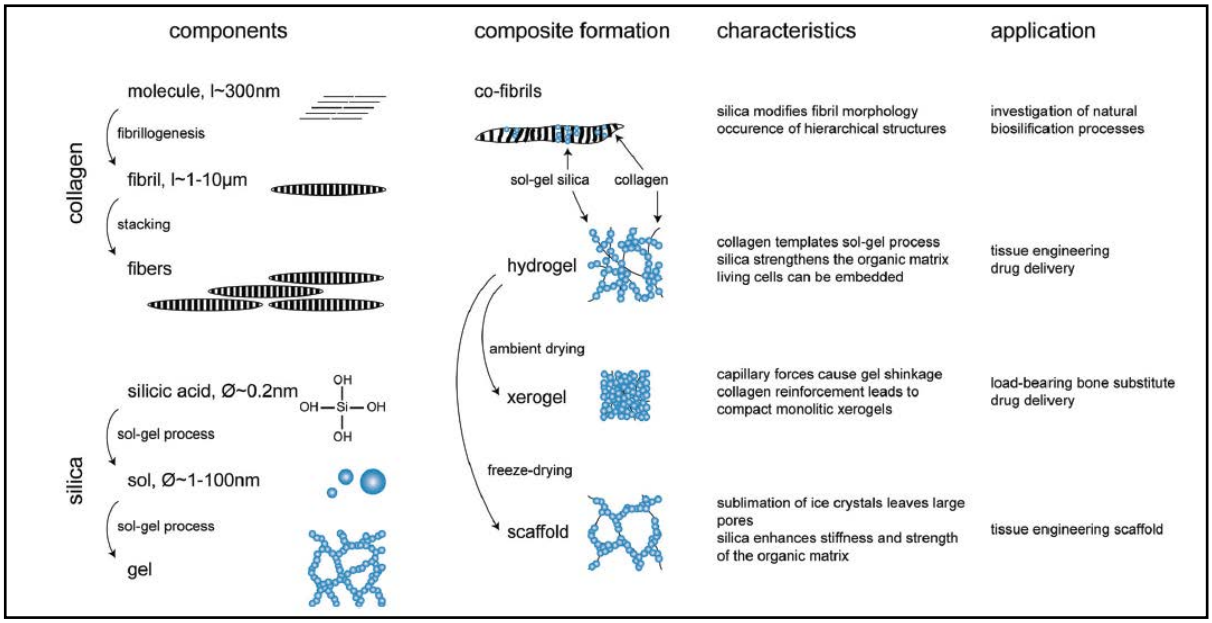

Figure 1-29: Overview of silica–collagen materials. Starting components, conditions of composite formation, main characteristics and potential applications.[110]

The ease to prepare collagen hydrogel facilitates the incorporation of other ingredients (e.g. cell culture medium, bioactive proteins, drugs), which makes collagen-based materials appealing candidates for bioactive wound dressing fabrication. However, fast release of biomolecules and limited mechanical strength remains drawbacks of this system.[136] In this context, it has been suggested that the combination of collagen hydrogels with silica could improve their performance.[137] Various silica species have been reported for silicification of soluble collagen, fibrils, fibers, films, gels or scaffolds for different medical applications (**Figure 1-29**).[110] Increasing studies are being carried out on silica-collagen hydrogels for tissue engineering, including nerve regeneration[111], bone repair[112], artificial cornea[113] and wound healing[114]. Preliminary biocompatibility studies by subcutaneous implantation in rats showed the absence of significant inflammation, infiltration of fibroblast cells and initiation of vascularization.[138]

Compared with other silicification approaches, the physical incorporation of silica nanoparticles within collagen hydrogel should allow to take full advantage of their drug delivery potential. By tuning particle size, surface chemistry and porosity, it may be possible to achieve controlled release kinetics. Whether this strategy can be applied to gene delivery systems is the central question that has motivated this work.

REFERENCES

1. Yin, H.; Kanasty, R. L.; Eltoukhy, A. A.; Vegas, A. J.; Dorkin, J. R.; Anderson, D. G., Non-viral vectors for gene-based therapy. *Nat Rev Genet* **2014,** *15* (8), 541-555.

2. Shier, D.; Butler, J.; Lewis, R., *Hole's Human Anatomy*. McGraw-Hill: 1996.

3. MacNeil, S., Progress and opportunities for tissue-engineered skin. *Nature* **2007,** *445* (7130), 874-880.

4. Hynes, R. O., The extracellular matrix: not just pretty fibrils. *Science* **2009,** *326* (5957), 1216-1219.

5. Arwert, E. N.; Hoste, E.; Watt, F. M., Epithelial stem cells, wound healing and cancer. *Nat Rev Cancer* **2012,** *12* (3), 170-180.

6. Falanga, V., Wound healing and its impairment in the diabetic foot. *The Lancet* **2005,** *366* (9498), 1736-1743.

7. Barrientos, S.; Stojadinovic, O.; Golinko, M. S.; Brem, H.; Tomic‐Canic, M., Growth factors and cytokines in wound healing. *Wound Repair Regen.* **2008,** *16* (5), 585-601.

8. Clark, R. A.; Ghosh, K.; Tonnesen, M. G., Tissue engineering for cutaneous wounds. *J. Invest. Dermatol.* **2007,** *127* (5), 1018-1029.

9. Baltzis, D.; Eleftheriadou, I.; Veves, A., Pathogenesis and Treatment of Impaired Wound Healing in Diabetes Mellitus: New Insights. *Adv. Ther.* **2014,** *31* (8), 817-836.

10. James, G. A.; Swogger, E.; Wolcott, R.; Pulcini, E. d.; Secor, P.; Sestrich, J.; Costerton, J. W.; Stewart, P. S., Biofilms in chronic wounds. *Wound Repair Regen.* **2008,** *16* (1), 37-44.

11. Koh, T. J.; DiPietro, L. A., Inflammation and wound healing: the role of the macrophage. *Expert reviews in molecular medicine* **2011,** *13*, e23.

12. Mosser, D. M.; Edwards, J. P., Exploring the full spectrum of macrophage activation. *Nat Rev Immunol* **2008,** *8* (12), 958-969.

13. Bonecchi, R.; Galliera, E.; Borroni, E. M.; Corsi, M. M.; Locati, M.; Mantovani, A., Chemokines and chemokine receptors: an overview. *Frontiers in bioscience (Landmark edition)* **2008,** *14*, 540-551.

14. Howes, A.; Stimpson, P.; Redford, P.; Gabrysova, L.; O'Garra, A., Interleukin-10: Cytokines in Anti-inflammation and Tolerance. In *Cytokine Frontiers*, Yoshimoto, T.; Yoshimoto, T., Eds. Springer Japan: 2014; pp 327-352.

15. Saraiva, M.; O'Garra, A., The regulation of IL-10 production by immune cells. *Nature Reviews Immunology* **2010,** *10* (3), 170-181.

16. Potas, J. R.; Haque, F.; Maclean, F. L.; Nisbet, D. R., Interleukin-10 conjugated electrospun polycaprolactone (PCL) nanofibre scaffolds for promoting alternatively activated (M2) macrophages around the peripheral nerve in vivo. *J. Immunol. Methods* **2015,** *420* (0), 38-49.

17. Jain, S.; Tran, T.-H.; Amiji, M., Macrophage repolarization with targeted alginate nanoparticles containing IL-10 plasmid DNA for the treatment of experimental arthritis. *Biomaterials* **2015,** *61*, 162-177.

18. Gower, R. M.; Boehler, R. M.; Azarin, S. M.; Ricci, C. F.; Leonard, J. N.; Shea, L. D., Modulation of leukocyte infiltration and phenotype in microporous tissue engineering scaffolds via vector induced IL-10 expression. *Biomaterials* **2014,** *35* (6), 2024-2031.

19. Futrega, K.; King, M.; Lott, W. B.; Doran, M. R., Treating the whole not the hole: necessary coupling of technologies for diabetic foot ulcer treatment. *Trends Mol. Med.* **2014,** *20* (3), 137-142.

20. Barrientos, S.; Brem, H.; Stojadinovic, O.; Tomic-Canic, M., Clinical application of growth factors and cytokines in wound healing. *Wound Repair Regen.* **2014,** *22* (5), 569-578.

21. Da Costa, R. M.; Jesus, F. M. R.; Aniceto, C.; Mendes, M., Randomized, double‐blind, placebo‐controlled, dose‐ranging study of granulocyte‐macrophage colony stimulating factor in patients with chronic venous leg ulcers. *Wound Repair Regen.* **1999,** *7* (1), 17-25.

22. Cruciani, M.; Lipsky, B. A.; Mengoli, C.; de Lalla, F., Granulocyte‐colony stimulating factors as adjunctive therapy for diabetic foot infections. *The Cochrane Library* **2013**.

23. Sun, D.-P.; Yeh, C.-H.; So, E.; Wang, L.-Y.; Wei, T.-S.; Chang, M.-S.; Hsing, C.-H., Interleukin (IL)-19 promoted skin wound healing by increasing fibroblast keratinocyte growth factor expression. *Cytokine* **2013,** *62* (3), 360-368.

24. Smiell, J. M.; Wieman, T. J.; Steed, D. L.; Perry, B. H.; Sampson, A. R.; Schwab, B. H., Efficacy and safety of becaplermin (recombinant human platelet‐derived growth factor‐BB) in patients with nonhealing, lower extremity diabetic ulcers: a combined analysis of four randomized studies. *Wound Repair Regen.* **1999,** *7* (5), 335-346.

25. Lipiäinen, T.; Peltoniemi, M.; Sarkhel, S.; Yrjönen, T.; Vuorela, H.; Urtti, A.; Juppo, A., Formulation and Stability of Cytokine Therapeutics. *J. Pharm. Sci.* **2015,** *104* (2), 307-326.

26. Cheng, F.; Gao, J.; Wang, L.; Hu, X. Y., Composite chitosan/poly(ethylene oxide) electrospun nanofibrous mats as novel wound dressing matrixes for the controlled release of drugs. *J. Appl. Polym. Sci.* **2015,** *132* (24).

27. Sarhan, W. A.; Azzazy, H. M. E., High concentration honey chitosan electrospun nanofibers: Biocompatibility and antibacterial effects. *Carbohydr. Polym.* **2015,** *122*, 135-143.

28. Wang, W.; Lin, S.; Xiao, Y.; Huang, Y.; Tan, Y.; Cai, L.; Li, X., Acceleration of diabetic wound healing with chitosan-crosslinked collagen sponge containing recombinant human acidic fibroblast growth factor in healing-impaired STZ diabetic rats. *Life Sci.* **2008,** *82* (3), 190-204.

29. Lee, Y.-H.; Chang, J.-J.; Yang, M.-C.; Chien, C.-T.; Lai, W.-F., Acceleration of wound healing in diabetic rats by layered hydrogel dressing. *Carbohydr. Polym.* **2012,** *88* (3), 809-819.

30. Baier, G.; Cavallaro, A.; Vasilev, K.; Mailander, V.; Musyanovych, A.; Landfester, K., Enzyme Responsive Hyaluronic Acid Nanocapsules Containing Polyhexanide and Their Exposure to Bacteria To Prevent Infection. *Biomacromolecules* **2013,** *14* (4), 1103-1112.

31. You, H. J.; Han, S. K.; Rhie, J. W., Randomised controlled clinical trial for autologous fibroblast-hyaluronic acid complex in treating diabetic foot ulcers. *J. Wound Care* **2014,** *23* (11), 521-530.

32. Xu, S. S.; Li, J. X.; He, A. H.; Liu, W. W.; Jiang, X. Y.; Zheng, J. F.; Han, C. C.; Hsiao, B. S.; Chu, B.; Fang, D. F., Chemical crosslinking and biophysical properties of electrospun hyaluronic acid based ultra-thin fibrous membranes. *Polymer* **2009,** *50* (15), 3762-3769.

33. Matsumoto, Y.; Kuroyanagi, Y., Development of a Wound Dressing Composed of Hyaluronic Acid Sponge Containing Arginine and Epidermal Growth Factor. *Journal of Biomaterials Science-Polymer Edition* **2010,** *21* (6-7), 715-726.

34. Abbruzzese, L.; Rizzo, L.; Fanelli, G.; Tedeschi, A.; Scatena, A.; Goretti, C.; Macchiarini, S.; Piaggesi, A., Effectiveness and safety of a novel gel dressing in the management of neuropathic leg ulcers in diabetic patients: a prospective double-blind randomized trial. *The international journal of lower extremity wounds* **2009,** *8* (3), 134-140.

35. Jung, R.; Kim, Y.; Kim, H.-S.; Jin, H.-J., Antimicrobial properties of hydrated cellulose membranes with silver nanoparticles. *J. Biomater. Sci. Polym. Ed.* **2009,** *20* (3), 311-324.

36. LAZARO-MARTINEZ, J. L.; ARAGON-SANCHEZ, F. J.; García-Morales, E.; BENEIT-MONTESINOS, J. V.; González-Jurado, M., A retrospective analysis of the cost-effectiveness of a collagen/oxidized regenerated cellulose dressing in the treatment of neuropathic diabetic foot ulcers. *Ostomy wound management* **2010,** *56* (11A), 4-8.

37. Serafica, G.; Mormino, R.; Oster, G. A.; Lentz, K. E.; Koehler, K., Microbial cellulose wound dressing for treating chronic wounds. Google Patents: 2010.

38. Straccia, M. C.; d'Ayala, G. G.; Romano, I.; Laurienzo, P., Novel zinc alginate hydrogels prepared by internal setting method with intrinsic antibacterial activity. *Carbohydr. Polym.* **2015,** *125*, 103-112.

39. Straccia, M. C.; d'Ayala, G. G.; Romano, I.; Oliva, A.; Laurienzo, P., Alginate hydrogels coated with chitosan for wound dressing. *Mar. Drugs* **2015,** *13* (5), 2890-908.

40. Shaw, J.; Hughes, C.; Lagan, K.; Stevenson, M.; Irwin, C.; Bell, P., The effect of topical phenytoin on healing in diabetic foot ulcers: a randomized controlled trial1. *Diabet. Med.* **2011,** *28* (10), 1154-1157.

41. Kawai, K.; Suzuki, S.; Tabata, Y.; Nishimura, Y., Accelerated wound healing through the incorporation of basic fibroblast growth factor-impregnated gelatin microspheres into artificial dermis using a pressure-induced decubitus ulcer model in genetically diabetic mice. *Br. J. Plast. Surg.* **2005,** *58* (8), 1115-1123.

42. Norouzi, M.; Shabani, I.; Ahvaz, H. H.; Soleimani, M., PLGA/gelatin hybrid nanofibrous scaffolds encapsulating EGF for skin regeneration. *Journal of Biomedical Materials Research Part A* **2015,** *103* (7), 2225-2235.

43. Helary, C.; Abed, A.; Mosser, G.; Louedec, L.; Letourneur, D.; Coradin, T.; Giraud-Guille, M. M.; Meddahi-Pellé, A., Evaluation of dense collagen matrices as medicated wound dressing for the treatment of cutaneous chronic wounds. *Biomaterials Science* **2015,** *3* (2), 373-382.

44. Raftery, R. M.; Tierney, E. G.; Curtin, C. M.; Cryan, S.-A.; O'Brien, F. J., Development of a gene-activated scaffold platform for tissue engineering applications using chitosan-pDNA nanoparticles on collagen-based scaffolds. *Journal of controlled release : official journal of the Controlled Release Society* **2015,** *210*, 84-94.

45. Arul, V.; Masilamoni, J.; Jesudason, E.; Jaji, P.; Inayathullah, M.; John, D. D.; Vignesh, S.; Jayakumar, R., Glucose oxidase incorporated collagen matrices for dermal wound repair in diabetic rat models: a biochemical study. *J. Biomater. Appl.* **2011**, 0885328210390402.

46. Kanda, N.; Morimoto, N.; Ayvazyan, A. A.; Takemoto, S.; Kawai, K.; Nakamura, Y.; Sakamoto, Y.; Taira, T.; Suzuki, S., Evaluation of a novel collagen–gelatin scaffold for achieving the sustained release of basic fibroblast growth factor in a diabetic mouse model. *Journal of tissue engineering and regenerative medicine* **2014,** *8* (1), 29-40.

47. Losi, P.; Briganti, E.; Errico, C.; Lisella, A.; Sanguinetti, E.; Chiellini, F.; Soldani, G., Fibrin-based scaffold incorporating VEGF- and bFGF-loaded nanoparticles stimulates wound healing in diabetic mice. *Acta Biomater.* **2013,** *9* (8), 7814-7821.

48. Seetharaman, S.; Natesan, S.; Stowers, R. S.; Mullens, C.; Baer, D. G.; Suggs, L. J.; Christy, R. J., A PEGylated fibrin-based wound dressing with antimicrobial and angiogenic activity. *Acta Biomater.* **2011,** *7* (7), 2787-2796.

49. Pedroso, D.; Tellechea, A.; Moura, L.; Fidalgo-Carvalho, I.; Duarte, J.; Carvalho, E.; Ferreira, L., Improved survival, vascular differentiation and wound healing potential of stem cells co-cultured with endothelial cells. *PloS one* **2011,** *6* (1), e16114.

50. Inpanya, P.; Faikrua, A.; Ounaroon, A.; Sittichokechaiwut, A.; Viyoch, J., Effects of the blended fibroin/aloe gel film on wound healing in streptozotocin-induced diabetic rats. *Biomedical Materials* **2012,** *7* (3), 035008.

51. Jeong, L.; Kim, M. H.; Jung, J.-Y.; Min, B. M.; Park, W. H., Effect of silk fibroin nanofibers containing silver sulfadiazine on wound healing. *International Journal of Nanomedicine* **2014,** *9*, 5277-5287.

52. Frampton, J. P.; Lai, D.; Lounds, M.; Chung, K.; Kim, J.; Eld, J. F. M.; Takayama, S., Elongation of Fibers from Highly Viscous Dextran Solutions Enables Fabrication of Rapidly Dissolving Drug Carrying Fabrics. *Advanced Healthcare Materials* **2015,** *4* (2), 313-319.

53. Sun, G.; Zhang, X.; Shen, Y.-I.; Sebastian, R.; Dickinson, L. E.; Fox-Talbot, K.; Reinblatt, M.; Steenbergen, C.; Harmon, J. W.; Gerecht, S., Dextran hydrogel scaffolds enhance angiogenic responses and promote complete skin regeneration during burn wound healing. *Proceedings of the National Academy of Sciences* **2011,** *108* (52), 20976-20981.

54. Anh, T. T. H.; Xing, M.; Le, D. H. T.; Sugawara-Narutaki, A.; Fong, E., Elastin-based silver-binding proteins with antibacterial capabilities. *Nanomedicine* **2013,** *8* (4), 567-575.

55. Koria, P.; Yagi, H.; Kitagawa, Y.; Megeed, Z.; Nahmias, Y.; Sheridan, R.; Yarmush, M. L., Self-assembling elastin-like peptides growth factor chimeric nanoparticles for the treatment of chronic wounds. *Proceedings of the National Academy of Sciences* **2011,** *108* (3), 1034-1039.

56. Vasconcelos, A.; Gomes, A. C.; Cavaco-Paulo, A., Novel silk fibroin/elastin wound dressings. *Acta Biomater.* **2012,** *8* (8), 3049-3060.

57. Marcilli, R. H.; de Oliveira, M. G., Nitric oxide-releasing poly (vinyl alcohol) film for increasing dermal vasodilation. *Colloids Surf. B. Biointerfaces* **2014,** *116*, 643-651.

58. Manju, S.; Antony, M.; Sreenivasan, K., Synthesis and evaluation of a hydrogel that binds glucose and releases ciprofloxacin. *Journal of materials science* **2010,** *45* (15), 4006-4012.

59. Choi, J. S.; Leong, K. W.; Yoo, H. S., In vivo wound healing of diabetic ulcers using electrospun nanofibers immobilized with human epidermal growth factor (EGF). *Biomaterials* **2008,** *29* (5), 587-596.

60. Choi, J. S.; Choi, S. H.; Yoo, H. S., Coaxial electrospun nanofibers for treatment of diabetic ulcers with binary release of multiple growth factors. *J. Mater. Chem.* **2011,** *21* (14), 5258-5267.

61. Huang, Z.; Lu, M.; Zhu, G.; Gao, H.; Xie, L.; Zhang, X.; Ye, C.; Wang, Y.; Sun, C.; Li, X., Acceleration of diabetic‐wound healing with PEGylated rhaFGF in healing‐impaired streptozocin diabetic rats. *Wound Repair Regen.* **2011,** *19* (5), 633-644.

62. Yang, Y.; Xia, T.; Chen, F.; Wei, W.; Liu, C.; He, S.; Li, X., Electrospun fibers with plasmid bFGF polyplex loadings promote skin wound healing in diabetic rats. *Mol. Pharm.* **2011,** *9* (1), 48-58.

63. Rasekh, M.; Karavasili, C.; Soong, Y. L.; Bouropoulos, N.; Morris, M.; Armitage, D.; Li, X.; Fatouros, D. G.; Ahmad, Z., Electrospun PVP-indomethacin constituents for transdermal dressings and drug delivery devices. *Int. J. Pharm.* **2014,** *473* (1-2), 95-104.

64. Li, Y.; Lee, P. I., Controlled nitric oxide delivery platform based on S-nitrosothiol conjugated interpolymer complexes for diabetic wound healing. *Mol. Pharm.* **2010,** *7* (1), 254-266.

65. Halpenny, G. M.; Steinhardt, R. C.; Okialda, K. A.; Mascharak, P. K., Characterization of pHEMA-based hydrogels that exhibit light-induced bactericidal effect via release of NO. *Journal of Materials Science-Materials in Medicine* **2009,** *20* (11), 2353-2360.

66. Wu, J. Y.; Li, C. W.; Tsai, C. H.; Chou, C. W.; Chen, D. R.; Wang, G. J., Synthesis of antibacterial TiO2/PLGA composite biofilms. *Nanomedicine-Nanotechnology Biology and Medicine* **2014,** *10* (5), 1097-1107.

67. Merrell, J. G.; McLaughlin, S. W.; Tie, L.; Laurencin, C. T.; Chen, A. F.; Nair, L. S., Curcumin‐loaded poly (ε‐caprolactone) nanofibres: Diabetic wound dressing with anti‐oxidant and anti‐inflammatory properties. *Clin. Exp. Pharmacol. Physiol.* **2009,** *36* (12), 1149-1156.

68. Chu, Y.; Yu, D.; Wang, P.; Xu, J.; Li, D.; Ding, M., Nanotechnology promotes the full‐thickness diabetic wound healing effect of recombinant human epidermal growth factor in diabetic rats. *Wound Repair Regen.* **2010,** *18* (5), 499-505.

69. Yang, Y.; Xia, T.; Zhi, W.; Wei, L.; Weng, J.; Zhang, C.; Li, X., Promotion of skin regeneration in diabetic rats by electrospun core-sheath fibers loaded with basic fibroblast growth factor. *Biomaterials* **2011,** *32* (18), 4243-4254.

70. Cheng, A. Y.; García, A. J., Engineering the matrix microenvironment for cell delivery and engraftment for tissue repair. *Curr. Opin. Biotechnol.* **2013,** *24* (5), 864-871.

71. Wirth, T.; Parker, N.; Ylä-Herttuala, S., History of gene therapy. *Gene* **2013,** *525* (2), 162-169.

72. Sheridan, C., Gene therapy finds its niche. *Nat. Biotechnol.* **2011,** *29* (2), 121-128.

73. Giacca, M.; Zacchigna, S., Virus-mediated gene delivery for human gene therapy. *J. Controlled Release* **2012,** *161* (2), 377-388.

74. Waehler, R.; Russell, S. J.; Curiel, D. T., Engineering targeted viral vectors for gene therapy. *Nature Reviews Genetics* **2007,** *8* (8), 573-587.

75. Huang, S.; Kamihira, M., Development of hybrid viral vectors for gene therapy. *Biotechnol. Adv.* **2013,** *31* (2), 208-223.

76. Munch, R. C.; Muth, A.; Muik, A.; Friedel, T.; Schmatz, J.; Dreier, B.; Trkola, A.; Pluckthun, A.; Buning, H.; Buchholz, C. J., Off-target-free gene delivery by affinity-purified receptor-targeted viral vectors. *Nature Communications* **2015,** *6*.

77. Yang, Z.; Jiang, Z. Z.; Cao, Z.; Zhang, C.; Gao, D.; Luo, X. G.; Zhang, X. F.; Luo, H. Y.; Jiang, Q.; Liu, J., Multifunctional non-viral gene vectors with enhanced stability, improved cellular and nuclear uptake capability, and increased transfection efficiency. *Nanoscale* **2014,** *6* (17), 10193-10206.

78. Aied, A.; Greiser, U.; Pandit, A.; Wang, W., Polymer gene delivery: overcoming the obstacles. *Drug Discov. Today* **2013,** *18* (21–22), 1090-1098.

79. Kakimoto, S.; Tanabe, T.; Azuma, H.; Nagasaki, T., Enhanced internalization and endosomal escape of dual-functionalized poly (ethyleneimine) s polyplex with diphtheria toxin T and R domains. *Biomed. Pharmacother.* **2010,** *64* (4), 296-301.

80. Morille, M.; Passirani, C.; Vonarbourg, A.; Clavreul, A.; Benoit, J.-P., Progress in developing cationic vectors for non-viral systemic gene therapy against cancer. *Biomaterials* **2008,** *29* (24), 3477-3496.

81. Felgner, P. L.; Gadek, T. R.; Holm, M.; Roman, R.; Chan, H. W.; Wenz, M.; Northrop, J. P.; Ringold, G. M.; Danielsen, M., Lipofection: a highly efficient, lipid-mediated

DNA-transfection procedure. *Proceedings of the National Academy of Sciences* **1987,** *84* (21), 7413-7417.

82. Lee, S.; Koo, H.; Na, J. H.; Lee, K. E.; Jeong, S. Y.; Choi, K.; Kim, S. H.; Kwon, I. C.; Kim, K., DNA Amplification in Neutral Liposomes for Safe and Efficient Gene Delivery. *ACS Nano* **2014,** *8* (5), 4257-4267.

83. Boussif, O.; Lezoualch, F.; Zanta, M. A.; Mergny, M. D.; Scherman, D.; Demeneix, B.; Behr, J. P., A Versatile Vector for Gene and Oligonucleotide Transfer into Cells in Culture and in-Vivo - Polyethylenimine. *Proc. Natl. Acad. Sci. U. S. A.* **1995,** *92* (16), 7297-7301.

84. Lungwitz, U.; Breunig, M.; Blunk, T.; Göpferich, A., Polyethylenimine-based non-viral gene delivery systems. *Eur. J. Pharm. Biopharm.* **2005,** *60* (2), 247-266.

85. Kesharwani, P.; Iyer, A. K., Recent advances in dendrimer-based nanovectors for tumor-targeted drug and gene delivery. *Drug Discov. Today* **2015,** *20* (5), 536-547.

86. Miyata, K.; Nishiyama, N.; Kataoka, K., Rational design of smart supramolecular assemblies for gene delivery: chemical challenges in the creation of artificial viruses. *Chem. Soc. Rev.* **2012,** *41* (7), 2562-2574.

87. Nitta, S. K.; Numata, K., Biopolymer-based nanoparticles for drug/gene delivery and tissue engineering. *International journal of molecular sciences* **2013,** *14* (1), 1629-1654.

88. Xu, J.; Ganesh, S.; Amiji, M., Non-condensing polymeric nanoparticles for targeted gene and siRNA delivery. *Int. J. Pharm.* **2012,** *427* (1), 21-34.

89. Guo, X.; Huang, L., Recent Advances in Nonviral Vectors for Gene Delivery. *Acc. Chem. Res.* **2011,** *45* (7), 971-979.

90. Cam, C.; Segura, T., Matrix-based gene delivery for tissue repair. *Curr. Opin. Biotechnol.* **2013,** *24* (5), 855-863.

91. Hortensius, R. A.; Becraft, J. R.; Pack, D. W.; Harley, B. A. C., The effect of glycosaminoglycan content on polyethylenimine-based gene delivery within three-dimensional collagen-GAG scaffolds. *Biomaterials Science* **2015,** *3* (4), 645-654.

92. Tarn, D.; Ashley, C. E.; Xue, M.; Carnes, E. C.; Zink, J. I.; Brinker, C. J., Mesoporous Silica Nanoparticle Nanocarriers: Biofunctionality and Biocompatibility. *Acc. Chem. Res.* **2013,** *46* (3), 792-801.

93. Cano, M.; de la Cueva-Mendez, G., Self-assembly of a superparamagnetic raspberry-like silica/iron oxide nanocomposite using epoxy-amine coupling chemistry. *Chem. Commun.* **2015,** *51* (17), 3620-3622.

94. Solange Alvarez, G.; Helary, C.; Mathilde Mebert, A.; Wang, X.; Coradin, T.; Federico Desimone, M., Antibiotic-loaded silica nanoparticle-collagen composite hydrogels with prolonged antimicrobial activity for wound infection prevention. *Journal of Materials Chemistry B* **2014,** *2* (29), 4660-4670.

95. Chen, C.; Geng, J.; Pu, F.; Yang, X.; Ren, J.; Qu, X., Polyvalent Nucleic Acid/Mesoporous Silica Nanoparticle Conjugates: Dual Stimuli‐Responsive Vehicles for Intracellular Drug Delivery. *Angew. Chem. Int. Ed.* **2011,** *50* (4), 882-886.

96. Lee, D.; Hong, J. W.; Park, C.; Lee, H.; Lee, J. E.; Hyeon, T.; Paik, S. R., Ca2+-Dependent Intracellular Drug Delivery System Developed with "Raspberry-Type" Particles-on-a-Particle Comprising Mesoporous Silica Core and α-Synuclein-Coated Gold Nanoparticles. *ACS Nano* **2014,** *8* (9), 8887-8895.

97. Kneuer, C.; Sameti, M.; Bakowsky, U.; Schiestel, T.; Schirra, H.; Schmidt, H.; Lehr, C.-M., A Nonviral DNA Delivery System Based on Surface Modified Silica-Nanoparticles Can Efficiently Transfect Cells in Vitro. *Bioconjug. Chem.* **2000,** *11* (6), 926-932.

98. Paunescu, D.; Fuhrer, R.; Grass, R. N., Protection and Deprotection of DNA—High-Temperature Stability of Nucleic Acid Barcodes for Polymer Labeling. *Angew. Chem. Int. Ed.* **2013,** *52* (15), 4269-4272.

99. Li, X.; Xie, Q. R.; Zhang, J.; Xia, W.; Gu, H., The packaging of siRNA within the mesoporous structure of silica nanoparticles. *Biomaterials* **2011,** *32* (35), 9546-9556.

100. Wu, M.; Meng, Q.; Chen, Y.; Du, Y.; Zhang, L.; Li, Y.; Zhang, L.; Shi, J., Large-Pore Ultrasmall Mesoporous Organosilica Nanoparticles: Micelle/Precursor Co-templating Assembly and Nuclear-Targeted Gene Delivery. *Adv. Mater.* **2015,** *27* (2), 215-222.

101. Kneuer, C.; Sameti, M.; Haltner, E. G.; Schiestel, T.; Schirra, H.; Schmidt, H.; Lehr, C.-M., Silica nanoparticles modified with aminosilanes as carriers for plasmid DNA. *Int. J. Pharm.* **2000,** *196* (2), 257-261.

102. Yang, H.; Zheng, K.; Zhang, Z.; Shi, W.; Jing, S.; Wang, L.; Zheng, W.; Zhao, D.; Xu, J.; Zhang, P., Adsorption and protection of plasmid DNA on mesoporous silica nanoparticles modified with various amounts of organosilane. *J. Colloid Interface Sci.* **2012,** *369* (1), 317-322.

103. Li, X.; Chen, Y.; Wang, M.; Ma, Y.; Xia, W.; Gu, H., A mesoporous silica nanoparticle – PEI – Fusogenic peptide system for siRNA delivery in cancer therapy. *Biomaterials* **2013,** *34* (4), 1391-1401.

104. Ngamcherdtrakul, W.; Morry, J.; Gu, S.; Castro, D. J.; Goodyear, S. M.; Sangvanich, T.; Reda, M. M.; Lee, R.; Mihelic, S. A.; Beckman, B. L.; Hu, Z.; Gray, J. W.; Yantasee, W.,

Cationic Polymer Modified Mesoporous Silica Nanoparticles for Targeted siRNA Delivery to HER2+ Breast Cancer. *Adv. Funct. Mater.* **2015,** *25* (18), 2646-2659.

105. Gao, F.; Botella, P.; Corma, A.; Blesa, J.; Dong, L., Monodispersed Mesoporous Silica Nanoparticles with Very Large Pores for Enhanced Adsorption and Release of DNA. *The Journal of Physical Chemistry B* **2009,** *113* (6), 1796-1804.

106. Na, H.-K.; Kim, M.-H.; Park, K.; Ryoo, S.-R.; Lee, K. E.; Jeon, H.; Ryoo, R.; Hyeon, C.; Min, D.-H., Efficient Functional Delivery of siRNA using Mesoporous Silica Nanoparticles with Ultralarge Pores. *Small* **2012,** *8* (11), 1752-1761.

107. Hartono, S. B.; Nghia Truong, P.; Yu, M.; Jia, Z.; Monteiro, M. J.; Qiao, S.; Yu, C., Functionalized large pore mesoporous silica nanoparticles for gene delivery featuring controlled release and co-delivery. *Journal of Materials Chemistry B* **2014,** *2* (6), 718-726.

108. Niu, D.; Liu, Z.; Li, Y.; Luo, X.; Zhang, J.; Gong, J.; Shi, J., Monodispersed and Ordered Large‐Pore Mesoporous Silica Nanospheres with Tunable Pore Structure for Magnetic Functionalization and Gene Delivery. *Adv. Mater.* **2014,** *26* (29), 4947-4953.

109. Walters, B.; Stegemann, J., Strategies for directing the structure and function of three-dimensional collagen biomaterials across length scales. *Acta Biomater.* **2014,** *10* (4), 1488-1501.

110. Heinemann, S.; Coradin, T.; Desimone, M. F., Bio-inspired silica-collagen materials: applications and perspectives in the medical field. *Biomaterials Science* **2013,** *1* (7), 688-702.

111. Jing, S.; Jiang, D.; Wen, S.; Wang, J.; Yang, C., Preparation and characterization of collagen/silica composite scaffolds for peripheral nerve regeneration. *J. Porous Mater.* **2014,** *21* (5), 699-708.

112. Heinemann, S.; Heinemann, C.; Wenisch, S.; Alt, V.; Worch, H.; Hanke, T., Calcium phosphate phases integrated in silica/collagen nanocomposite xerogels enhance the bioactivity and ultimately manipulate the osteoblast/osteoclast ratio in a human co-culture model. *Acta Biomater.* **2013,** *9* (1), 4878-4888.

113. Patel, S. V.; Divito, M. D.; Rudisill, S. G.; Stein, A.; McLaren, J. W.; Hubel, A., Silica-collagen hybrid artificial cornea. *Acta Ophthalmol. (Copenh).* **2013,** *91*.

114. Alvarez, G. S.; Alvarez Echazu, M. I.; Olivetti, C. E.; Desimone, M. F., Synthesis and Characterization of Ibandronate-Loaded Silica Nanoparticles and Collagen Nanocomposites. *Curr. Pharm. Biotechnol.* **2015,** *16* (7), 661-667.

115. Stöber, W.; Fink, A.; Böhn, E. Controlled growth of monodispersed silica spheres in the micron size range. *J. Colloid Interface Sci.* **1968**, *26*, 62-69

116. Ciriminna, R.; Sciortino, M.; Alonzo, G.; de Schrijver, A.; Pagliaro, M. From molecules to systems: sol-gel microencapsulation in silica-based materials. *Chem. Rev.* **2011**, *111*, 765-789.

117. Mamaeva, V.; Sahlgren, C.; Lindén, M. Mesoporous silica nanoparticles in medicine—Recent advances. *Adv. Drug Del. Rev.* **2013,** *65*, 689-702.

118 Niu, D.; Liu, Z.; Li, Y.; Luo, X.; Zhang, J.; Gong, J.; Shi, J., Monodispersed and Ordered Large-Pore Mesoporous Silica Nanospheres with Tunable Pore Structure for Magnetic Functionalization and Gene Delivery. *Adv. Mater.* **2014,** *26*, 4947-4953.

119. Knezevic, N. Z.; Durand, J. O., Large pore mesoporous silica nanomaterials for application in delivery of biomolecules. *Nanoscale* **2015,** *7*, 2199-2209.

120. Du, X.; Shi, B.; Liang, J.; Bi, J.; Dai, S.; Qiao, S. Z., Developing Functionalized Dendrimer-Like Silica Nanoparticles with Hierarchical Pores as Advanced Delivery Nanocarriers. *Adv. Mater.* **2013,** *25* (41), 5981-5985.

121. Wu, M.; Meng, Q.; Chen, Y.; Du, Y.; Zhang, L.; Li, Y.; Zhang, L.; Shi, J., Large-Pore Ultrasmall Mesoporous Organosilica Nanoparticles: Micelle/Precursor Co-templating Assembly and Nuclear-Targeted Gene Delivery. *Adv. Mater.* **2015,** *27*, 215-222.

122. Voisin, H.; Aimé, C.; Coradin, T. Understanding and tuning bioinorganic interfaces for the design of bionanocomposites. *Eur. J. Inorg. Chem*. DOI:10.1002/ejic.201500403

123. Treccani, L.; Yvonne Klein, T.; Meder, F.; Pardun, K.; Rezwan, K., Functionalized ceramics for biomedical, biotechnological and environmental applications. *Acta Biomater.* **2013,** *9*, 7115-7150.

124. Hu, S.; Wiench, J.W.; Yoo, J.-C.; Pruski, M.; Lin, V.S.Y. Organic Functionalization and Morphology Control of Mesoporous Silicas via a Co-Condensation Synthesis Method. *Chem. Mater*. **2003**, *15*, 4247-4256.

125. Barbé, C.J. ; Bartlett, J. ; Kong, L. ; Finnie, K. ; Lin, H.Q. ; Larkin, M. ; Calleja, S., Bush, A. ; Calleja, G., Silica particles: A novel drug-delivery system. *Adv. Mater*., **2004**, *16*, 1959-1966.

126 Li, Z.X.; Barnes, J.C.; Bosoy, A.; Stoddart, J.F.; Zink, J.I., Mesoporous silica nanoparticles in biomedical applications. *Chem. Soc. Rev*., **2012**, *41*, 2590-2605.

127. Vallet-Regi, M.; Ramila, A.; del Real, R. P.; Perez-Pariente, J., A new property of MCM-41: Drug delivery system. *Chem. Mater*., **2001**, *13*, 308-311.

128. Manzano, M.; Vallet-Regi, M., New developments in ordered mesoporous materials for drug delivery. *J. Mater. Chem*., **2010**, *20*, 5593-5604

129. Slowing, I.I.; Trewyn, B.G.; Lin, V.S.Y. Mesoporous silica nanoparticles for intracellular delivery of membrane-impermeable proteins. *J. Am. Chem. Soc.* **2007**, *129*, 8845–8849

130. Ashley, C.E. et al. The targeted delivery of multicomponent cargos to cancer cells by nanoporous particle-supported lipid bilayers. *Nature Mater.* **2011**, *10*, 389-397.

131. Zhang, J.; Yuan, Z.-F.; Wang, Y.; Chen, W.-H.; Luo, G.-F.; Cheng, S.-X.; Zhuo, R.-X.; Zhang, X.-Z. Multifunctional envelope-type mesoporous silica nanoparticles for tumore-triggered targeting drug delivery. *J. Am. Chem. Soc*. **2013**, *135*, 5068-5073.

132. Rosenholm, J. M.; Sahlgren, C.; Linden, M., Towards multifunctional, targeted drug delivery systems using mesoporous silica nanoparticles - opportunities & challenges. *Nanoscale* **2010,** *2* (10), 1870-1883.

133. Gelse, K.; Pöschl, E.; Aigner, T. Collagens--structure, function and biosynthesis. *Adv. Drug. Deliv. Rev*. **2003**, *55*, 1531-1546.

134. Friess, W. Collagen – biomaterial for drug delivery. *Eur. J. Pharm. Biopharm.* **1998,** *45* , 113-136.

135. Chattopadhyay, S.; Raines, R.T. Review collagen-based biomaterials for wound healing. *Biopolymers*, **2014**, *101*, 821-833.

136. Wallace, D.G.; Rosenblatt, J. Collagen-based systems for sustained delivery and tissue engineering. *Adv. Drug Delivery Rev*., **2003**, *55*, 1631–1649.

137. Desimone, M. F.; Helary, C.; Rietveld, I. B.; Bataille, I.; Mosser, G.; Giraud-Guille, M. M.; Livage, J.; Coradin, T. Silica–collagen bionanocomposites as three-dimensional scaffolds for fibroblast immobilization *Acta Biomater.* **2010**, *6*, 3998–4004.

138 Desimone, M. F.; Helary, C.; Quignard, S.; Rietveld, I. B.; Bataille, I.; Copello, G.; Mosser, G.; Giraud-Guille, M. M.; Livage, J.; Meddahi-Pellé, A.; Coradin, T. In vitro Studies and Preliminary In vivo Evaluation of Silicified Concentrated Collagen Hydrogels. *ACS Appl. Mater. Interfaces*, **2011**, *3*, 3831–3838.

139. Gurtner, G.C.; Werner, S.; Barrandon, Y.; Longaker, M.T. Wound repair and regeneration. *Nature* **2008,** *453*, 314-321.

140. Li, J.; Chen, J.; Kirsner, R. Pathophysiology of acute wound healing. *Clin. Dermatol.* **2007**, *25*, 9-18.

141. Menke, N.B.; Ward, K.R.; Witten, T.M.; Bonchev, D.G.; Diegelmann, R.F. Impaired wound healing. *Clin. Dermatol.* **2007**, *25*, 19-25.

142. Zaulyanov, L.; Kirsner, R.S. A review of a bilayered living cell treatment (Apligraf) in the treatment of venous leg ulcers and diabetic foot ulcers. *Clin. Interv. Aging* **2007,** *2*, 93-98.

143. Raffeto, J.D. Dermal pathology, cellular biology, and inflammation in chronic venous disease. *Thrombosis Res*. **2009**, *123*, S66-71

144 Schultz, G.S.; Wysocki, A. Interactions between extracellular matrix and growth factors in wound healing. *Wound Repair Regen.* **2009,** *17*, 153-162.

145. Gary Sibbald, R.; Woo, K.Y. The biology of chronic foot ulcers in persons with diabetes. *Diabetes Metab. Re.s Rev.* **2008**, *24*, S25-30.

146. Chen, W.Y.; Rogers, A.A. Recent insights into the causes of chronic leg ulceration in venous diseases and implications on other types of chronic wounds. *Wound Repair Regen.* **2007**, *15*, 434-449.

147. Eming, S.A.; Krieg, T.; Davidson, J.M. Inflammation in wound repair: molecular and cellular mechanisms. *J. Invest. Dermatol.* **2007,** *127*, 514-525.

148. Ehrenreich, M.; Ruszczak, Z. Update on tissue-engineered biological dressings. *Tissue Eng.* **2006,** *12*, 2407-2424.

149. Agren, M.S.; Werthen, M. The extracellular matrix in wound healing: a closer look at therapeutics for chronic wounds. *Int. J. Low Extrem. Wounds* **2007,** *6*, 82-97.

150. Martinez, F.; Gordon, S. The M1 and M2 paradigm of macrophage activation: time for reassessment. *F1000Prime Rep.* **2014**, *6*, 13.

CHAPITRE II

Délivrance locale et soutenue de gènes dans des nanocomposites silice-collagène

CHAPITRE II

Délivrance locale et soutenue de gènes dans des nanocomposites silice-collagène

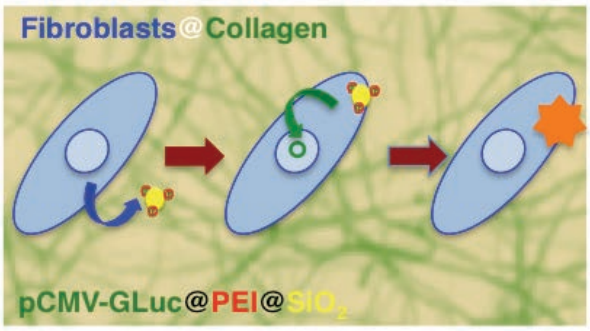

Résumé

Nous avons développé des matériaux nanocomposites associant des complexes formés par l'association de nanoparticules de silice, de polyethylèneimine et d'ADN avec des hydrogels de collagène colonisés par des fibroblastes 3T3. Grâce à la modulation de la taille de la particule de silice et de la masse moléculaire du polymère, il a été possible de réaliser la transfection des fibroblastes au sein du gel, permettant l'expression génique pendant une semaine. Des configurations alternatives consistant en l'addition des particules à des gels cellularisés ou impliquant la culture des cellules sur la surface d'hydrogels contenant les complexes ont aussi été étudiées. Ces études montrent que l'encapsulation des particules limite la dissémination du plasmide et de la silice hors de l'hydrogel. Elles montrent aussi le rôle clé joué par la prolifération et la migration cellulaire sur l'efficacité de la transfection.

Publié dans

X. Wang, C. Hélary, T. Coradin, Local and Sustained Gene Delivery in Silica-Collagen Nanocomposites, *ACS Appl. Mater. Interfaces*, 2015, 7, 2503-2511.

II-1. INTRODUCTION

In this work, collagen-based nanocomposite hydrogels integrating plain silica nanoparticles were evaluated as gene delivery systems to favour tissue repair. We hypothesized that the integration of plasmid-PEI-SiNP complexes within collagen hydrogels would allow for a sustained gene release. We show here that PEI-coated silica nanoparticles with optimal size and polymer molecular weight are efficient plasmid vectors when they are entrapped within cellularized collagen networks, allowing for a prolonged gene expression. We demonstrate that the transfection efficiency depends on both particle diffusion and cell proliferation/migration within the hydrogel. The encapsulation of the vectors within the collagen scaffold also has the advantage to avoid rapid dissemination of the plasmids and the particles, providing a safe solution for the development of biofunctional medical dressings favouring tissue regeneration.

II-2. EXPERIMENTAL SECTION

II-2-1. Preparation and Functionalization of Silica Nanoparticles

Silica nanoparticles (SiNP) with diameter *d* varying from 50 nm to 400 nm were synthesized by the Stöber method using ammonia, ethanol and tetraethylorthosilicate (TEOS) (Table II-1)

Particle size *d* (nm)	TEOS (mL)	25% NH_4OH (mL)	EthanoL (mL)	H_2O (mL)
50	7.6	9.6	200	-
100	7.4	7.3	200	5.7
200	7.6	9.7	200	6.0
400	7.0	16.0	200	11.0

Table II-1. Conditions for preparation of SiNP with different particle sizes

The as-synthesized particles were dialyzed against distilled water for 2 days, recovered by centrifugation and resuspended in 10 mM Phosphate Buffer Saline (PBS) (pH= 7.4). For PEI-SiNP particle preparation, 200 mg of branched PEI with different molecular weights (1.8 kDa, 10 kDa, 25 kDa, Sigma-Aldrich) was dissolved in 20 mL of 10 mM PBS (pH 7.4). Silica nanoparticles suspension (20 mL) with the same concentration was then

added dropwise into the PEI solution under stirring. The mixtures were further stirred for 48 h after which particles were recovered by centrifugation, washed 3 times in 10 mM PBS and finally resuspended in the buffer solution. Particle sizes and zeta potential (ζ) were measured in 10 mM PBS solution using a ZetaSizer Nano (Malvern Instruments Ltd., Worcestershire, UK). Particles were also imaged using Transmission Electron Microscopy (TEM) on a JEOL 1011 instrument. The amount of adsorbed PEI was determined by thermogravimetric analysis (TGA) and elemental analysis (C,H,O,N).

II-2-2. pDNA-PEI and pDNA-PEI-SiNP Complexation

Reporter plasmid pCMV-GLuc (pGluc) encoding Gaussia Luciferase (New England BioLabs, Ipswich, MA) was used for transfection experiments. This plasmid was amplified by one shot® BL21(DE3) pLysS kit (Invitrogen™, Life technologies), extracted by one PureLink® HiPure Plasmid kit (Invitrogen™, Life technologies) and finally stored in Tris-EDTA buffer at -20 °C. pDNA-PEI complexes were prepared at weight ratio of 1:2. pDNA-PEI-SiNP complexes were prepared at various pDNA:PEI-SiNP weight ratios. Complexes formation was examined by agarose gel electrophoresis. Briefly, 1 µL of pDNA solution (0.1 µg. μL^{-1}) were mixed homogeneously with a total volume of 9 µL of PEI-SiNP suspension or PEI solution (PBS 1x) by vortexing in a microcentrifuge tube. The resulting mixtures were left at room temperature for 2 h to achieve complete complexation, before being loaded onto 0.7% agarose gel with ethidium bromide (0.1 $\mu g.mL^{-1}$) and running with TAE buffer at 100 V for 40 min. DNA retardation was observed by irradiation with ultraviolet light.

II-2-3. Fibroblast Cell Culture

3T3 mouse fibroblasts were cultured in complete cell culture medium (Dulbecco's Modified Eagle's Medium (DMEM) supplemented with 10% fetal serum, 100 $U.mL^{-1}$ penicillin, 100 $\mu g.mL^{-1}$ streptomycin and 0.25 $\mu g.mL^{-1}$ Fungizone). Tissue culture flasks (75 cm^2) were kept at 37 °C in a 95 % air: 5 % CO_2 atmosphere. Before confluence, fibroblasts were removed from culture flasks by treatment with 0.1% trypsin and 0.02 % EDTA. Cells were rinsed and resuspended in the above culture medium before use.

II-2-4. Preparation of Collagen-Based Nanocomposites

Collagen type I was purified from rat tails and the concentration was estimated by hydroxyproline titration, as previously described.[1] Tubes separately filled with collagen solution (2 $mg.mL^{-1}$ in 17 mM acetic acid), whole cell culture medium, and 0.1 M NaOH were kept in ice bathes for 1 h before preparation to slow down the gelling kinetics of

collagen. Complexes were formed by adding 1 µg of pDNA to 25 µL of a solution containing PEI or PEI-SiNP in order to achieve the pDNA:PEI (or pDNA-PEI-SiNP) ratio obtained from gel electrophoresis. Three models were proposed in our study: particles on top of cellularized hydrogels (model 1), co-entrapped particles and cells (model 2), and cells beneath free-floating nanocomposites (model 3) (**Figure II-1**). For model 1, 500 µL of collagen solution and 400 µL of culture medium were added to a 1.5 mL tube and vortexed vigorously. After addition of 30 µL of 0.1 M NaOH and strong vortexing, 125 µL of the cell suspension at a density of 10^6 cells.mL^{-1} was added and mixed homogenously. Then 0.9 mL was sampled from the mixture and deposited into a 24-well plate. The plate was then incubated at room temperature for 10 min for complete gelling of collagen. After this delay, 25 µL of the complexes solution was added onto the surface of the materials. For model 2, a similar procedure was followed except that the 25 µL of complexes was mixed with 100 µL of the cell suspension before gel formation. Model 3 was similar to model 2 except that the cell suspension was replaced by culture medium and the hydrogels were left free-floating in the culture medium of plate-seeded cells (5.10^3 cells.mL^{-1}).

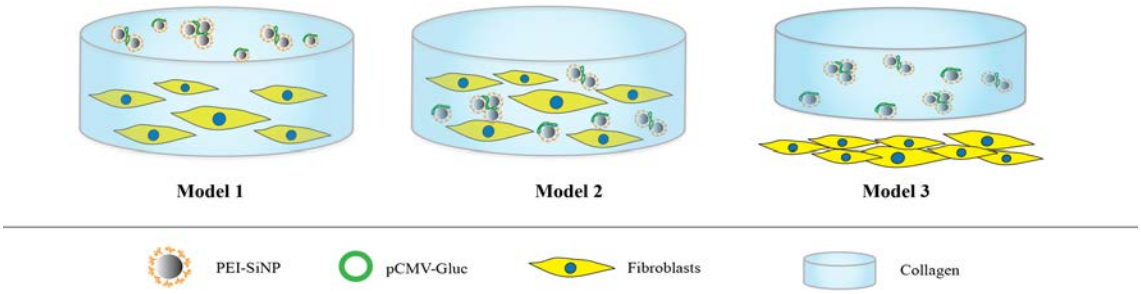

Figure II-1. Schematic representation of the three models

II-2-5. Cell Transfection and Cell Viability

Transfection efficiency of pDNA-PEI and pDNA-PEI-SiNP were evaluated by luciferase expression of pGLuc by 3T3 fibroblast cells in cell culture medium. To perform cell transfection in 2D, 3T3 mouse fibroblasts were plated at a density of 5.10^4 per well in a 24-well plate. pDNA-PEI or pDNA-PEI-SiNP complexes (25 µL, prepared as described above) were added to the cell culture medium. After 4 h, the supernatant was removed, the well was refreshed with 1 mL medium and the cells were then cultured for another 44 h in complete

medium for the expression of luciferase. To perform cell transfection in 3D, pDNA complexes were added on the top of the hydrogel (model 2) or mixed with the collagen solution (model 1 & 3). 1 mL of whole medium was then added in each well. At selected time points over a 1-week period, 0.5 mL of the culture medium was collected from the wells and replenished with equal volumes of fresh medium. For measurements of luciferase activity, a BioLux Gaussia Luciferase Assay Kit (New England Biolabs) was used and transgene expression of luciferase was reported as relative light units (RLU). Control groups were under the same culture conditions as the experiment groups except for the absence of DNA complexes.

Internalization of nanoparticles in 3T3 mouse fibroblasts was studied using fluorescence microscopy. For cells cultured in 2D, the pDNA-particle complexes along with cell culture medium were removed after 24 h incubation, rinsed 3 times with PBS and fixed with 4% paraformaldehyde for 1 hour at RT. The cell nucleus was then stained with DAPI (4',6-diamidino-2-phenylindole dihydrochloride, Life technologies, 300 nM in PBS) for 10 min and rinsed with PBS before observation. For cells immobilized in collagen hydrogels, gels were incubated for 48 h, rinsed 3 times with PBS and fixed with 4% paraformaldehyde overnight. Next, the fixed samples were dehydrated in ethanol and butanol and incorporated in paraffin to obtain 10 µm histological sections with a manual microtome. Before observation, the as-obtained samples were immersed in toluene, ethanol and then water for rehydration. The cell nucleus was stained with DAPI for 10 min and rinsed with PBS before observation. Model 2 was also studied by scanning electron microscopy (SEM). Collagen hydrogels were fixed using 3.63% glutaraldehyde in a cacodylate/saccharose buffer (0.05 M/0.3 M, pH 7.4) for 1 hour at 4 °C. Following fixation, samples were washed three times in a cacodylate/saccharose buffer (0.05 M/0.3 M, pH 7.4) and dehydrated through successive increasing concentration ethanol baths from 70% to 100% alcohol. Thereafter, samples were dried in a critical point dryer and gold sputtered (20 nm) for analysis. Samples were observed with Hitachi S-3400N SEM operating at 10 kV.

Cell viability was monitored using the Alamar Blue test. For the 2D model, cell culture medium was removed for luciferase activity test and 200 µL of the Alamar Blue solution (10% in cell culture medium) was added. The cells were then incubated at 37 °C with 5 % CO_2 for 4 h. The supernatant in each well was then collected, diluted with 800 µL water, and its absorbance was measured at λ = 570 nm and 600 nm. Cell viability was calculated and

reported as a percentage of the control group (n = 6). For the 3D model, cell viability was assessed in the same way except that the 800 µL water was first added to the collagen gel for 0.5 h at room temperature to extract the Alamar blue solution trapped in the gel and then collected for the absorbance measurements. To further understand the proliferation of cells in the collagen gel (1 mg/mL) over one week, cell viability was evaluated with Alamar Blue test as described before after 2, 5 and 7 days and was calculated as the percentage of that of 2 days.

II-2-6. Statistical analysis

Graphical results are presented as mean±SD (standard deviation). Statistical significance was assessed using one-way analysis of variance (ANOVA) followed by Tukey (compare all pairs of groups) or Dunnett (compare a control group with other groups) post-hoc test. The level of significance in all statistical analyses was set at a probability of $P< 0.05$.

II-3. RESULTS AND DISCUSSION

II-3-1 Silica particle characterization

Plain silica nanoparticles $SiNP_d$ with diameters ranging from 50 nm to 400 nm were obtained using the Stöber reaction, as indicated by DLS measurements in water (**Table II-2**) and confirmed by TEM observation (**Figure II-2**). Zeta potential (ζ) values were constant over the particle size variation and significantly negative (-25/-35 mV), as expected for silica near neutral pH. After contact with PEI_{25}, all particles have a positive ζ value in PBS, in agreement with the surface deposition of the polycation polymer. The amount of adsorbed PEI was maximum for $SiNP_{50}$ and $SiNP_{200}$ particles (*ca*. 15 w%) and lower for $SiNP_{100}$ and $SiNP_{400}$. DLS studies indicate that particles with intermediate sizes have a good stability in PBS whereas the smallest and largest ones show a tendency towards aggregation.

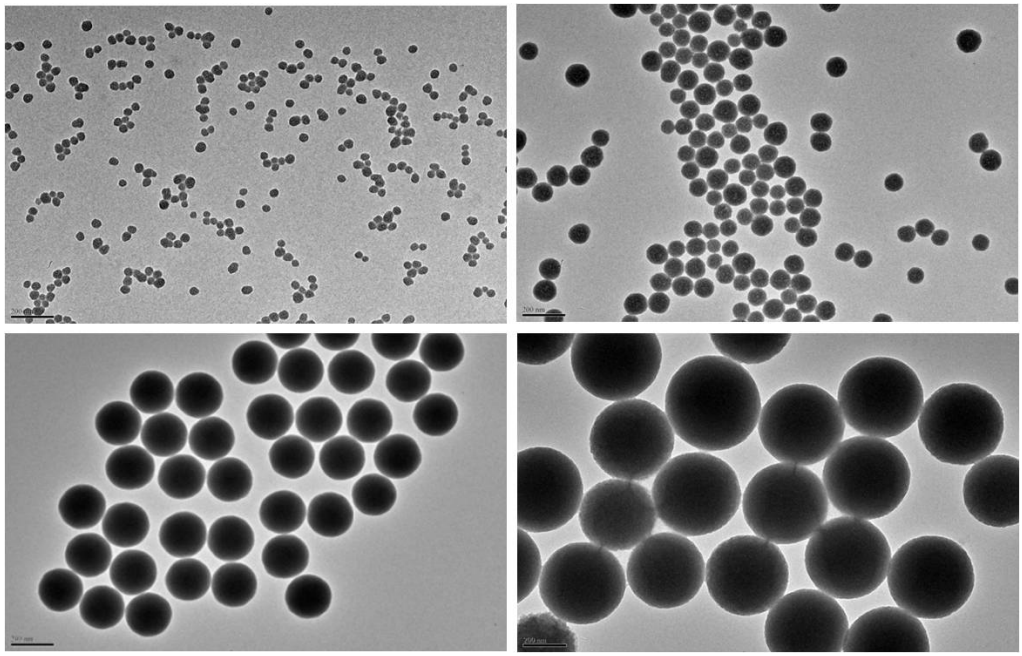

Figure II-2. TEM image of SiNP with different particle sizes 50 nm- 400 nm (×11,000)

bare particles		after coating		
d_{H2O}	ζ_{H2O}	d_{PBS}	ζ_{PBS}	PEI
[nm]	[mV]	[nm]	[mV]	[wt%]
50 ± 10	- 28 ± 12	140 ± 70	+ 18 ± 8	15
120 ± 20	- 27 ± 11	150 ± 40	+ 19 ± 6	10
210 ± 10	-26 ± 8	250 ± 40	+ 19 ± 6	15
390 ± 40	-35 ± 7	420 ± 150	+ 20 ± 9	5

Table II-2. Diameter (d) and zeta potential (ζ) and PEI amount for silica nanoparticles before and after coating with PEI-25kD

II-3-2. Cell transfection properties of silica nanoparticles in 2D

In a first step, the complexation ability of the different PEI_{25}-coated $SiNP_d$ was studied by electrophoretic mobility shift assays of pDNA (**Figure II-3**). The optimal plasmid :particle weight ratio ensuring full retention of pDNA by particles was 1:30 w/w% for $SiNP_{400}$ and $SiNP_{200}$ and 1:10 w/w% ratio for $SiNP_{100}$ and $SiNP_{50}$.

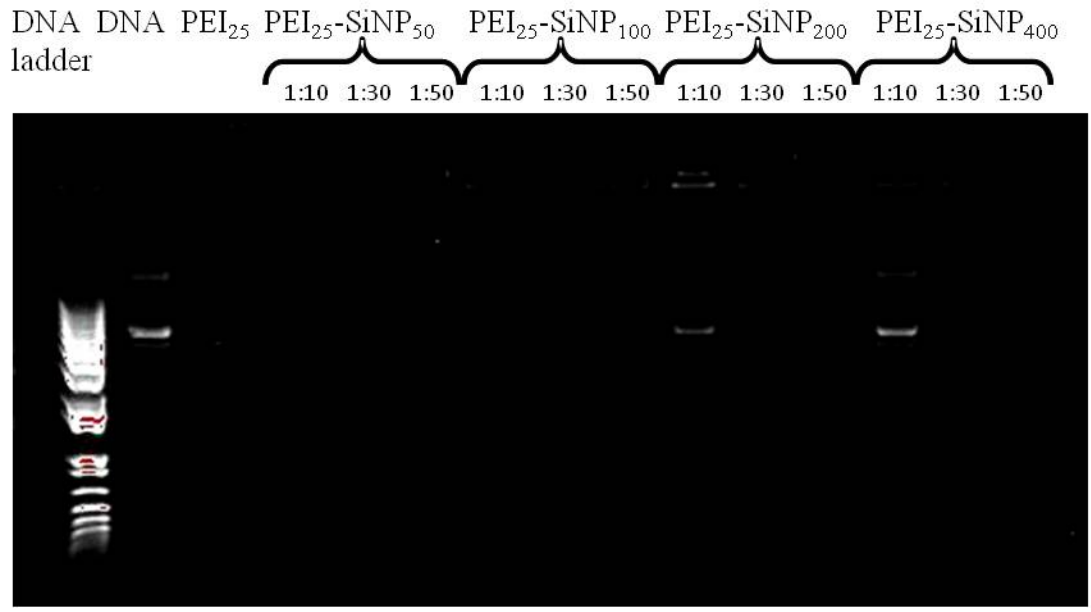

Figure II-3. Agarose gel electrophoresis showing the particle size effect on pDNA complexation by $PEI_{25}SiNP_d$. A constant amount of DNA was complexed with silica particles at different weight ratios 1:10, 1:30 and 1:50.

The cell transfection ability of these complexes was studied on 3T3 fibroblast cells seeded in 24-well plates (2D configuration). Luciferase expression, indicative of successful internalization and transport to the nucleus of the pDNA, was observed for all systems (**Figure II-4**).

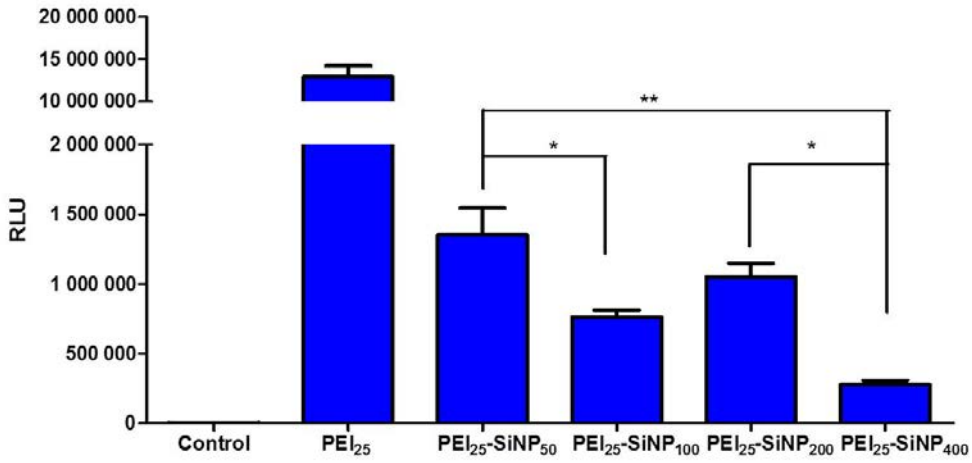

Figure II-4. Transfection of 3T3 mouse fibroblasts after 4 h incubation with free and silica-associated PEI_{25} expressed in Relative Light Units (RLU) (n=3). Variance of the luciferase expression among group PEI_{25}-$SiNP_{50}$, PEI_{25}-$SiNP_{100}$, PEI_{25}-$SiNP_{200}$ and group PEI_{25}-$SiNP_{400}$ was determined by one-way ANOVA with Tukey post-hoc test (*P<0.05, ** P<0.01).

Importantly, PEI_{25}, pDNA and $SiNP_d$ alone gave no significant signal. The PEI_{25} polymer alone was the most efficient transfecting agent whereas its adsorption on SiNP decreases its transfection ability by one order of magnitude regardless of the nanoparticle size. This may be attributed to the fact that a fraction of the positively-charged ammonium groups of PEI is interacting with the silica surface and is therefore no longer accessible for DNA complexation. Another explanation is related to the size of the complexes that can be less adequate for cell internalization by fibroblasts than PEI alone. Fibroblasts are able to internalize particles by endocytosis in a size dependent manner, with smaller particles being more rapidly engulfed by cells than larger ones. Noticeably, internalization of nanoparticles with a diameter larger than 500 nm is observed only in exceptional cases. PEI_{25} on its own has the best ability to compact DNA and generate 100 nm complexes suitable for cell uptake. In contrast, after PEI adsorption, SiNPs have diameters in the 150-420 nm range. This can explain why the largest PEI_{25}-$SiNP_{400}$ exhibited the lowest transfection efficiency.

Considering the effect of particle size in more detail, it is worth pointing out that adsorption of cationic polyelectrolytes on silica surface is a complex phenomenon where transitions from flat to extended configurations are observed as a function of polymer concentration. The particle size also has a major influence on the adsorption process from different points of view: it controls the density of silanol groups, and therefore particle surface

charge; it dictates the available surface for adsorption per particle; it defines the maximum packing density of polymers via its radius of curvature. Here a reliable comparison must be made from the PEI density on the particle surface rather the amount of PEI sorption per g of silica. Such a density can be estimated by the product of PEI wt% by particle radius, leading to PEI density decreasing as $SiNP_{200}$ > $SiNP_{400}$ > $SiNP_{100}$ > $SiNP_{50}$. It illustrates the fact that the decrease in available surface per particle with increasing size is compensated by the increase in maximum PEI packing density. Interestingly, electrophoresis data indicates that PEI_{25}-$SiNP_{100}$ and PEI_{25}-$SiNP_{50}$ bind more DNA than PEI_{25}-$SiNP_{200}$ and PEI_{25}-$SiNP_{400}$. However higher transfection is obtained for PEI_{25}-$SiNP_{50}$ and PEI_{25}-$SiNP_{200}$. This strongly suggests that transfection efficiency is not directly related to PEI amount nor to particle size. A more relevant parameter is DNA compaction that depends on PEI conformation. Here $SiNP_{50}$ and $SiNP_{200}$ have similar transfection efficiency although $SiNP_{50}$ has lower PEI density but binds more DNA than $SiNP_{200}$. That is to say, the PEI chains on $SiNP_{50}$ are more effective to bind DNA than the PEI chain on $SiNP_{200}$. As mentioned above, this can be explained considering that for small radius of curvature (i.e. large particles), PEI can adopt a flat configuration that is not favorable for DNA compaction. As the radius of curvature increase (i.e. the particle size decrease), PEI chains can adopt a more compact configuration to optimize their packing on the surface, a situation that is more favorable for DNA compaction

II.3.3 Effect of PEI Molecular Weight on Fibroblast Transfection in 2D

Taking into account their limited tendency to aggregate and high PEI loading, the $SiNP_{200}$ particles were selected for the following investigations.─For these $SiNP_{200}$ particles, decreasing the PEI molecular weight from 25 kDa to 10 kDa led to an increase of particle size polydispersity and an increase in the amount of adsorbed polymer (**Table II-3**). For short PEI chains (*MW* = 1.8 kDa), submicronic aggregates were detected by DLS in PBS whereas the amount of adsorbed PEI was similar to that of PEI_{25}. Large branched PEI chains are known to adopt compact conformation whose dimensions decrease with decreasing MW.[2] This allows for a higher density of PEI molecules on the surface, explaining the higher rate of adsorption of PEI_{10} compared to PEI_{25}. However, when decreasing further the polymer MW, short chains can adopt a more linear conformation and a flat configuration on the surface, leading to a lower density and therefore lower amount of adsorbed PEI. The observation of a significant

aggregation of the $PEI_{1.8}$-$SiNP_{200}$ confirms this hypothesis as flat PEI chains are less effective in improving colloidal stability via steric repulsion compared to extended conformations.[3]

MW [kDa]	d_{PBS} **[nm]**[a]	ζ_{PBS} **[mV]**	**PEI [wt%]**[b]
1.8	> 1000	+ 20 ± 12	15
10	310 ± 100	+ 19 ± 8	25
25	250 ± 40	+ 19 ± 6	15

Table II-3. Diameter (*d*) and zeta potential (ζ) and PEI amount for 200 nm-silica nanoparticles after coating with PEI of different molecular weight *MW*

Agarose gel experiments performed on pDNA-complexed PEI-coated particles showed that the optimal plasmid:particle weight ratio was 1:30 w/w% independently of the PEI molecular weight, in agreement with the fact that a similar ζ value of + 20 mV was found for all PEI-$SiNP_{200}$ particles (**Figure II-5**)

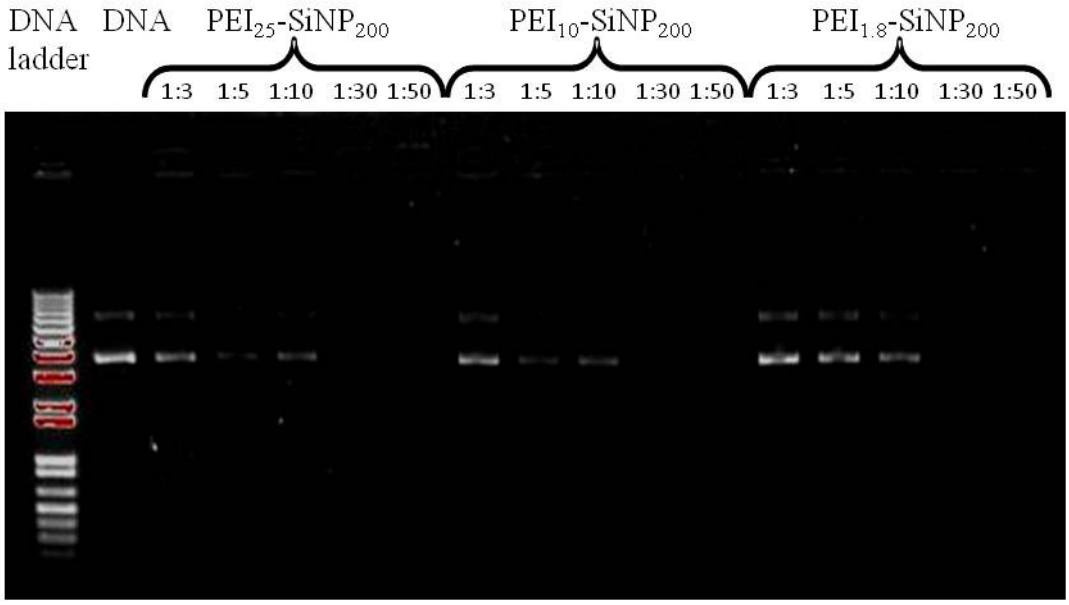

Figure II-5. Agarose gel electrophoresis showing the PEI molecular weight influence on PEI-Si_{200}/pDNA complexation. A constant amount of DNA was complexed with silica particles at different weight ratios 1:3, 1:5, 1:10, 1:30 and 1:50.

Transfection assays in 2D revealed an interesting phenomenon (**Figure II-6**). When PEI polymers alone were used as complexation reagents, an increase in transfection efficiency with increasing molecular weight was observed, in agreement with the literature.[4-6] When PEI-$SiNP_{200}$ systems were used, the optimal transfection was achieved with PEI_{10}. Moreover, the particles showed a higher transfection efficiency than the polymer alone. This beneficial influence of PEI adsorption was further evidenced at lower molecular weight since $PEI_{1.8}$ alone did not show any transfection capability whereas expression of luciferase was detectable for $PEI_{1.8}$-$SiNP_{200}$.

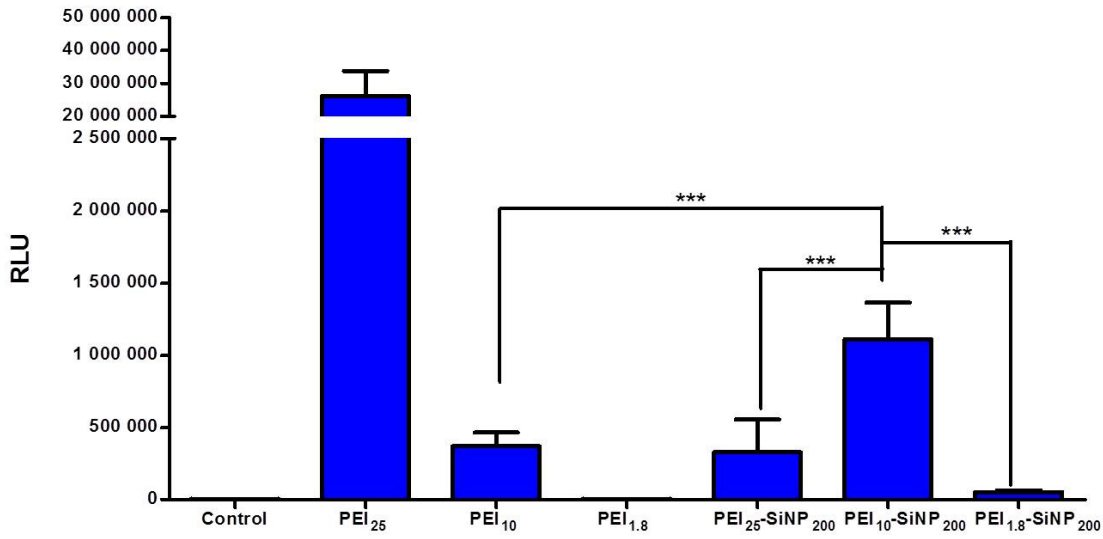

Figure II-6. Transfection of 3T3 mouse fibroblasts after 4 h incubation with free and $SiNP_{200}$ coated with PEI of various molecular weights (n=6). Variance of the luciferase expression between group PEI_{10}, PEI_{25}-$SiNP_{200}$, $PEI_{1.8}$-$SiNP_{200}$ and group PEI_{10}-$SiNP_{200}$ was determined by one-way ANOVA with Dunnett post-hoc test (*** P<0.001).

Whereas the higher amount of adsorbed PEI_{10} compared to PEI_{25} may, at least partially, account for the behavior of the corresponding particles, the observed improvement of transfection efficiency of shorter PEI upon coating suggests that another parameter should be considered. Importantly, the decrease in transfection efficiency of PEI chains with lower molecular weight was attributed to their decreased ability to compact DNA, a pre-requirement to its internalization. Thus, based on our observation of particle aggregation upon plasmid addition, it is possible to assume that several particles are conjointly involved in the compaction of one pDNA chain, allowing for its better compaction. Noticeably, such an aggregation process is known to be responsible for the transfection capabilities of cationic liposomal formulations (lipofection).[7]

To clarify the transfection pathway of PEI-coated SiNPs, FITC-containing silica nanoparticles were prepared and their internalization after complexation with pDNA by fibroblasts cells was followed by fluorescence microscopy. As shown in **Figure II-7**, the presence of silica particles (green fluorescence) within the cells and accumulating near the nucleus (blue fluorescence) was ascertained. Noticeably, significant particle aggregation was observed for $PEI_{1.8}$-Si_{200}, in agreement with the DLS data. Bare $SiNP_{200}$ nanoparticles put in contact with pDNA were also used as controls, showing a similar uptake as PEI-coated ones,

in agreement with the literature.[8] Therefore it is not possible to determine whether internalized particles bear PEI and pDNA or not.

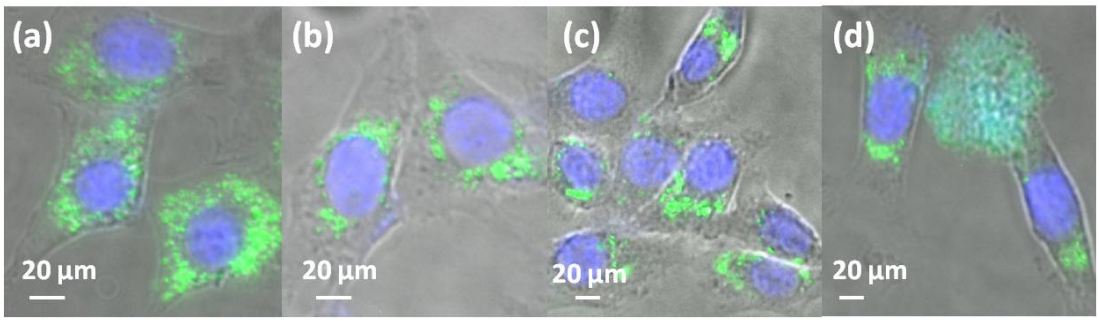

Figure II-7. Fluorescence microscopy images showing internalization of (a) pDNA-$SiNP_{200}$, (b) pDNA-PEI_{25}-$SiNP_{200}$, (c) pDNA-PEI_{10}-$SiNP_{200}$, (d) pDNA-$PEI_{1.8}$-$SiNP_{200}$ complexes by 3T3 fibroblasts after 24 h of incubation. Green fluorescence corresponds to FITC-labeled particles and blue to DAPI nuclei staining (scale bar = 20 µm).

However, solutions containing the pDNA-PEI-Si_{200} particles were regularly centrifuged and the absence of luciferase expression using the supernatant was checked. This evidences that transfection is not due to soluble pDNA-PEI complexes that may have been desorbed from the silica particle surface (**Figure II-8**).

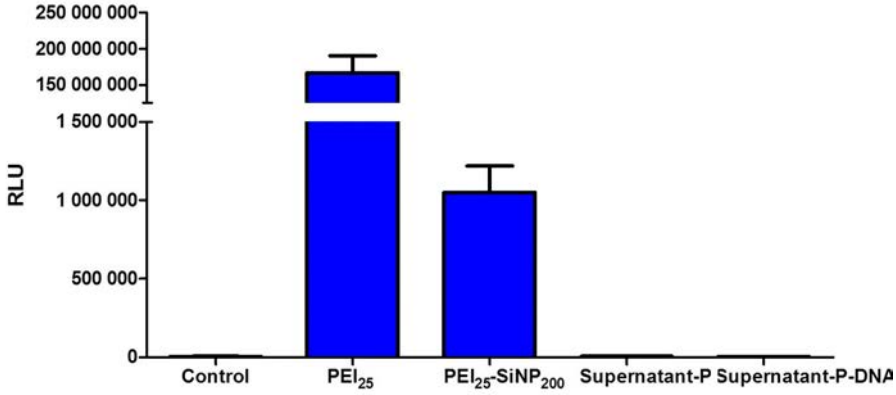

Figure II-8. Control transfection experiments with particle supernatant. Supernatant-P denotes the supernatant of PEI_{25}-$SiNP_{200}$ while Supernatant-P-DNA refers to the supernatant of DNA-PEI_{25}-$SiNP_{200}$ complexes. The former was further complexed with pDNA before transfection test. No luciferase expression was detected using neither of the supernatant as transfection reagent.

Altogether, these data indicate that PEI-coated silica nanoparticles *ca*. 200 nm in diameter are well-suited for plasmid delivery to fibroblast cells in 2D. Importantly, they reveal to be even more effective than PEI alone when using low molecular weight polymers. This is a very interesting result as the cytoxicity of PEI is know to increase with its molecular weight due to higher cationic charge. Here, for all experiments carried out, cells showed good viability even when PEI alone was used as the pDNA carrier (**Figure II-9**).

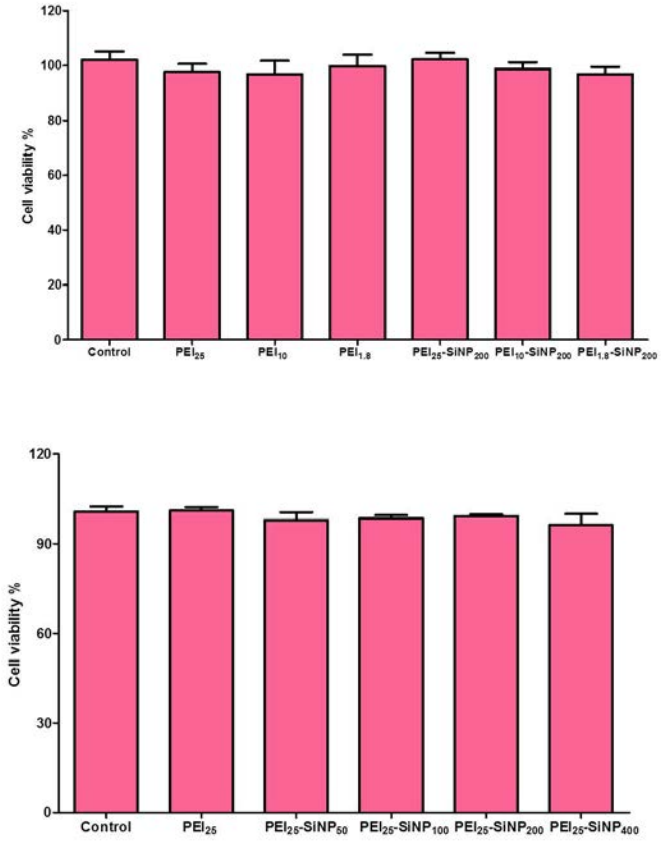

Figure II-9. Cell viability in 2D as influenced by different sizes of SiNP and different molecular weight of PEI. Cell viability was assessed after 4 h of contact with Alamar Blue test and calculated in the percentage of control (n=6).

This is probably due to the small amount of PEI (2 µg/mL) used in these experiments together with the fact that 3T3 mouse fibroblast is a robust cell line. To study this point further, the viability of fibroblasts after 4 h of contact with PEI and PEI-coated SiNP200 particles as a function of dose (0-100 µg/mL) was studied (**Figure II-10**). PEI_{25} showed significant cytotoxicity (*i.e*. cell viability < 80 %) above a 10 µg/mL concentration. This toxic dose increased to 50 µg/mL for PEI_{10} while no significant cytotoxicity was observed for

$PEI_{1.8}$ in the studied concentration range. Strikingly, PEI_{25}-$SiNP_{200}$ and PEI_{10}-$SiNP_{200}$ showed a very limited impact on cell viability (> 90 %) at all investigated doses. This clearly demonstrates the beneficial effect of PEI adsorption on the silica nanoparticle surface on its cytotoxicity. As indicated earlier, this can be attributed to the fact that the apparent positive charge of the PEI chain is decreased by interaction of some of the protonated amine groups with the silica surface.

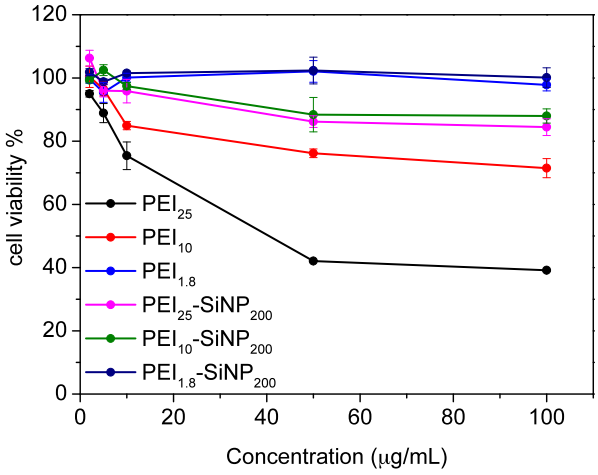

Figure II-10: Impact of PEI and PEI-coated $SiNP_{200}$ nanoparticles after 4 h of contact as monitored by the Alamar Blue viability test.

II-3-4. Cellularized collagen hydrogels as models for 3D transfection

Cellularized collagen hydrogels can be considered as good model of dermis to evaluate biomolecules effects in more physiologically-relevant 3D conditions. pDNA-PEI-$SiNP_{200}$ particles were placed onto hydrogels to assess their diffusion through the collagen network and their ability to transfect immobilized 3T3 fibroblasts, using pDNA-PEI polyplexes as controls (model 1). For PEI_{25}-based polyplexes, an efficient transfection was detected from day 2 until the end of the experiment. In contrast, no luciferase expression was detected at day 2 when PEI_{25} was absorbed onto $SiNP_{200}$. The transfection became significant after day 5 only and was enhanced after day 7 but remained one order of magnitude lower than the pDNA-PEI_{25} polyplexe alone. **(Figure II-11)** A similar trend was observed for PEI_{10} except that after day 7, the particles showed a level of luciferase expression similar to the polyplexes. In the case of $PEI_{1.8}$, a weak transfection was detected at day 7 but only for particles. Overall, similar transfection efficiencies were obtained in these 3D models compared to 2D

configuration, except for a delay in luciferase expression. This is in good agreement with our recent study showing that silica nanoparticles with sizes ranging from 10 nm to 200 nm can diffuse through cellularized hydrogels, with the diffusion rate decreasing with increasing particle size.[9] Moreover, these particles could be internalized by immobilized fibroblasts. Interestingly, these data also suggest that the particles aggregates that were suggested to be responsible for pDNA compaction are preserved during diffusion.

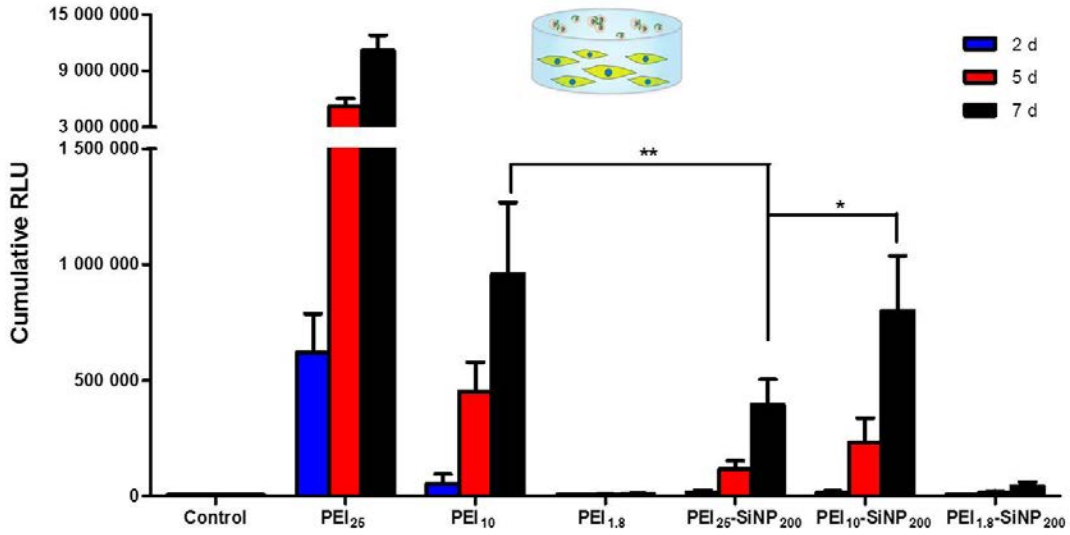

Figure II-11. Transfection of 3T3 mouse fibroblasts immobilized in collagen hydrogels after 2, 5 and 7 d of contact with diffused free and Si_{200}-associated PEI of various molecular weight (model 1, n=6). Variances among the cumulative luciferase expression on 7 d of PEI_{10}, PEI_{25}-$SiNP_{200}$ and PEI_{10}-$SiNP_{200}$ were determined by one-way ANOVA with Tukey post-hoc test (*P<0.05, ** P<0.01).

II-3-5. Evaluation of Cellularized Nanocomposites as Cell Factories

Two different configurations for the use of plasmid-loaded particles associated with collagen hydrogels can be envisioned. The first strategy relies on the implantation of cellularized scaffolds incorporating the functional nanoparticles (model 2, **Figure II-12(a)**). The advantage of this configuration is that DNA cargos can rapidly transfect cells encapsulated in the implant. Cells start to produce the biomolecules of interest in a short range of time. With this strategy, we can produce a cell factory to promote wound healing. In addition, the implantation of collagen hydrogels in the wound bed limits the risk of infection while preventing dehydration.[10-11] However, in this situation, it is important to check that particle

internalization by the cells is still possible within the hydrogel. For this purpose, collagen hydrogels encapsulating both 3T3 fibroblasts and pDNA-PEI-Si_{200} were prepared. Using fluorescent carriers, it was possible to observe the accumulation of particles within immobilized cells (**Figure II-12(b)-(d)**).

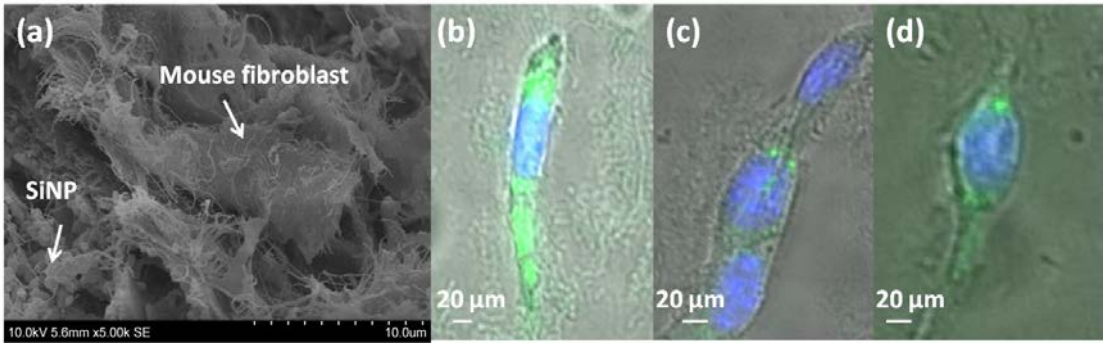

Figure II-12. (a) SEM image of nanocoposites, displaying SiNP and fibroblast immobilized in collagen scaffold. Fluorescence microscopy image showing internalization of (b) pDNA-PEI_{25}-Si_{200}, (c) pDNA-PEI_{10}-Si_{200}, (d) pDNA-$PEI_{1.8}$-Si_{200} complexes by 3T3 fibroblasts within collagen hydrogels after 48 h of incubation, in which green fluorescence corresponds to FITC-labeled particles and blue to DAPI nuclei staining (scale bar = 20 µm).

Transfection assays performed in collagen hydrogels encapsulating both 3T3 fibroblasts and p-DNA-PEI or pDNA-PEI-Si_{200} also confirm internalization and gene expression (**Figure II-13**). The luciferase expression followed similar trends in terms of the effect of PEI chain length, both as such or associated with Si_{200} particles, compared to the complexes in solution. The main difference between the two systems lies on the lower expression rate for encapsulated complexes, suggesting that more vectors can enter in contact with the cells upon diffusion than after immobilization.

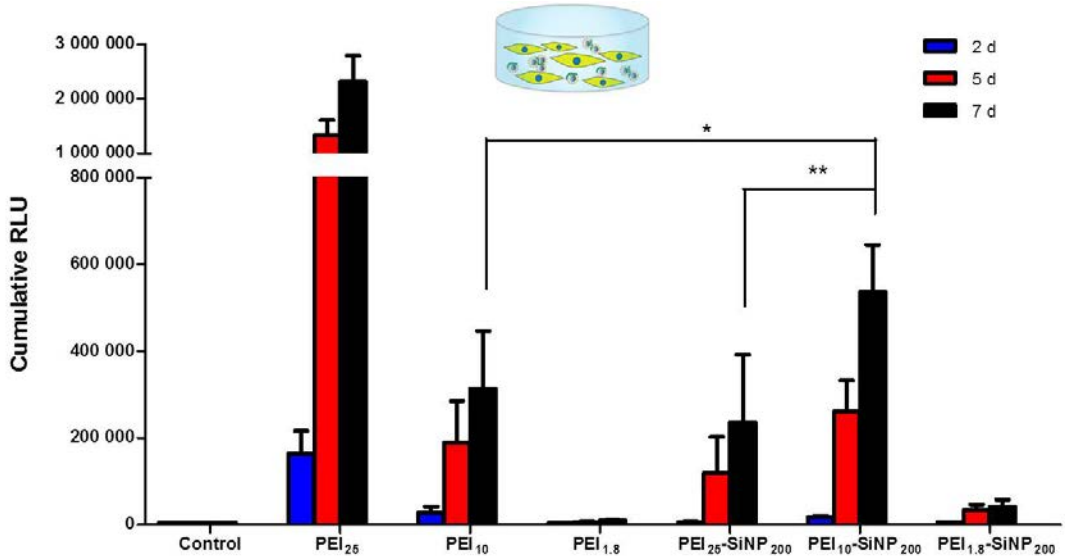

Figure II-13. Transfection of 3T3 mouse fibroblasts co-immobilized with free and Si_{200}-associated PEI of various molecular weight in collagen hydrogels after 2, 5 and 7 d of incubation (model 2, n=6). Variance among the cumulative luciferase expression on 7 d of PEI_{10}, PEI_{25}-$SiNP_{200}$ and PEI_{10}-$SiNP_{200}$ was determined by one-way ANOVA with Tukey post-hoc test ($*P<0.05$, $**$ $P<0.01$).

It was previously shown that silica nanoparticles entrapped within the fibrillar collagen network are in close interaction with protein fibrils.[12] As a consequence, nanoparticles are expected to have a restricted mobility. The alternative possibility is that cells proliferate and migrate within the collagen network, meet complexes and internalize them.[13-14] This assumption is supported by the measured proliferation of fibroblasts within the hydrogels (**Figure II-14**) The time needed for cell proliferation and migration can explain the observed delay in luciferase expression compared to the 2D situation. Nevertheless, the trends obtained for these nanocomposites as a function of PEI molecular weight and adsorption are in good agreement with that obtained for 2D transfection as well as for particle diffusion assays (model 1). This indicates that the pDNA-PEI-Si_{200} complexes preserve their integrity upon encapsulation.

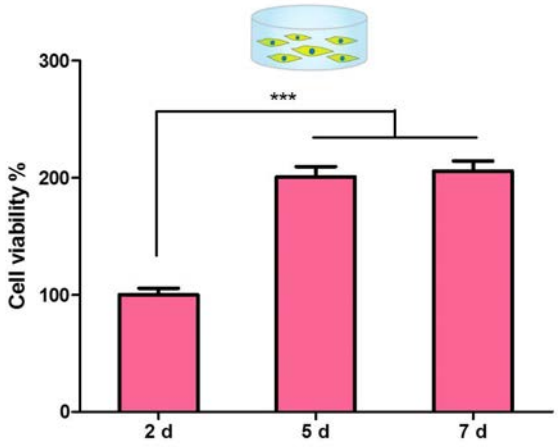

Figure II-14. Proliferation of cells in a particle-free collagen gel (1 mg/mL) evaluated with Alamar Blue test and presented as cell viability, which is calculated in the percentage of 2d (n=3). Significant increase of viability was detected for 5d and 7d vs 2d determined by one-way ANOVA with Tukey post-hoc test (*** $P< 0.001$).

Importantly, no evidence for cytotoxicity was observed for model 1 (particle diffusion through cellularized gels) and model 2 (co-immobilized particles and cells) after 24 h of contact with PEI and PEI-coated particles during transfection experiments (**Figure II-15**). Increasing the dose to 50 µg/mL showed high cytotoxicity for PEI_{25} and PEI_{10} whereas coated silica nanoparticles had a limited impact on cell viability.

(a)

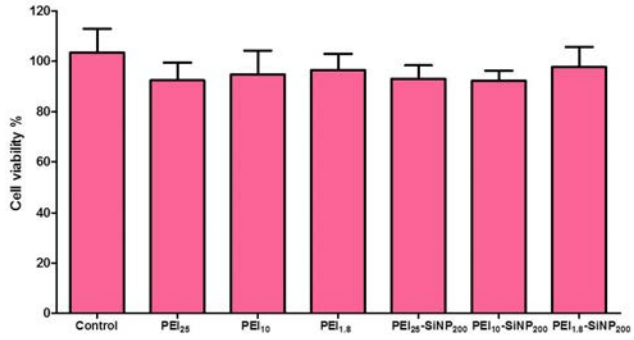

(b)

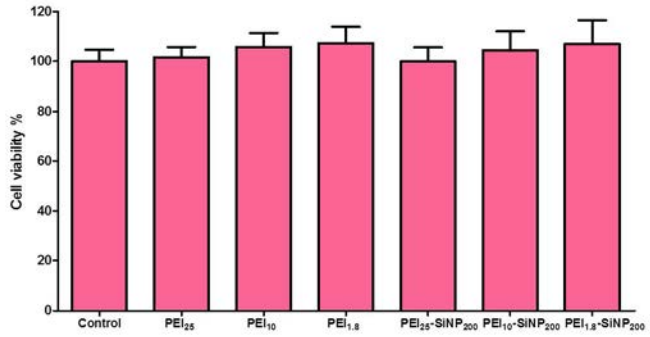

(c)

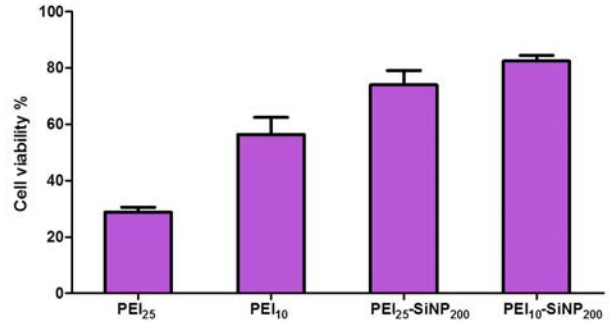

Figure II-15. Cell viability as assessed with Alamar Blue test and calculated in the percentage of control (n=6). (a) model 1 and (b) model 2 configurations after 24 h of contact in the conditions of cell transfection. (c) model 2 after 24 h of contact with a 50 μg/mL dose.

II-3-6.Evaluation of Nanocomposites as Gene Delivery Systems.

We then studied a second situation where the collagen scaffolds incorporating functional nanoparticles could act as a medicated dressing to deliver genes to tissue cells at the site of implantation. To test this configuration, hydrogels containing p-DNA-PEI or pDNA-PEI-Si200 were left free-floating in the culture medium covering 3T3 cell-seeded well plates (model 3). As shown in **Figure II-16**, significant level of luciferase expression was only observed for pDNA-PEI25 after 5 days, but this level remains one order of magnitude below the transfection efficiency achieved in model 2. This strongly support the hypothesis that entrapped vectors have a very limited mobility within the collagen hydrogels so that internalization is possible only if cells can migrate inside the protein network. One important

outcome of this study is that complexing DNA with PEI-SiNP provides an efficient method to confine gene expression within the scaffold and avoid plasmid and silica particles dissemination in the surrounding tissue, at least before colonization of the material by host cells.

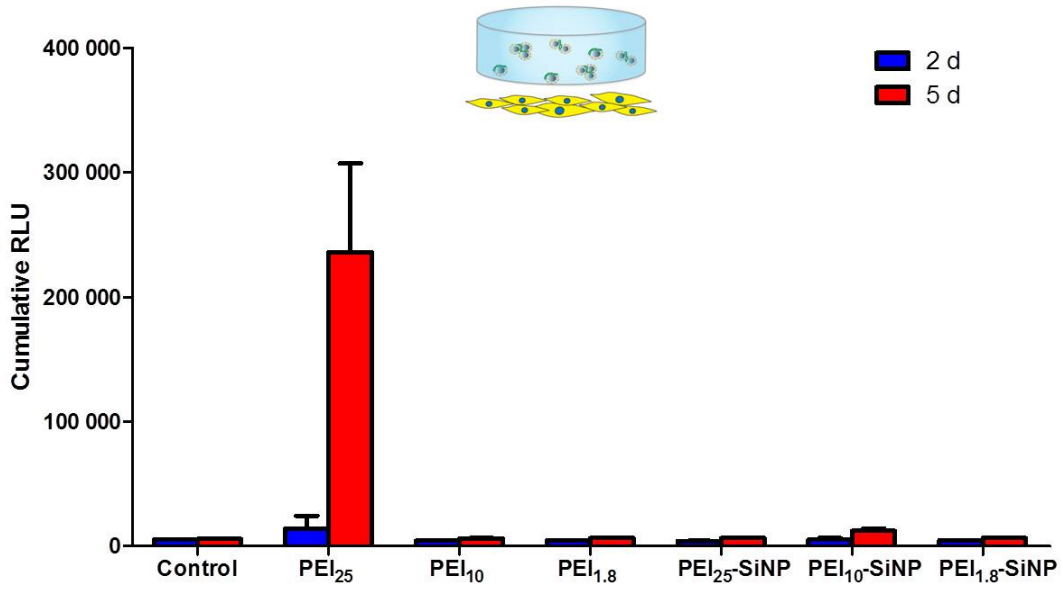

Figure II-16. Transfection of 3T3 mouse fibroblasts in contact with free-floating collagen hydrogels containing free and Si_{200}-associated PEI of various molecular weight after 2, 5 and 7 d of incubation (model 3, n=3).

II-3-7. Implication in Gene Delivery and Tissue Engineering

Coupling PEI with plain spherical SiNP seems to be a very interesting strategy for targeted cell transfection. The cytocompatibility of SiNPs has been widely studied and discussed in the literature. Dissolution of silica nanoparticles into silicic acid has been demonstrated both in cells and in animals.[9, 15] The spherical shape of SiNPs is also an important factor. Although needles or rods have the most appropriate shape to be engulfed by fibroblasts, they are more cytotoxic as they inflict mechanical damage when they penetrate biological membrane.[4, 16-17] Moreover spheres are more suitable to favour gene expression as they approach the nucleus more rapidly than elliptical particles.[17] Noticeably, most previous attempts to use silica nanoparticles as gene carriers have been made using mesoporous nanoparticles (MSNs). Regular MSNs are not good carriers of plasmidic DNA because of their small pores (2 nm), that prevent internal plasmid diffusion and compaction.[18] As a consequence, pDNA is stuck at

the surface and is not protected against cellular nucleases. To overcome this problem, MSN with ultra-large pores (23 nm) have been prepared.[19-20] These particles were able to pack pDNA and succeeded in transfecting cells. Alternatively, MSNs loaded with an anticancer drug were coated with PEI allowing for DNA SiRNA conjugation and delivery.[4] Our approach has the advantage of technical simplicity and short reaction time. Moreover, the possibility to encapsulate active drugs within Stöber particles has already been demonstrated so that combination of drug and gene delivery using such plain SiNPs appears feasible.[12]

Considering the applications of the here-described nanocomposites, it is first important to point out that tissue repair involves the formation of new healthy tissue in the wound site requires several phases well-orchestrated to guide the tissue formation. Inflammation is crucial for the debridement of necrotic tissue and to kill bacteria. In absence of modulation, a chronic inflammation can occur.[21] The incorporation of a therapeutic gene modulating inflammation such as IL-10 within collagen nanocomposites could be useful to promote wound healing. In addition inflammatory cells that infiltrate the implant could be directed towards a wound healing phenotype instead of an inflammatory one. Synthetic matrices made from biodegradable polymers such as PLGA or Polycaprolactone were previously evaluated for gene delivery.[22-23] DNA/PEI complexes are mixed with the polymer in solution before matrix synthesis. In this case, polyplexes are encapsulated within material walls. This allows for a controlled and sustained delivery of polyplexes but requires a large porosity for cell infiltration. Moreover, synthetic polymers are not the natural support of fibroblasts and are not remodelled by cells. Alternatively, several collagen based-materials have been developed. Most of them are cross-linked collagen sponges rehydrated with a polyplexes solution (Transfecting reagent/pDNA). Polyplexes are therefore adhering to the sponge wall and easily detached under flow. As a consequence a rapid diffusion of polyplexes occurs preventing a precise spatio-temporal control of the gene delivery process.[24] In this perspective, the silica-collagen materials combine several advantages. As demonstrated earlier, the stiffness of collagen hydrogels at 1 $mg.mL^{-1}$ promote fibroblast proliferation over one week and favour cell infiltration thanks to a pore size of ca. 5 μm.[1] This is highly beneficial to the target application as proliferating cells are more willing to be transfected than quiescent ones.[25] The other major advantage of the nanocomposites approach is that the DNA-loaded particles cannot diffuse out of the hydrogel. Therefore, in the first period after implantation, the delivery of plasmids to the immobilized cells would allow for the production and release of proteins. In a second phase, silica-collagen hydrogels will be

colonized by inflammatory and connective cells.[26] Our data suggest that cells from the host organism could also be transfected during implant infiltration. Overall, it should allow for a prolonged production and delivery of active proteins at the implantation site and in its surrounding, favoring neotissue formation.

II.4 CONCLUSION

We have demonstrated that PEI-coated plain silica nanoparticles are able to deliver therapeutic genes in a controlled and sustained manner within collagen hydrogels. The gene delivery properties of these particles were evidenced when they are transported through pre-formed cellularized hydrogels or co-entrapped with fibroblasts, whereas no transfection was observed for cells external to the material. This offers various and safe options to combine silica and collagen to design gene delivery systems promoting wound healing.

These results lead to two important questions. One of more fundamental nature is related to the mechanisms of the transfection process when silica particles are used as vectors. In fact we have observed that best transfection levels were obtained for free PEI_{25} and that the highest transfection efficiency for silica-based systems was at least one order below these values. One possible approach to address this important question is to modifiy the mode of association between the silica particles and PEI, which should impact on the intracellular process of plasmid delivery. The second point that needs to be addressed is related to the possible applications of these materials. Above-described results were obtained using immortalized mouse fibroblast cells, which constitute a robust and easy-to-work model. However, if medical applications are foreseen, the technology has to be transferred to human cells. Therefore it was of primary importance to study the transfection efficiency of the silica@PEI vectors in primary skin cells, both in 2D and 3D configurations.

REFERENCES

(1) Helary, C.; Bataille, I.; Abed, A.; Illoul, C.; Anglo, A.; Louedec, L.; Letourneur, D.; Meddahi-Pellé, A.; Giraud-Guille, M. M. Concentrated Collagen Hydrogels as Dermal Substitutes. *Biomaterials* **2010**, *31*, 481-490.

(2) Rejman, J.; Oberle, V.; Zuhorn, I. S.; Hoekstra, D. Size-dependent Internalization of Particles via the Pathways of Clathrin- and Caveolae-mediated Endocytosis. *Biochem. J.* **2004**, *377*, 159-169.

(3) Wightman, L.; Kircheis, R.; Rossler, V.; Carotta, S.; Ruzicka, R.; Kursa, M.; Wagner, E. Different Behavior of Branched and Linear Polyethylenimine for Gene Delivery In vitro and In vivo. *J. Gene Med.* **2001**, *3*, 362-372.

(4) Xia, T.; Kovochich, M.; Liong, M.; Meng, H.; Kabehie, S.; George, S.; Zink, J. I.; Nel, A. E. Polyethyleneimine Coating Enhances the Cellular Uptake of Mesoporous Silica Nanoparticles and Allows Safe Delivery of siRNA and DNA Constructs. *ACS Nano* **2009**, *3*, 3273-3286.

(5) Godbey, W. T.; Wu, K. K.; Mikos, A. G. Poly(ethylenimine) and Its Role in Gene Delivery. *J. Controlled Release* **1999**, *60*, 149-160.

(6) Godbey, W. T.; Ku, K. K.; Hirasaki, G. J.; Mikos, A. G., Improved Packing of Poly(ethylenimine)/DNA Complexes Increases Transfection Efficiency. *Gene Ther.* **1999**, *6*, 1380-1388.

(7) Felgner, P. L.; Gadek, T. R.; Holm, M.; Roman, R.; Chan, H. W.; Wenz, M.; Northrop, J. P.; Ringold, G. M.; Danielsen, M. Lipofection - a Highly Efficient, Lipid-Mediated DNA-Transfection Procedure. *Proc. Natl. Acad. Sci. U. S. A.* **1987**, *84*, 7413-7417.

(8) Quignard, S.; Mosser, G.; Boissière, M.; Coradin, T. Long-term Fate of Silica Nanoparticles Interacting with Human Dermal Fibroblasts. *Biomaterials* **2012**, *33*, 4431-4442.

(9) Quignard, S.; Helary, C.; Boissiere, M.; Fullana, J.-M.; Lagree, P.-Y.; Coradin, T. Behaviour of Silica Nanoparticles in Dermis-like Cellularized Collagen Hydrogels. *Biomater. Sci.* **2014**, *2*, 484-492.

(10) Powers, J. G.; Morton, L. M.; Phillips, T. J. Dressings for Chronic Wounds. *Dermatol. Ther.* **2013**, *26*, 197-206.

(11) Slaughter, B. V.; Khurshid, S. S.; Fisher, O. Z.; Khademhosseini, A.; Peppas, N. A. Hydrogels in Regenerative Medicine. *Adv. Mater.* **2009**, *21*, 3307-3329.

(12) Alvarez, G. S.; Helary, C.; Mebert, A. M.; Wang, X. L.; Coradin, T.; Desimone, M. F. Antibiotic-loaded Silica Nanoparticle-collagen Composite Hydrogels with Prolonged Antimicrobial Activity for Wound Infection Prevention. *J. Mater. Chem. B.* **2014**, *2*, 4660-4670.

(13) Grinnell, F. Fibroblast Biology in Three-Dimensional Collagen Matrices. *Trends Cell Biol.* **2003**, *13*, 264-269.

(14) Grinnell, F.; Petroll, W. M. Cell Motility and Mechanics in Three-Dimensional Collagen Matrices. *Annu. Rev. Cell Dev. Biol.* **2010**, *26*, 335-361.

(15) Chen, K. H.; Zhang, J. X.; Gu, H. C. Dissolution from Inside: A Unique Degradation Behaviour of Core-shell Magnetic Mesoporous Silica Nanoparticles and the Effect of Polyethyleneimine Coating. *J. Mater. Chem.* **2012**, *22*, 22005-22012.

(16) Ferrari, M. Beyond Drug Delivery. *Nat. Nanotechnol.* **2008**, *3*, 131-132.

(17) Kettiger, H.; Schipanski, A.; Wick, P.; Huwyler, J. Engineered Nanomaterial Uptake and Tissue Distribution: from Cell to Organism. *Int. J. Nanomed.* **2013**, *8*, 3255-3269.

(18) Mamaeva, V.; Sahlgren, C.; Linden, M. Mesoporous Silica Nanoparticles in Medicine-Recent advances. *Adv. Drug Delivery Rev.* **2013**, *65*, 689-702.

(19) Kim, M.-H.; Na, H.-K.; Kim, Y.-K.; Ryoo, S.-R.; Cho, H. S.; Lee, K. E.; Jeon, H.; Ryoo, R.; Min, D.-H. Facile Synthesis of Monodispersed Mesoporous Silica Nanoparticles with Ultralarge Pores and Their Application in Gene Delivery. *ACS Nano* **2011**, *5*, 3568-3576.

(20) Gao, F.; Botella, P.; Corma, A.; Blesa, J.; Dong, L. Monodispersed Mesoporous Silica Nanoparticles with Very Large Pores for Enhanced Adsorption and Release of DNA. *J. Phys. Chem. B* **2009**, *113*, 1796-1804.

(21) Eming, S. A.; Krieg, T.; Davidson, J. M. Inflammation in Wound Repair: Molecular and Cellular Mechanisms. *J. Invest. Dermatol.* **2007**, *127*, 514-525.

(22) Shea, L. D.; Smiley, E.; Bonadio, J.; Mooney, D. J. DNA Delivery From Polymer Matrices for Tissue Engineering. *Nat. Biotechnol.* **1999**, *17*, 551-554.

(23) Holladay, C.; Keeney, M.; Greiser, U.; Murphy, M.; O'Brien, T.; Pandit, A. A Matrix Reservoir for Improved Control of Non-viral Gene Delivery. *J. Controlled Release* **2009**, *136*, 220-225.

(24) Jang, J. H.; Rives, C. B.; Shea, L. D. Plasmid Delivery In vivo From Porous Tissue-Engineering Scaffolds: Transgene Expression and Cellular Transfection. *Mol. Ther.* **2005**, *12*, 475-483.

(25) Cam, C.; Segura, T. Matrix-based Gene Delivery for Tissue Repair. *Curr. Opin. Biotechnol.* **2013**, *24*, 855-863.

(26) Desimone, M. F.; Helary, C.; Quignard, S.; Rietveld, I. B.; Bataille, I.; Copello, G. J.; Mosser, G.; Giraud-Guille, M. M.; Livage, J.; Meddahi-Pelle, A.; Coradin, T. In vitro Studies and Preliminary In vivo Evaluation of Silicified Concentrated Collagen Hydrogels. *ACS Appl. Mater. Interfaces* **2011**, *3*, 3831-3838.

CHAPITRE III

Influence de la chimie des particules de silice et du type cellulaire sur l'efficacité de la transfection

CHAPITRE III

Influence de la chimie des particules de silice et du type cellulaire sur l'efficacité de la transfection

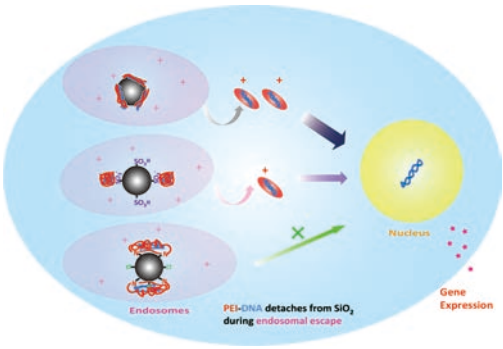

Résumé

Dans ce chapitre, nous avons exploré plus avant les capacités de transfection des particules de silice. Nous avons tout d'abord tenté de moduler l'efficacité de transfection en changeant la nature de l'interaction silice-PEI. Pour cela, des groupements sulfonates et chlorure d'alkyle ont été introduits en surface. Les particules non modifiées ont montré une quantité maximale de PEI adsorbé et une efficacité de transfection optimale. La présence de sulfonates diminue ces deux paramètres malgré un ratio optimal particule:ADN similaire aux particules nues. La liaison covalente a un impact négatif sur l'ensemble des propriétés. Ces résultats indiquent que le renforcement des interactions silice-PEI peut être défavorable à la transfection. Ceci suggère que le détachement du complexe PEI:ADN de la particule dans les endosomes est une étape clé de ce processus. Dans un deuxième temps, nous avons étudié la transfection de cellules humaines primaires, en vue d'applications in vivo. Nous montrons que la transfection en 2D par des particules silice-PEI est possible avec des fibroblastes et des keratinocytes humains et en 3D avec les fibroblastes, mais avec des efficacités moindres que pour les cellules 3T3. Ceci est attribué au plus faible taux de prolifération des cellules primaires.

En révision dans *Langmuir*

III-1. GENERAL INTRODUCTION

Despite the success of our strategy based on collagen-based nanocomposite hydrogels, further steps were required before being able to propose a fully functional biomaterial. First, the performances of PEI-coated silica particles in terms of transfection efficiency were significantly smaller than PEI (25 kD) alone. We hypothesized that the modulation of the silica-PEI interactions may impact on the plasmid loading, complex internalization and/or transfer to the cell nucleus. As shown hereafter, varying the strength of interaction between the particle surface and the polymer indeed has a deep impact on the transfection efficiency. This study also provides interesting insights on the intracellular mechanism of transfection.

The second point to be addressed was related to the extension of our approach from immortalized fibroblasts to human primary cells, a necessary step if cellularized dressings are targeted. The study illustrates the cell-dependent efficiency of the transfection, particularly emphasizing the relationship between the cell proliferation rate and the protein expression efficiency.

III-2. IMPACT OF POLYETHYLENEIMINE CONJUGATION MODE ON CELL TRANSFECTION EFFICIENCY OF SILICA NANOPARTICLES

III-2-1. Preparation and Functionalization of Silica Nanoparticles

In order to study the influence of the conjugation mode of PEI on the transfection efficiency of the silica nanoparticles, we have prepared three different particles : naked particles SiO_2, particles grafted with propylsulfonate moieties SiO_2-SO_3, both of which can adsorb PEI via electrostatic interactions, and particles grafted with propylchloride moieties, allowing for its covalent grafting. Naked silica nanoparticles SiO_2 (200 nm) and PEI (25 kD)-coated SiO_2@PEI were prepared following the procedure described in section **II-2-1**.

For SiO_2-SO_3@PEI particle preparation,[1] the SiNP was first functionalized with thiol groups by silylation with 3-mercaptopropyltrimethoxysilane (MPTMS). Typically, 1 g of silica was dispersed in a mixture of 100 ml ethanol and 2.2 ml ammonium hydroxide solution before addition of 1 ml MPTMS. The mixture was stirred for 40 min at room temperature. Subsequently, the reaction mixture was heated to 80 °C and the total volume was reduced by 2/3 by distillation of ethanol and ammonia at ambient pressure. Then, the mixture was cooled back to room temperature, centrifuged, washed 3 times with ethanol and dried at 60 °C.

The amount of –SH was determined by Ellman test.[2] For this test, a phosphate buffer (0.2 M, pH = 7.3) was prepared and labeled as solution A. Solution B (10 mM EDTA) was produced by dissolving 372 mg of EDTA in 100 mL of solution A, and solution C (6 mM 5-(3-Carboxy-4-nitrophenyl)disulfanyl-2-nitrobenzoic acid -DTNB) was prepared by dissolving 238 mg of DTNB in 100 mL of solution A. Several vials were filled with a mixture of 8 ml of solution A, 1 mL of solution B and 1 mL of solution C. A series of masses of SiO_2-SH, less than 50 mg, were measured and then each dispersed into a vial mixture solution. Simultaneously, several known quantities of thiol (obtained from a solution of MPTMS) were also introduced in the same mixture solution to determine the molar extinction coefficient by linear regression. After 45 minutes of stirring, the particle dispersion is filtered through a syringe filter. The absorbance of the filtrate and standard MPTMS solutions are determined by spectrophotometry. The absorbance of the solutions MTPMS can be traced back to the value for the experience of the molar extinction coefficient of NTB^{2-} by linear regression.

Then 0.9 g of the thus-obtained SiO_2-SH was suspended in 45 mL hydrogen peroxide (H_2O_2 35%, Acros Organics) under stirring at RT for 48 hours. The solid product was washed by centrifugation with distilled water before addition of 35 mL of concentrated sulfuric acid (H_2SO_4 95.0-98.0%, Sigma Aldrich) and stirred for 2 hours at RT. Finally the as-synthesized SiO_2-SO_3 particles were washed with water, suspended in PBS and coated with PEI as described above.

For SiO_2-Cl@PEI particle preparation**,** 400 mg of SiO_2 nanoparticles was dispersed in 20 mL of dried toluene, and 1.3 mL of chloropropyltriethoxysilane (Cl-PTES) was added to the suspension, that was further kept under reflux for 24 h. The product was washed thoroughly with toluene and ethanol, and dried at room temperature. Then, 200 mg SiO_2-Cl was dispersed in 20 ml ethanol, and 0.8 g of PEI was added to the suspension. The suspension was refluxed for 24 h. The final solid product was recovered by washing with ethanol and dried at room temperature. The as-synthesized SiNP-Cl@PEI was suspended in 10 mM PBS (pH 7.4) before use.

III-2-2. Particle characterization

Silica nanoparticles SiO_2 were synthesized by the Stöber method and obtained with a low size dispersity (210 ± 20 nm, from TEM with a polydispersity index PDI = 0.005) (**Figure III-1**).

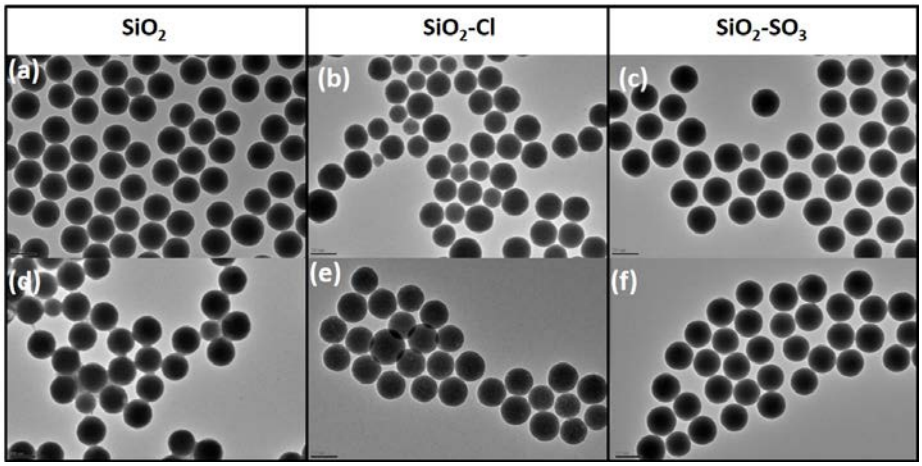

Figure III-1. TEM images of SiO_2, SiO_2-SO_3, SiO_2-Cl before(A-C) and after (D-F) modification with PEI 25 kDa

	d (nm)	ζ (mV)	Cl:Si (wt%)	N:Si (wt%)	PEI (wt%)	silane/ particle	amine/ particle
SiO_2	214 ± 17	-15 ± 6	-	-	-	-	-
SiO_2@PEI	188 ± 68	+20 ± 7	-	11.0	12.7	-	510[6]
SiO_2-SO_3	233 ± 38	-21 ± 8	-	-	-	1.510[4a]	-
SiO_2-SO_3@PEI	221 ± 20	+21 ± 9	-	3.8	4.2	ND[b]	1.510[6]
SiO_2-Cl	518 ± 308	-13 ± 6	2.7	-	-	1.710[6]	
SiO_2-Cl@PEI	806 ± 642	+18 ± 9	1.1	3.1	3.4	ND[b]	10[6]

[a]from Ellman titration; [b]ND= not determined

Table III-1. Hydrodynamic diameter (*d*), zeta potential ζ in PBS, elemental analysis and calculated composition of the particles

After coating with PEI, the particle hydrodynamic diameter (*d*) in PBS was not significantly modified but the PDI significantly increased to 0.127. The zeta potential (ζ) value turned from negative to positive in PBS, in agreement with the deposition of a cationic polymer (**Table III-1**). In the case of sulfonated SiO_2-SO_3 particles, neither surface

functionalization nor PEI sorption significantly impacted on the colloidal size distribution. The mean ζ value of SiO_2-SO_3 particles was slightly more negative than for bare silica, due to the presence of acidic sulfonate moieties, but the ζ value after PEI coating was similar for both particles. The SiO_2-Cl nanoparticles showed a high tendency to aggregate, as such and after PEI conjugation, with high PDIs in both situations. However, the ζ values were not significantly different from the two previous systems (**Table III-1**).

Elemental analysis allowed for the quantification of grafted moieties and amount of surface PEI (**Table III-1**). From the Cl:Si weight ratio, it was possible to estimate grafting density per particle of *ca*. $1.5x10^6$ silanes for SiO_2-Cl. For SiO_2-SO_3, the S content was below 0.1 wt% so that the silane density was obtained by the Ellman test, yielding to a grafting density per particle of *ca*. $1.5x10^4$ groups. The Cl:Si ratio decreased from 2.7:100 to 1.1:100 upon reaction with PEI, supporting the occurrence of a nucleophilic substitution reaction between the propylchloride moiety and some amine groups of the polymer. In parallel, the highest amount of bound PEI was obtained for SiO_2@PEI (12 w%) while the two other systems had a significantly lower binding capacity (4 wt% for SiO_2-SO_3@PEI and 3 wt% for SiO_2-Cl@PEI).

Surface modified particles before PEI sorption were studied using ^{29}Si solid-state magic angle spinning (MAS) NMR measurements. These experiments, and all other NMR studies reported hereafter, were performed by S. Masse and G. Laurent (LCMCP) on a Bruker Avance III 300 MHz equipment.

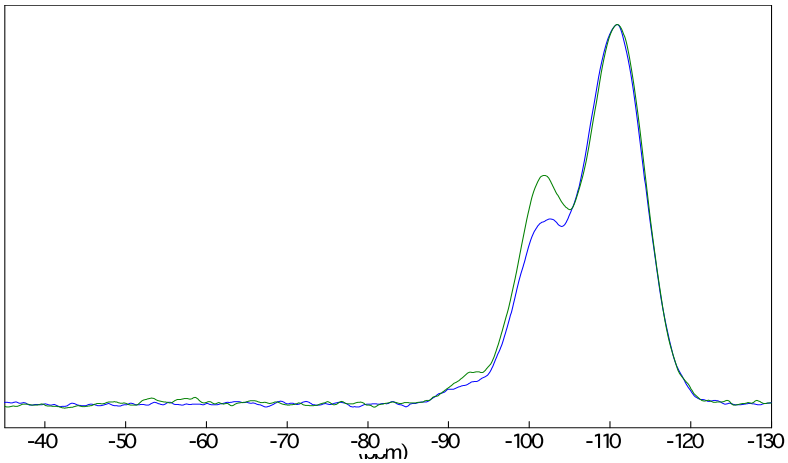

Figure III-2. ^{29}Si MAS NMR spectra of (blue line) SiO_2-SO_3 and (green line) SiO_2-Cl. Experiments were carried out using a single-pulse technique and high power ^{1}H decoupling (HPDEC) at a 5 kHz spinning rate with 30° pulses and a recycling delay of 60 s with 720 and 840 scans, respectively

As seen on **Figure III-2**, three main peaks at ca. -110 ppm, -100 ppm and -90 ppm are obtained for both SiO_2-Cl and SiO_2-SO_3. These resonances correspond to Q_4 ($Si(OSi)_4$), Q_3 ($Si(OSi)_3OR$) and Q_2 ($Si(OSi)_2(OR)_2$) silicon atoms (where R can be an organic group or an hydrogen atom). The predominance of Q_4 species indicates that the particles have a high degree of condensation. When SiO_2-Cl and SiO_2-SO_3 are compared, the former has a higher relative amount of Q_3 and Q_2 compared to the latter, in agreement with the larger grafting density.

More information about the grafting reaction was obtained using ^{29}Si-{^{1}H} cross-polarization (CP) MAS experiment.[3] This technique allows to enhance the signal of silicon species that are in close proximity to hydrogen atoms. As seen on **Figure III-3,** two additional signals of weak intensity are present of the spectra of SiO_2-SO_3 at *ca*. -65 ppm and -57 ppm. They are more clearly evidenced of the spectra of SiO_2-Cl, together with another signal at - 48 ppm. These signals correspond to T_3 ($SiR'(OSi)_3$), T_2 ($SiR'(OSi)_2OR$) and T_1 ($SiR'(OSi)(OR)_2$) silicon species, respectively, where R' is an organic group covalently bound to Si. Although these species have long been attributed to organosilanes that are individually attached to the silica surface by 1 to 3 Si-O-Si bonds, it is now well-accepted that silanization of silica particle surface leads to more complex situations where pre-condensed short chains of silanes are formed before grafting.[4]

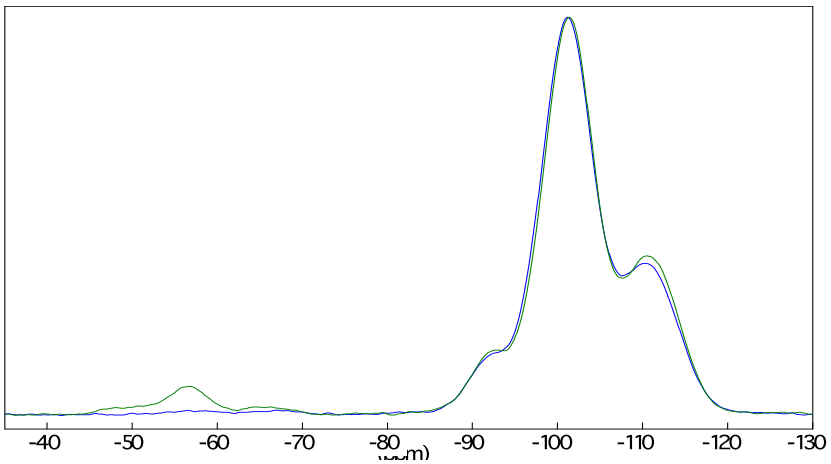

Figure III-3. ^{29}Si-{^{1}H} CP MAS NMR spectra of (blue line) SiO_2-SO_3 and (green line) SiO_2-Cl. Experiments were carried out with a recycling delay of 1 s, a 1 ms contact time with 4096 scans for both samples

The surface composition of the particles was studied by X-Ray Photoelectron Spectroscopy in collaboration with C. Méthivier, Laboratoire de Réactivité de Surface. The surveys of uncoated and coated particles, together with pure PEI are shown in **Figure III-4**, together with the relative abundance (in atom %) of each element. Detailed spectra for each region are provided at the end of this chapter, except for N_{1S} provided as **Figure III-5.**

For PEI, carbon and nitrogen elements are identified in a C:N atomic ratio of 70:30, in fair agreement with the overall C_2H_5N formula of ethylene imine. The C_{1s} data show an asymmetric peak in the 284-288 eV region, corresponding to the overlap of C-C (285 eV) and C-N (287 eV) signals.[5] The N_{1s} signal consists of a single peak centered à 399 eV that can be attributed to primary/secondary/tertiary amines. For SiO_2, the typical peaks of amorphous silica are observed at 103 eV (Si_{2p}) and 534 eV (O_{1s}).[6] A weak C_{1s} signal is also obtained that can be attributed to carbon surface contamination as well as possible unhydrolyzed $Si(OC_2H_5)$ moieties.

The XPS spectrum of SiO_2@PEI particles combines the Si, O and C peaks of SiO_2 and PEI. However, the N_{1S} data showed two populations at 399 eV and 401 eV in a 56:44 intensity ratio, the latter corresponding quartenary amines (**Figure III-5**).[7] The presence of sulfonate groups could be ascertained by the presence of a S_{2s} signal at 232 eV for SiO_2-SO_3.[8] Compared to SiO_2, the C_{1s} region showed an additional signal near 289 eV that can be attributed to the C-S bond. PEI coating did not significantly modify the C, O, Si and S signals. At the N_{1s} level, the 399 eV and 401 eV peaks are again identified but with an intensity ratio of 64:36. For SiO_2-Cl, the Cl_{2p} peak near 200 eV confirms the successful grafting of Cl-PTES.[9] Similarly to SiO_2-SO_3, the C_{1s} signal shows a high energy contribution corresponding to C-Cl bond. For SiO_2-Cl@PEI, the Cl_{2p} signal was still clearly evidenced but a slight decrease of the Cl:Si ratio was found, in qualitative agreement with the elemental analysis results. The signal at the N_{1s} level indicates a unprotonated:protonated amine ratio of 72:28, the highest value in this series.

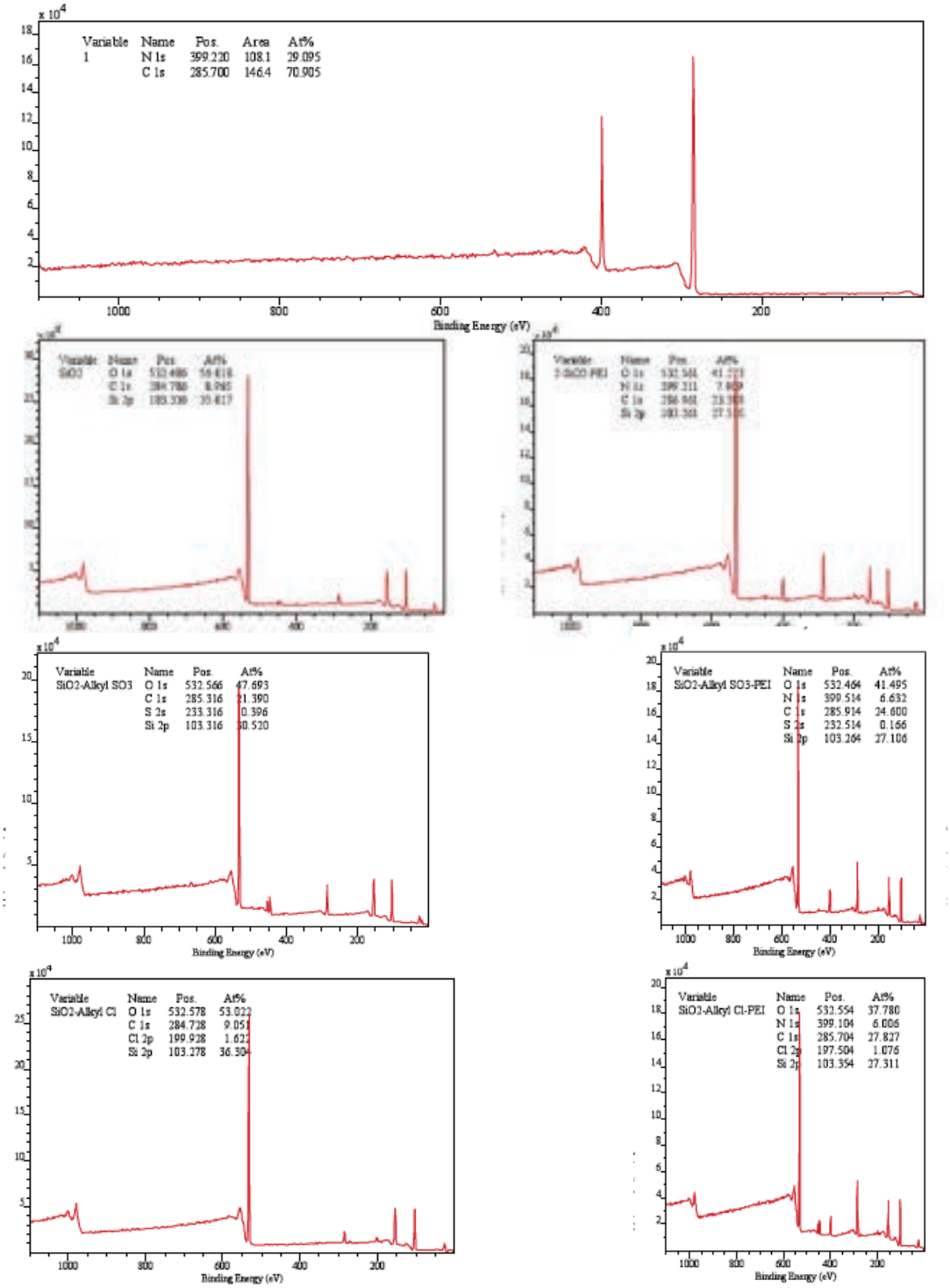

Figure III-4. XPS survey spectra of PEI (top image) and particles before (left hand column) and after (right hand column) reaction with PEI.

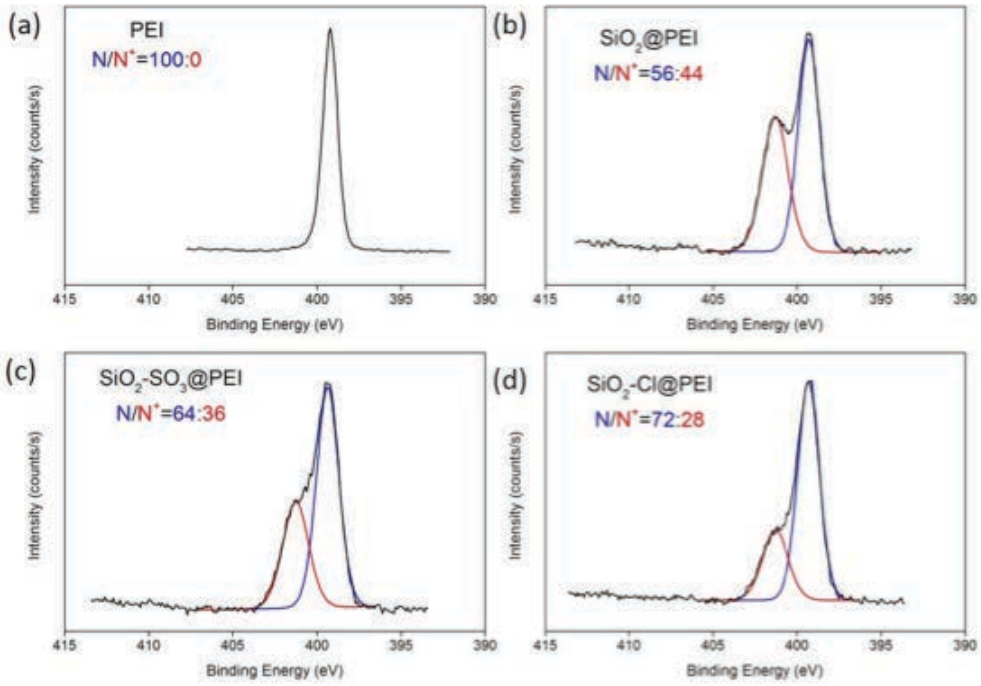

Figure III-5. XPS spectra at the N1s level and their deconvolution for pure PEI and PEI-coated particles.

Attempts were made to further characterize PEI immobilized on the particle surface using ^{13}C NMR. Although the main idea was to compare the ^{13}C-{^{1}H} CP-MAS NMR spectra of the polymer before and after sorption, the problem was faced that pure PEI is a liquid. Therefore the CP-MAS approach cannot be applied to this sample and the only spectra that could be recorded was the ^{13}C High Power Decoupled (HPDec)-MAS spectra. This spectrum is shown on **Figure III-6** and compared to the ^{13}C-{^{1}H} CP-MAS NMR spectra of SiO_2@PEI. As expected, PEI in the liquid state shows well-defined narrow resonance peaks in the 35-60 ppm region. In contrast, adsorbed PEI shows two broad bands in the same region due to its low mobility. It is clear from this comparison that it is not possible to draw any conclusion on the chemical or structural modification of PEI after sorption from this technique.

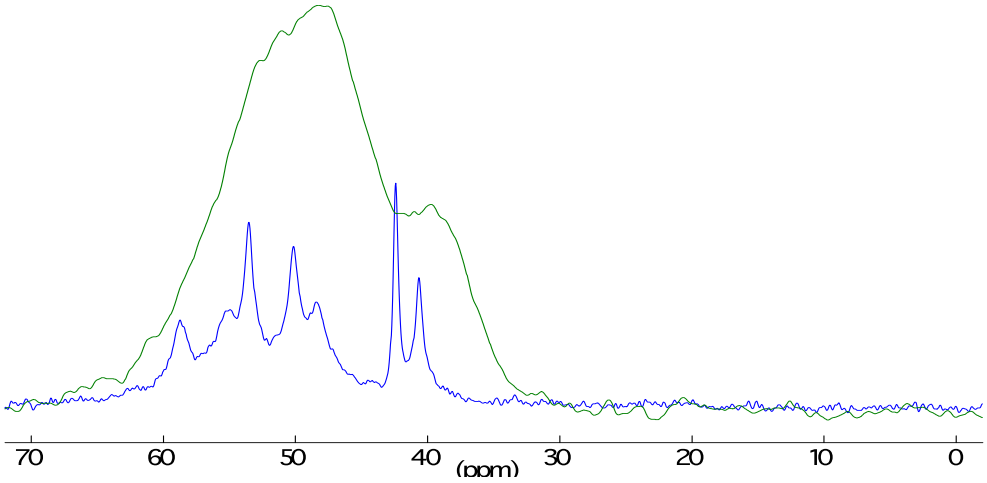

Figure III-6 Blue line: ^{13}C HPDec spectra of PEI (Recycle time: 3s@30°; NS: 280; rotation: 300 Hz); green line: ^{13}C-{^{1}H} CP-MAS NMR of SiO_2@PEI (Recycle time: 1s; contact time: 1ms; NS: 4096; rot: 5 kHz)

The possibility to focus on the grafted moieties rather than PEI itself was then studied. This allows for the comparison of these functions before and after PEI reaction in the solid state. The drawback is that, based on the chemical composition of the particles, the intensity of the resonances belonging to the grafted groups were expected to be smaller than that of PEI and that some overlap may exist between the peaks of the two systems. This happened to be the case for SiO_2-SO_3 that was not further studied. In contrast, for SiO_2-Cl (that has a significantly higher amount of grafted moieties compared to SiO_2-SO_3), some resonances of high intensity could be observed outside the chemical shift region of PEI (**Figure III-7**). However, although a comparison between the two spectra shows some modifications of the relative intensities of the peaks, it is still difficult to draw any useful conclusion from these spectra.

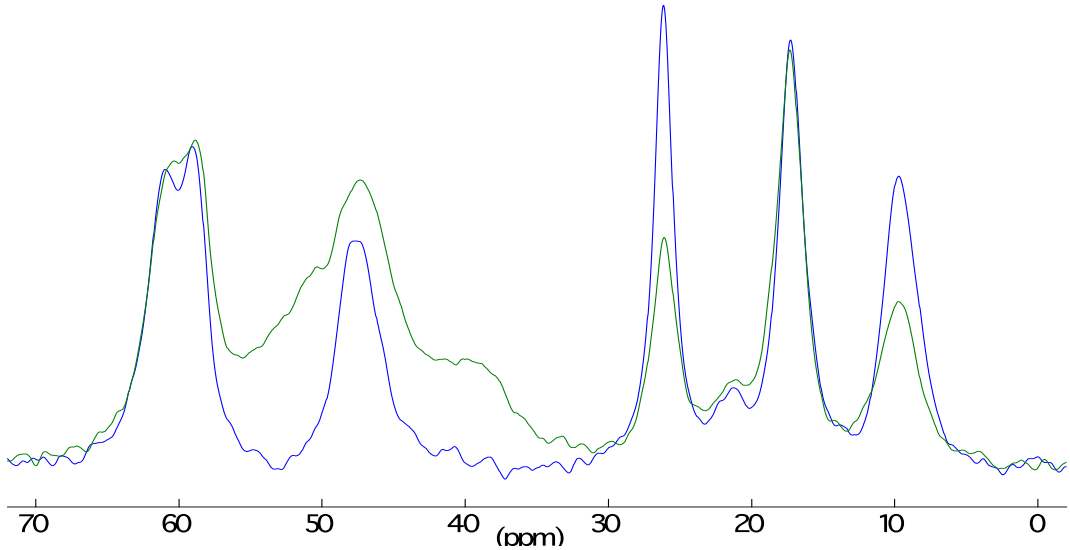

Figure III-7 ^{13}C-{^{1}H} CP-MAS NMR of (blue) SiO_2-Cl and (green) SiO_2-Cl@PEI (Recycle time: 1s; contact time: 1ms; NS: 4096; ro: 5 kHz).

It was then hypothesized that the covalent binding of the propylchloride chain to PEI may have an effect on the propyl chain mobility. To check this, an inversion recovery cross polarization (IRCP) approach was used.[10] This technique allows for the discrimination of elements of different mobilities in a single system but also to compare the mobility of different systems. This mobility can be estimated from the inversion time t_i at which a given NMR signal turns from positive to negative. The IRCP-MAS NMR spectra of SiO_2-Cl is shown in the upper part of **Figure III-8**. Resonances at 10 ppm, 28 ppm and 48 ppm correspond to the propyl chain whereas the peaks at 17 ppm and 59 ppm correspond to unhydrolyzed ethoxy groups of TEOS. Focusing on the 48 ppm signal corresponding to the C atom in α position of the Cl atom, its inversion time lies in the 200-300 µs range. The lower part of Figure III-9 shows the IRCP-MAS NMR spectra of SiO_2-Cl@PEI. In this case, t_i can be estimated in the 50-70 µs range. Such a decrease in inversion time is correlated with an increase of the cross-polarization rate and therefore a decrease in mobility of the Cα atom, supporting the occurrence of a strong interaction between the end of the propyl chains and PEI.

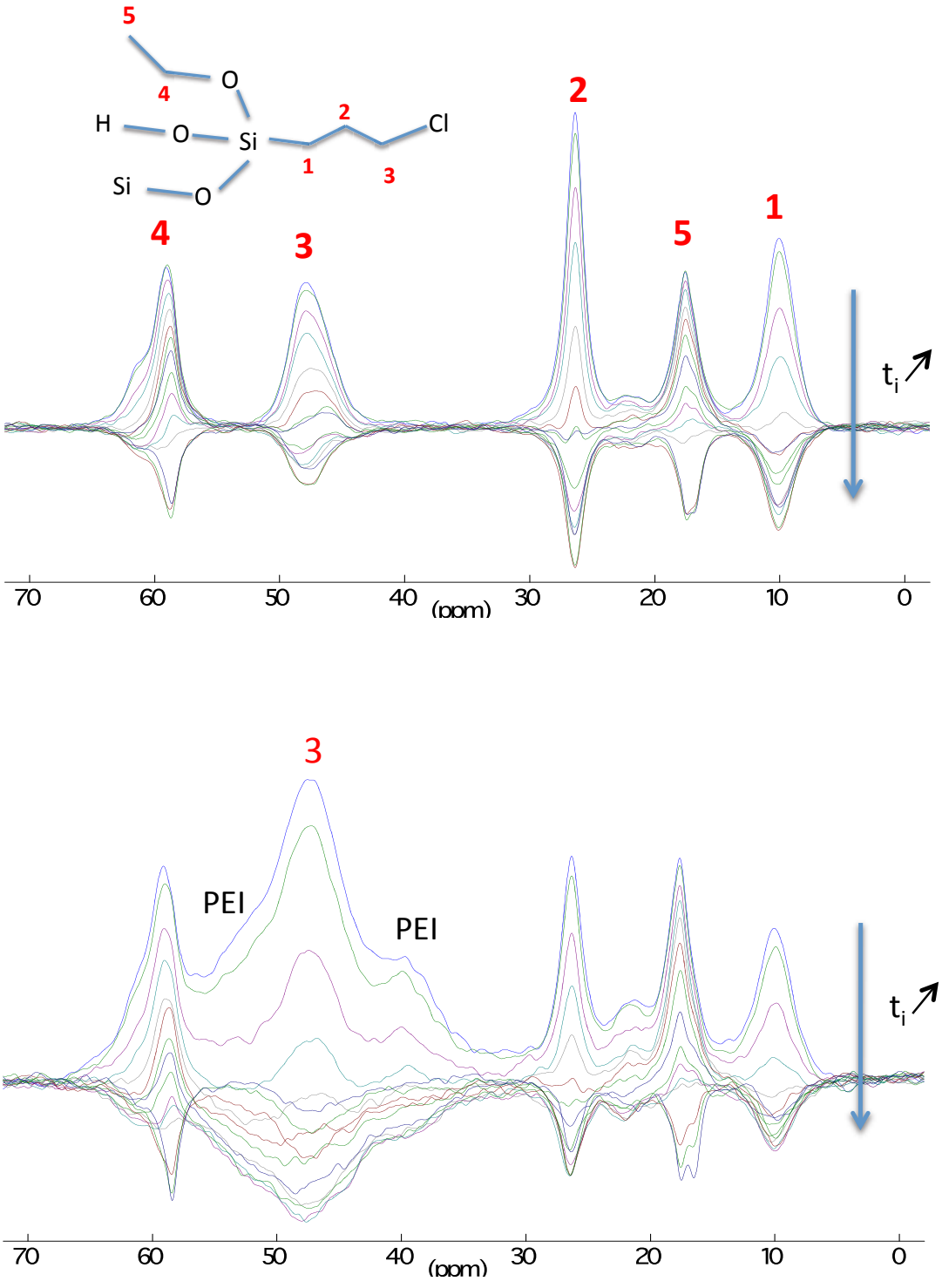

Figure III-8. ^{13}C Inversion recovery cross polarization (IRCP)-MAS NMR spectra of (a) SiO_2-Cl and (b) SiO_2-Cl@PEI. Main acquisition parameters used for the IRCP exp.: Recycle time: 1s; contact time: 1ms; NS: 4096; ro: 5 kHz; inversion time t_i (from top to bottom): 5, 10, 20, 30, 50, 70, 100, 200, 300, 500, 700, 1.000, 3.000, 5.000, 10.000 µs.

III-2-3. Transfection experiments

Protocols used in the following section were the same as those described in **Chapter II**, except for the additional use of primary normal human keratinocytes (NHK) that were cultured in keratinocytes growth medium 2 (Promocell) supplemented with $CaCl_2$.

In a first step, the optimal p-Gluc:particle ratio was determined by gel electrophoresis using the procedure described in section **II-2-2** (**Figure III-9**). Full retention was achieved for pGLuc:SiO_2@PEI and pGLuc:SiO_2-SO_3@PEI: weight ratios of 1:30 whereas a 1:50 ratio was optimal for pGLuc:SiO_2-Cl@PEI. These ratios were used to evaluate the potential of particles@PEI systems to deliver G-Luc plasmids into 3T3 fibroblasts and human primary keratinocytes.

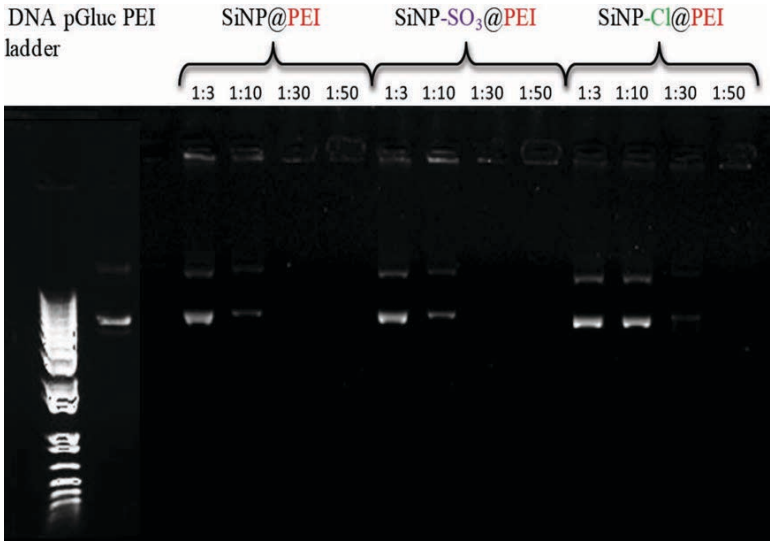

Figure III-9. Agarose gel electrophoresis showing the influence of PEI conjugation mode on pGLuc complexation. A constant amount of pGLuc (1µg) was complexed with particles at 1:3, 1:10, 1:30 and 1:50 weight ratios.

Delivery of therapeutic genes from PEI-coated silica nanoparticles requires the particles uptake by cells. Particle internalization within mouse 3T3 fibroblasts was checked using fluorescent FITC-silica nanoparticles after 48 h of contact. Observations by fluorescence microscopy evidenced the accumulation of colloids near the cell nucleus for SiO_2@PEI and

SiO_2-Cl@PEI (**Figure III-10A)**. Bleaching of the FITC probes during sulfonate particle preparation hindered their intracellular observation. Cytotoxicity of uncoated and PEI-coated particles was also studied on 3T3 fibroblasts. This study consisted in the measure of cell viability of fibroblasts incubated with increasing doses of particles (**Figure III-11B**). For particle@PEI systems, cell viability was always higher than 80 %, indicating the absence of significant cytotoxicity up to 50 µg.mL^{-1} in PEI. In contrast, PEI alone was detrimental to cell viability at a dose > 5 µg.mL^{-1}. Uncoated particles were evaluated using the same silica weights, showing no visible cytotoxicity effect.

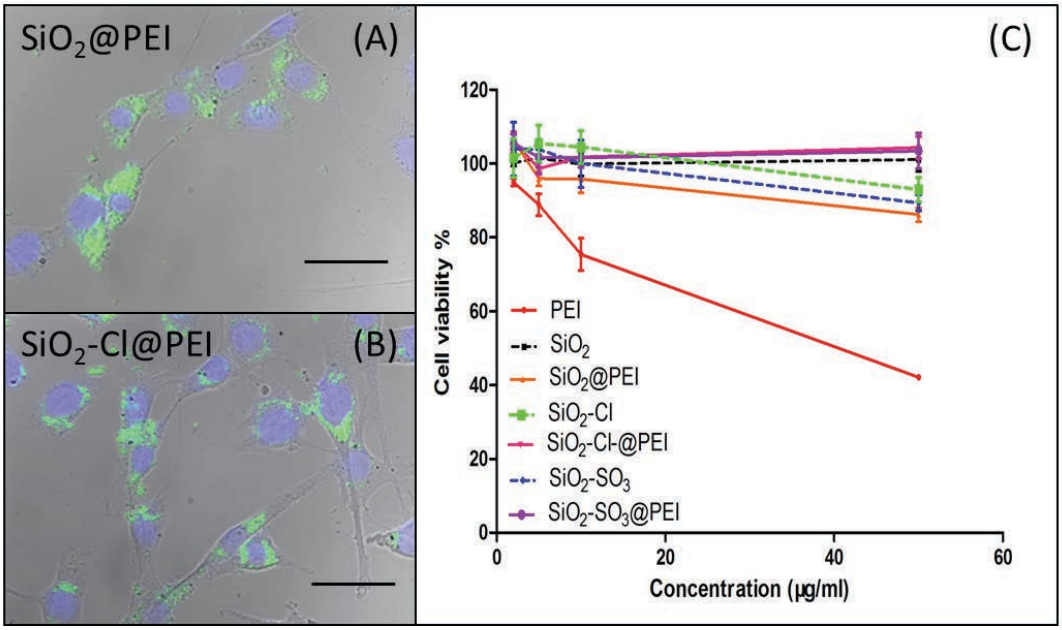

Figure III-10. (A and B) Fluorescence microscopy image showing internalization of pGLuc:particle@PEI by 3T3 fibroblasts after 48 h of incubation (green: FITC-labeled particles, blue : DAPI nuclei staining, scale bar = 20 µm) ; (C) Impact of PEI, particles and particle@PEI systems on 3T3 cell viability at the end of transfection experiments as monitored by the Alamar Blue test. Bar: 50µm.

The transfection efficiency of the particles was evaluated in 3T3 mouse fibroblasts and primary human keratinocytes using a plasmid encoding for Luciferase (pG-Luc) (**Figure III-11)**. Quantities of polymers used in this experiment were not toxic for cells with the aim of comparing the abilities of transfection of the different systems. The ability of transfection was first analyzed on immortalized 3T3 fibroblasts (**Figure III-11A)**. Among particles, the highest bioluminescence level was obtained with SiO_2@PEI, that was one order of magnitude below that of PEI alone. The efficiency of SiO_2-SO_3@PEI particles was ten times lower than

that measured with SiO_2@PEI. Last, a very weak luciferase activity was observed with the SiO_2-Cl@PEI system.

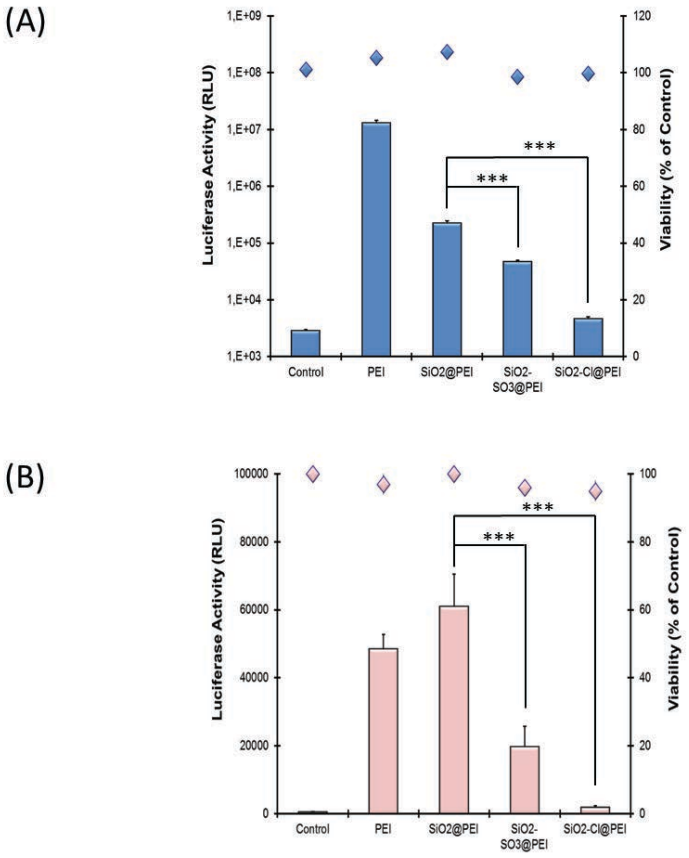

Figure III-11. Transfection of mouse 3T3 fibroblasts (A) and human primary keratinocytes (B) after a 4 h incubation period with pGLuc :particle@PEI systems. Variance of the luciferase expression among particle groups was determined by one-way ANOVA with Tukey posthoc test (*** $P < 0.001$)

Indeed, the luciferase activity was only the double of the basal level quantified in controls samples (without pG-Luc). The potential of PEI@particles to delivery genes was also investigated on primary normal human keratinocytes **(Figure III-11B**). The bioluminescene levels measured after incubation with the different systems of particles revealed the same profiles of transfection as those observed in 3T3 cells. The best ability of transfection was obtained with SiO_2@PEI. The transfection efficiency was three times lower with SiO_2-SO_3@PEI particles and that measured with the SiO_2-Cl@PEI system was very low. Compared with the performance of the different particles@PEI systems on 3T3 cells, the bioluminescence levels measured with keratinocytes were two times lower.

III-2-4. Discussion

III-2-4-1. Influence of conjugation mode on PEI attachment

These data indicate that the conjugation mode impacts on PEI content, charge and plasmid binding ability. For SiO_2@PEI, using a particle radius of 100 nm and a silica density of 2 $g.cm^{-3}$, the total amount of amine groups per particle can be estimated to *ca*. 5.10^6 from elemental analysis (**Table III-1**). The ammonium/total amine ratio obtained by XPS is *ca*. 45 % (i.e. *ca*. $2.2x10^6$ ammonium per particle). As a comparison a 30 % value was reported for PEI in a buffer solution (pH 7.4), suggesting that partial PEI protonation occurred during the adsorption process.[11] A density of 3-5 silanol per nm^2 was reported for amorphous silica surfaces, *i.e*. 4-$6x10^5$ SiOH for 200 nm particles, with 20 % of acidic (pKa = 4.5) and 80 % of basic (pKa = 8.5) groups.[12] The increase in PEI protonation may therefore arise from an acid-base reaction with the silanol groups. Comparing $5x10^5$ SiOH with $2.2x10^6$ N^+ per particle, the silanol:ammonium ratio is 1:4-5 so that the positive charge of PEI is not balanced by the negative charge of silica, explaining the positive ζ value of these systems.

For SiO_2-SO_3@PEI, the protonation degree of PEI is closer to the reported value in buffer (36 % vs. 30 %). Sulfonate groups are fully deprotonated at pH 7 so that proton exchange with PEI was not expected. The fact that the silanol groups do not significantly interact with the polymer suggests that PEI is kept apart from the silica surface. Interestingly, combined elemental analysis and XPS indicate that there are $5x10^5$ ammonium groups per particle to be compared with $1.5x10^4$ sulfonate groups. This observation can be compared with a recent study devoted to the sorption of collagen triple helices on the surface of silica particles.[1] For bare particles, a large amount of collagen was readily adsorbed, suggesting that the protein adopts a flat configuration on the particle surface. In contrast, sulfonate-bearing particles could adsorb less collagen but the proteins had a more ordered organization. It was suggested that the sulfonate groups could act as anchoring points for the protein chains that protrude out of the surface rather than laying flat, so that the amount of sorbed collagen was limited by the steric constraints of the triple helices packing. A similar situation can be reasonable assumed for the present system (**Figure III-12**). Noticeably, naked particles have a lower initial negative charge, bind more PEI with a higher degree of protonation than sulfonated ones, so that it was expected that they exhibit a higher positive surface charge after coating. However the two systems show close ζ values. This can be explained considering that silanol groups of the surface can contribute to the overall particle charge for SiO_2 whereas these moieties are

screened by the sulfonate/PEI layer, strengthening our model of a flat vs. compact organization of the polymer in the two systems.

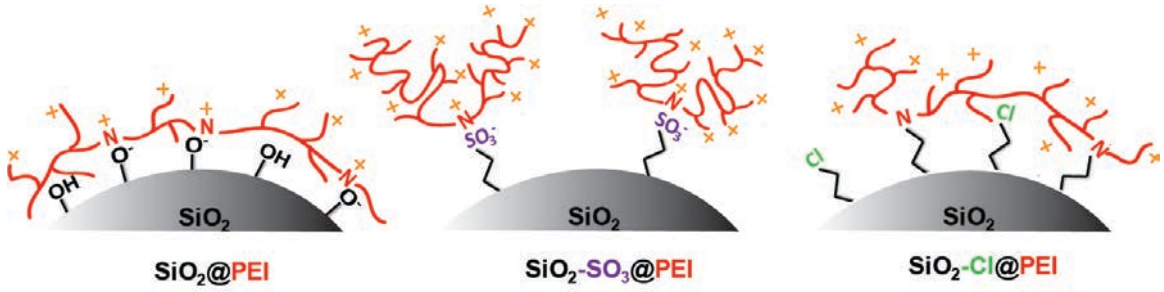

Figure III-12. Schematic representation of the different conjugation modes of polyethyleneimine (PEI) with silica particles and proposed PEI configuration: non-specific adsorption on silica particles (SiO_2@PEI), strong electrostatic interactions with sulfonate-modified silica particles (SiO_2-SO_3@PEI) and covalent bond with propylchloride-grafted silica particles (SiO_2-Cl@PEI).

For SiO_2-Cl@PEI, the protonation degree of PEI is similar to its free form in buffer and the number of amines per particle is *ca*. 10^6. This value is in the same range as the initial density of propylchloride groups ($1.5x10^6$). Elemental analysis indicate that one half of the Cl atoms are no longer present after reaction with PEI. Taken together these data suggest that an important fraction of the PEI amine groups have reacted with the propylchloride moieties. It is therefore possible to assume that each PEI chain is bound to the particle surface by several anchoring points, decreasing its conformational flexibility and therefore its maximum packing density on the surface, resulting in a low PEI loading (**Figure III-12**). Noticeably, SiO_2-Cl@PEI has a similar ζ value to SiO_2@PEI, which can be explained considering that the less negative surface charge of the chlorinated surface compared to bare particles is compensated by lower PEI loading and lower PEI protonation.

Considering the optimal plasmid:PEI ratio, it depends on the positive charge of PEI, as the PEI-plasmid system is a polyelectrolyte complex, as well as on the PEI flexibility, that determines its ability to wrap and compact DNA.[13,14] The amount of PEI per particle must also be considered for the optimal plasmid:particle ratio. SiO_2@PEI and SiO_2-SO_3@PEI particles have a similar optimal pGLuc:particle@PEI ratio although the former has a higher polymer loading with a larger proportion of ammonium groups than the latter. As pointed out earlier, the ζ value is not a suitable parameter to compare the complexing ability of the systems as it can include a contribution of the silica particle surface that is not involved in the DNA

wrapping process. Rather PEI conformation has to be considered (**Figure III-8**). For SiO_2, the extended conformation of the polyelectrolyte is not favorable for DNA wrapping whereas the local anchoring of PEI on the surface of Si-SO_3 should better preserve its structural flexibility. For SiO_2-Cl, as mentioned earlier, its flexibility should be limited by the high density of covalent bonds, resulting in a low pG-Luc:particle@PEI ratio.

III-2-4-2. Influence of conjugation mode on transfection efficiency

Despite their extensive study, the exact mechanisms driving cell transfection by non-viral vectors are still controversial.[15] Yet the main steps of the process have been identified. First, the DNA complex must be internalized by endocytosis, a process that depends on its size and charge. Here, the three particles exhibit similar positive charges compatible with internalization. SiO_2@PEI and Si-SO_3@PEI particles have similar dimensions (*ca*. 200 nm) in PBS whereas SiO_2-Cl@PEI dispersions show a tendency to aggregate into larger species (*ca*. 800 nm). Nevertheless fluorescence images suggest the successful internalization of a fraction of SiO_2-Cl@PEI particles. This could be explained by the de-aggregation of SiO2-Cl@PEI, allowing the uptake of individual particles. A second hypothesis relies on the polydispersity of SiO2-Cl@PEI particles. According to the results obtained by DLS, a small fraction of particles possesses the appropriate size (less than 400 nm) to be engulfed by cells. Despite the fact that the uptake abilities are cell dependent, it is generally admitted that particles larger than 500 nm are not likely to be internalized by endocytosis in mammalian cells.[16,17] This could explain the very low level of transfection. The question of the particle size, rather the covalent bonding seems to a crucial parameter for cellular uptake of SiO_2-Cl@PEI. Several groups have functionalized PEI by covalent attachment on mesoporous silica nanoparticles or on hyaluronic acid chains. They obtained particles:DNA complexes with a limited aggregation (less than 350 nm), thereby permitting cellular uptake and transfection.[18-20] In addition, some of these particles were functionalized with mannose facilitating the engulfment by receptor-mediated endocytosis.[19] Last, the studied cells were macrophages that are cells with high efficiency of engulfment.

In a second step, DNA must be released in the cytoplasm. This is possible via endosome acidification leading to endosomal membrane disruption. The plasmid carrier can play a role both in the destabilization of the endosome via the proton sponge effect and in the protection of DNA against acidic degradation. The first effect increases with the amount of PEI and should therefore be more favorable with SiO_2. The protecting effect depends on the PEI quantity, its conformation and flexibility. The ratio PEI:DNA for SiO_2@PEI , Si-SO_3@PEI,

SiO2-Cl@PEI were 3.8, 1.2 and 1.7, respectively. According to the results of cell viability, these ratios were not associated with any cytotoxicity. It is well-admitted that the transfection capabilities increase when the PEI:DNA ratio rises.[21] Hence, the quantity of PEI on SiO_2 particles could explain in part its higher transfection ability because of its impact on DNA compaction and protection against nucleases. Nevertheless, the conformation of PEI at the surface also plays an important role and is expected to be optimal for the Si-SO_3@PEI system.

In a following step, the released plasmid must diffuse to the nucleus and enter, either during mitosis or via the nuclear import machinery. Importantly, the stage at which PEI and DNA are dissociated is still a matter of debate.[15] However, focusing on the particle-PEI interactions, it is interesting to note that in the acidic conditions of the endosomes, an important fraction of the silanolate groups of the bare silica particles become protonated. This decreases the negative charge of the carrier, favoring PEI desorption. On the opposite, sulfonate functions should remain negatively-charged, preserving their attractive interactions with PEI. Finally, for SiO_2-Cl, the existing covalent bonds are not expected to be cleaved, limiting the possibility for complexes to escape. These trends in PEI detachment from particles nicely follow the measured transfection efficiencies, suggesting that such a release is a relevant event in the plasmid delivery process.

Surprisingly, the performance of PEI alone was not better than that of the SiO_2@PEI system for keratinocytes, in contrast to the results obtained with 3T3 cells. The highest cell transfection observed with PEI compared to particles on immortalized cells could be explained by the particle size and the metabolic activity of 3T3 fibroblasts. PEI/DNA complexes measure about 100 nm in diameter.[22] These complexes are rapidly uptaken by cells *via* the chlatrin-mediated endocytosis. In contrast, larger particles@PEI systems are more internalized by the caveolin-mediated endocytosis.[23] Therefore the chlatrin pathway seems to be more efficient in 3T3 fibroblasts to engulf complexes. Second, 3T3 cells proliferate rapidly, facilitating plasmid transfer by disruption of the nuclear membrane during cell division. Thus it can be proposed that PEI complexes are rapidly uptaken, transported to the nucleus and that protein expression occurs at a very high rate thanks to fast proliferation. In contrast, the uptake of particles being less efficient, there is a delay required for sufficient plasmid accumulation before significant protein expression is achieved. In the case of primary cells such as keratinocytes, the cells proliferate at a lower rate. Therefore the overall protein expression rate is slower for both systems. Moreover, in these conditions, it is possible for silica particles to accumulate in a higher quantity between two cellular division event, so that the protein expression level becomes comparable to that of PEI.

III.2.5 Conclusion

One of the starting hypothesis of this study was that enhancing the interactions between the silica surface and PEI would allow to immobilize more polymer on the particle so as to complex more DNA and possibly enhance transfection efficiency. However, our study showed that the opposite situation occurs. The naked silica surface offers an open area of silanolate groups available for unspecific adsorption of extended PEI chains. The introduction of well-defined moieties provides a smaller number of binding sites leading to a decrease in the amount of immobilized PEI. Moreover, the persistence of significant interactions between the silica surface and PEI in the acidic conditions of the endosomes appears detrimental to the gene delivery. Yet data obtained with sulfonated particles suggest that this situation leads to a more favorable PEI conformation. Therefore it would be interesting to change the nature of the grafted moiety, for instance using carboxylate groups whose pKa is closer to endosomal pH, and also to achieve a better control of the grafting density. In parallel, our hypothesis concerning PEI:DNA detachment has to be supported by further experiments. In particular, the use of fluorescence resonance energy transfer (FRET)[24] techniques would be particularly useful to monitor the fate of SiO_2:PEI:DNA complexes in the intracellular media.

III.3 IMPACT OF CELL TYPE ON THE TRANSFECTION EFFICIENCY OF POLYETHYLENEIMINE-COATED SILICA NANOPARTICLES

III-3-1. Cell Culture and Experimental Conditions

In this study, human primary dermal fibroblasts and epidermal keratinocytes were selected as they are relevant cells in the pathophysiology of cutaneous chronic wounds. Human primary fibroblasts culture was performed using the same protocol than that for 3T3 cells. For keratinocytes, the protocol was also similar except for the culture medium as described in the section III-2-2. The protocols used for collagen-silica hydrogels preparation and transfection experiments in 2D and 3D were the same as those described in **Chapter II**, except when noted.

III-3-2. Human Primary Dermal fibroblasts

III-3-2-1. 2D experiments

Transfection studies were performed with dermal fibroblasts seeded in culture wells and bare silica nanoparticles 200 nm (SiNP) in diameter coated with PEI 25 kDa and 10 kDa. Pure PEIs of same molecular weight were evaluated in parallel. As shown in **Figure III-13**, the transfection efficiency follows a similar trend as found for 3T3 cells (see **Figure II-6** in previous chapter). When coated on silica nanoparticles, PEI_{10} exhibited a higher ability to deliver plasmidic DNA compared to its soluble form. Interestingly, silica nanoparticles coated with PEI_{10} and PEI_{25} showed the same performance of transfection. However some differences were found between immortalized and primary fibroblasts. First the RLU values for human primary fibroblasts are at least one order of magnitude below that of 3T3, the difference reaching two orders of magnitude for PEI_{25}. Second, PEI_{10} is significantly less efficient than PEI_{25}-coated particles for human cells.

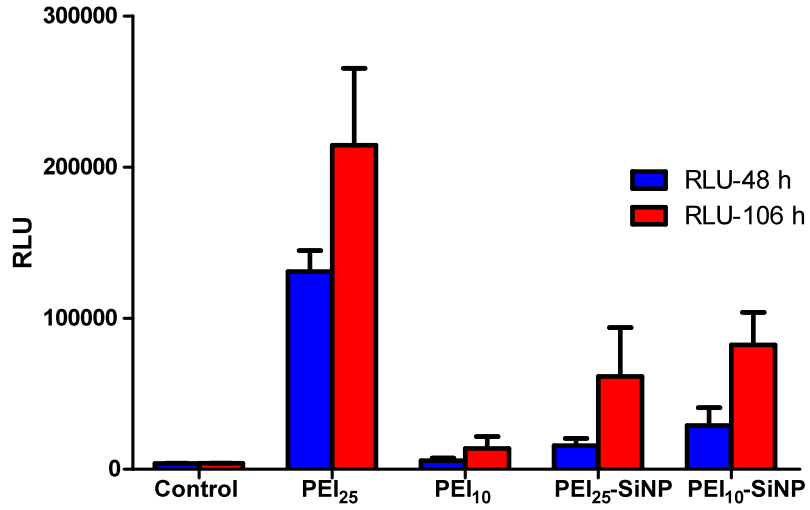

Figure III-13. Transfection of human fibroblasts after 4 h incubation with free and SiNP coated with PEI of various molecular weights (n=3).

The cytotoxicity of the different systems towards human fibroblasts was also evaluated after 4 h of contact using the Alamar Blue test (**Figure III-14**), evidencing no significant impact on cell viability.

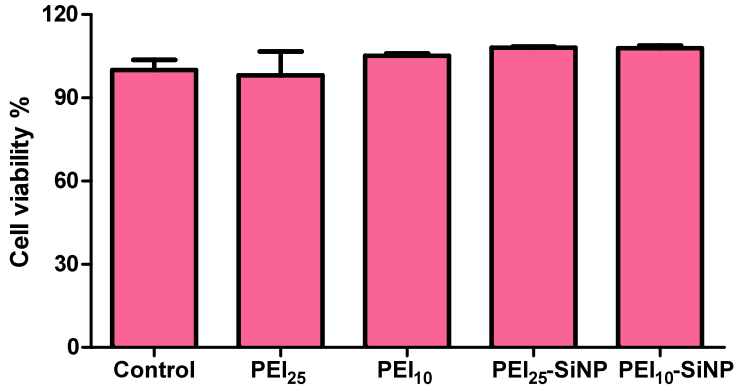

Figure III-14. Human fibroblast viability in 2D as influenced by different molecular weight of PEI without or with SiNP. Cell viability was assessed after 4 h of contact with Alamar Blue test and calculated in the percentage of control (n=3).

III-3-2-2. 3D experiments

These experiments were performed by co-encapsulation of human fibroblasts and plasmid-PEI or plasmid-SiNP@PEI complexes in 1 $mg.mL^{-1}$ hydrogels. In order to optimize plasmid content, a first series of experiments was performed with PEI_{25} only with pGLuc content between 2 and 8 µg/gel and a pGLuc:PEI weight ratio of 1:2. As seen on **Figure III-15**, maximum transfection was observed over 7 days for the intermediate plasmid content (4 µg)

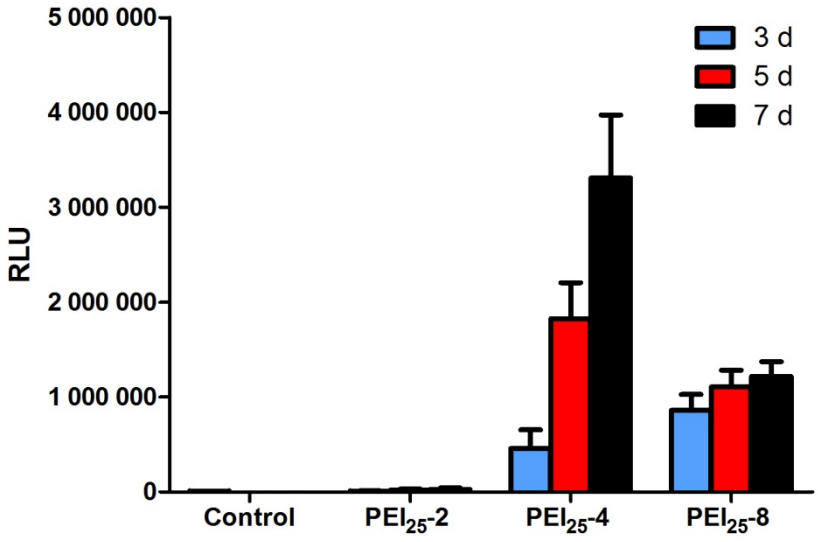

Figure III-15. Transfection of human fibroblasts co-immobilized with pGluc-PEI_{25} complexes in collagen hydrogels after 3, 5 and 7 d of contact, using 2, 4 and 8 µg of plasmid /gel

Viability tests performed over the same period showed that the system containing the highest plasmid content has a significant but limited cytotoxicity, that can correspond to the associated high concentration of PEI (**Figure III-16**). Hence the observation of an optimal value at 4 µg can be attributed to the achieved compromise between low plasmid content (2 µg) and cytotoxicity of PEI (8 µg).

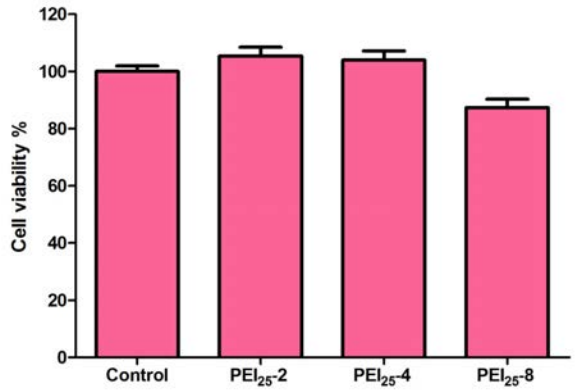

Figure III-16. Cell viability of human fibroblasts co-immobilized with pGluc-PEI_{25} complexes in collagen hydrogels after 7 days, using 2, 4 and 8 µg of plasmid /gel in collagen as evaluated with Alamar Blue test and calculated as the percentage of the control (n=3).

Transfection experiments using co-immobilized PEI-coated silica nanoparticles were therefore performed with a 4 µg plasmid content per gel (1 mL each). In these conditions, it was observed that the transfection efficiency of particles was much lower than that of free PEIs (**Figure III-17**). However, compared to the control, significant bioluminescence levels could be observed from day 5 to 12 for the two PEI-coated systems. At day 12, the RLU values were two orders of magnitudes higher than that measured in the control samples (**Figure II-13**). Nevertheless, the luciferase expression obtained with dermal fibroblasts was one order of magnitude below the values obtained with 3T3 cells. Some differences were observed in terms of profile of transfection between the different conditions. For instance,

PEI-coated systems did not have the same performance of transfection compared to the free PEI 10 kDa.

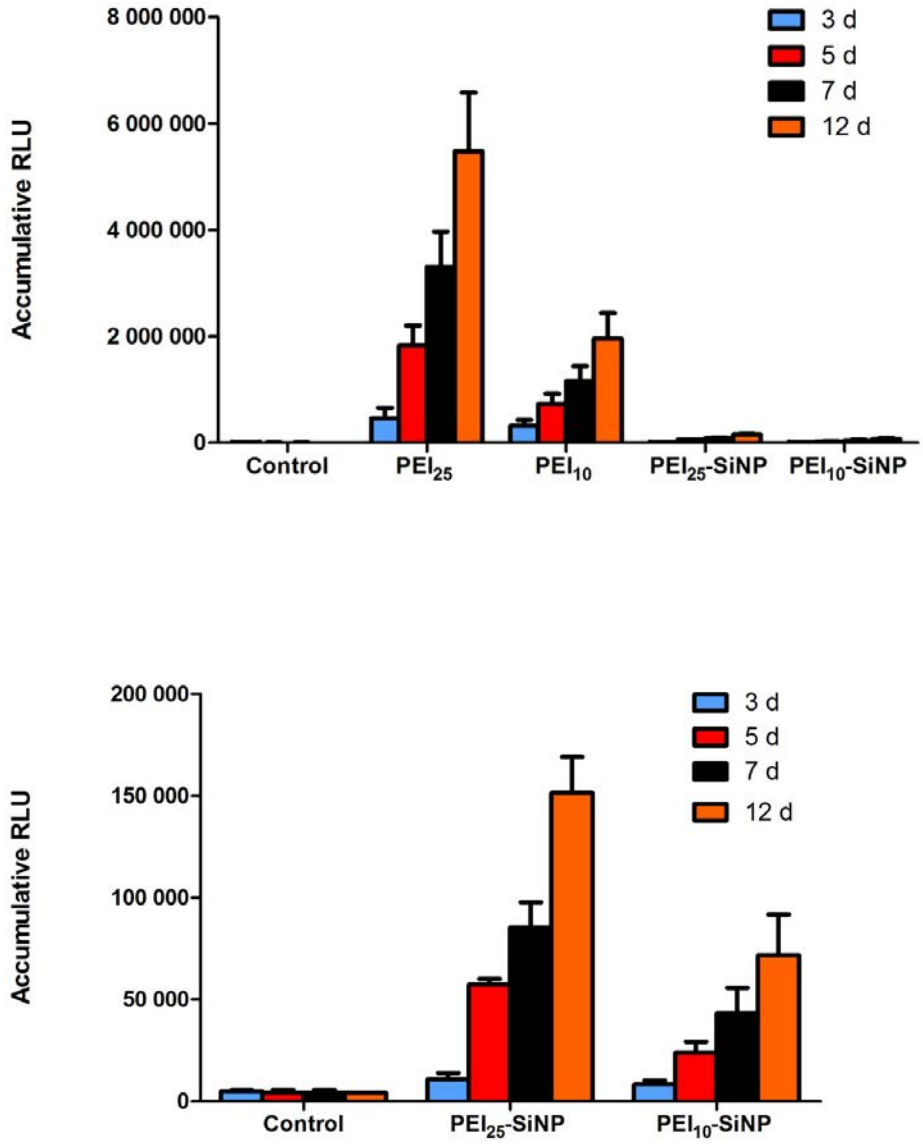

Figure III-17. Transfection of human fibroblasts co-immobilized with p-GLuc-PEI$_x$ and pGLuc-PEI$_x$-SiNP complexes in collagen hydrogels after 3, 5, 7 and 12 days of contact, 4 µg of plasmid /gel. Bottom graph focuses on the silica particle systems (n =3).

Viability tests indicated that these differences could not be attributed to cytotoxic effects of the plasmid carriers (**Figure III-18**)

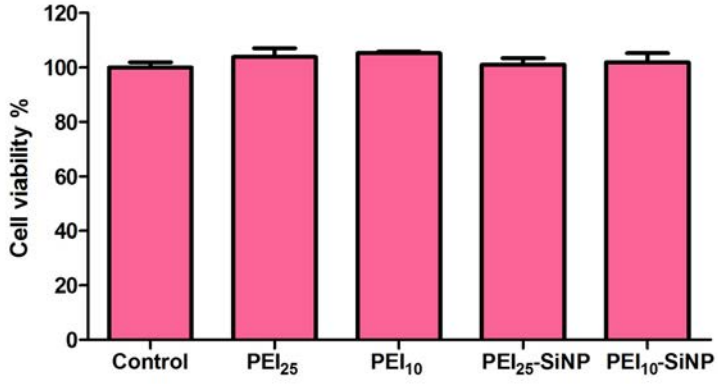

Figure III-18. Cell viability of human fibroblasts co-immobilized with p-GLuc-PEI_x and pGLuc-PEI_x-SiNP complexes in collagen hydrogels after 7 days as evaluated with Alamar Blue test and calculated as the percentage of the control (n=3).

III-3-3. Human keratinocytes

III-3-3-1. 2D experiments

In a first step, transfection experiments were performed using a pGluc:PEI_x-SiNP ratio of 1:30, similar to previous studies. However, in these conditions, very low transfections efficiencies were obtained that could be correlated with high cytotoxicity. Lower plasmid:particle weight ratios (from 1:5 to 1:20 at constant plasmid content) were therefore evaluated. As shown on **Figure III-19**, the cytotoxicity of the particles could efficiently be lowered by decreasing their concentration. The ratios used in these experiments are lower than the optimal ones. Hence it is possible than a small quantity of pDNA has not been complexed.

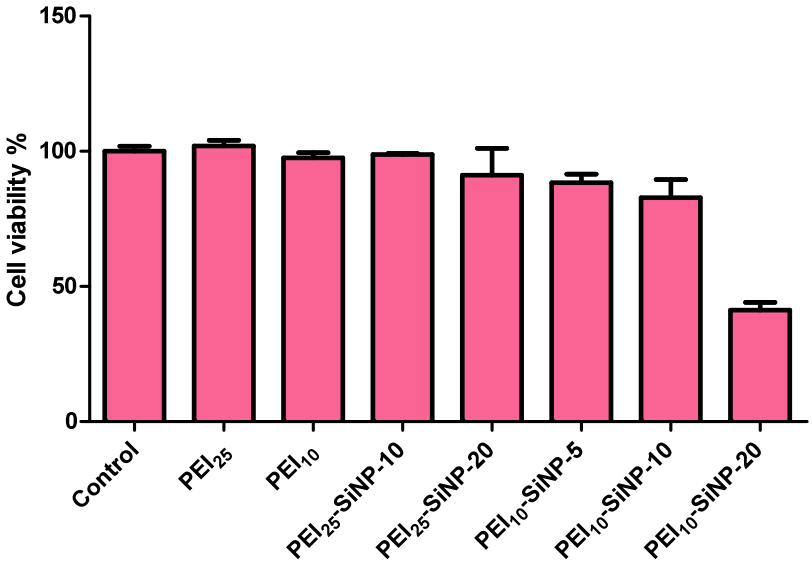

Figure III-19. Human keratinocyte viability as influenced by different molecular weight of PEI and different plasmid:particle ratio. Cell viability was assessed after 4 h of contact with Alamar Blue test and calculated in the percentage of control (n=3).

The transfection efficiency of these different systems was also studied (**Figure III-20**). Here again, the bioluminescence levels were lower than for 3T3 cells. This can be in part due to the lower plasmid:particle ratios used. Moreover PEI-coated particles had very similar efficiency to free PEI. The optimal conditions for particle systems resulted from a compromise between a low plasmid:carrier ratio that corresponds to a larger fraction of pGLuc interacting with the particles and therefore being able to be uptaken, and a high plasmid:carrier ratio that corresponds to a lower particle concentration and therefore lower cytotoxicity.

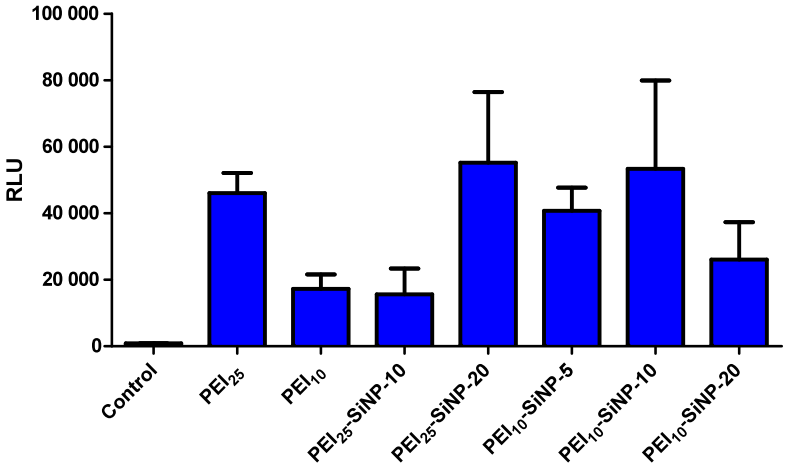

Figure III-20. Transfection of human keratinocytes after 4 h incubation as influenced by different molecular weight of PEI and different plasmid:particle ratio (n=3).

III-3-3-2. 3D experiments

Contrary to fibroblasts, keratinocytes do not survive within collagen hydrogels. Therefore a pseudo 3D model was used where the complexes, being pGLuc-PEI or pGLuc-SiNP@PEI, are immobilized in the collagen hydrogel and keratinocytes are seeded on its surface.

In these conditions, only free PEI_{25} led to a bioluminescence level that was statistically different from the control (**Figure III-21**). Again these differences could not be attributed to toxicity effects (**Figure III-22**). These results are in good agreement with the data obtained for 3T3 cells (see **Figure II-16**) and suggest that only the pGLuc-PEI_{25} complex can migrate out of the hydrogel.

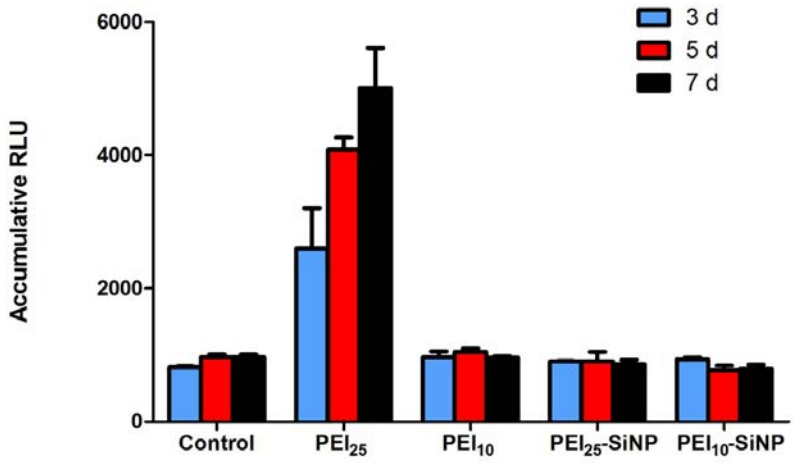

Figure III-21. Transfection of keratinocytes seeded on collagen hydrogels containing p-GLuc-PEI$_x$ and pGLuc-PEIx-SiNP complexes after 3, 5 and 7 d of contact.

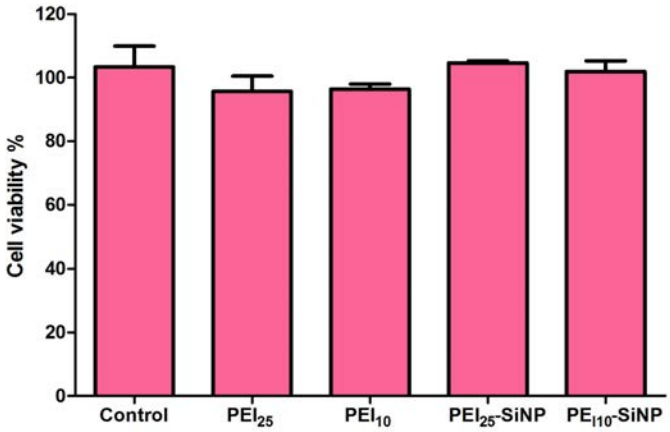

Figure III-22. Cell viability of human keratinocytes seeded on collagen hydrogels containing p-GLuc-PEI$_x$ and pGLuc-PEIx-SiNP complexes after 7 days of contact as evaluated with Alamar Blue test and calculated as the percentage of the control (n=3).

III-3-4. Discussion and conclusion

The efficiency of transfection depends on the ability of cells to uptake polyplexes. In addition, gene delivery and transgene expression is facilitated when the cells have a high proliferative rate. When used in their soluble form, the performance of PEI 25 KDa and PEI 10 KDa, is much lower than that observed with 3T3 cells. To reach the same amplitude of transfection, it

was necessary to increase the quantity of DNA by 4. This can be explained by the doubling time of primary cells that is much longer than immortalized cells. Fontana et al have shown that several micrograms of polyplexes were required to efficiently transfect adipose stem cells encapsulated in HA/collagen microgels.[25] However, the results obtained with primary cells are in agreement with the general scheme of cell transfection in 3D systems.

Unlike 3T3 cells, free forms of PEI are always more effective on dermal fibroblasts than the PEI-coated systems. Primary dermal fibroblasts do not have the same ability of migration as 3T3 cells. When immobilized in a 3D collagen gel, fibroblasts stop migrating after a few days. Then, they differentiate into myofibroblasts and acquire contractile faculties.[26,27] They contract the collagen network and their abilities to proliferate drastically decrease[28]. This weak proliferation could explain why gene delivery is less effective when the cells are encapsulated in a 3D collagen hydrogels compared to 2D conditions. Immortalized cells do not behave this way as they are unable to contract a 1 $mg.mL^{-1}$ collagen gels and keep their migratory faculties. When they move they can be in contact with particles and uptake them. In the case of primary fibroblasts, this is not possible. Cells pull on collagen fibrils to bring them closer and contract the collagen network.[26,27] This mechanism permits the interaction between the particles stuck on collagen fibrils and the cellular membrane. However, this mechanism is less effective to uptake particles compared to cell migration. This explains why the free forms of PEI are more effective to deliver genes because they can diffuse rapidly in the pores of the collagen network, encounter fibroblasts and transfect them.

Transfection of collagen-entrapped complexes put in contact with keratinocytes also gave similar trends than 3T3 cells concerning the influence of PEI molecular weight and the influence of the silica particles. Only the free form of PEI is able to transfect keratinocytes seeded on the surface. This evidences one more time the confinement of PEI-coated silica nanoparticles within the collagen network.

Noticeably, the viability of keratinocytes is more affected by the presence of silica particles than that of the primary fibroblasts. As a consequence, the ratios used in the experiments of transfections were lower. This result is surprising as the cytotoxicity of submicronic silica nanoparticles has not been described. Nabeshi et al have shown that 300 nm SiNPs do not present any toxicity on keratinocytes until a1 $mg.mL^{-1}$ dose is reached[29]. This dose is much higher than that used in this study. However comparison between different sets of experiments is often difficult due to variations in particle size, structure, surface functionality, etc. Its understanding would require a much deeper study of the cellular

response to the silica particles. One particularly interesting observation is the difference in particle toxicity between keratinocytes and fibroblasts. As a matter of fact we could not find any explanation for this difference in the literature. Noticeably, such studies may be particularly valuable in the field of biomaterials for wound healing as one of the current material in the market, Apligraf®, combines these two kinds of cell associated with collagen [30].

III.4 CONCLUSION

We have demonstrated that the mode of conjugation of PEI with the silica particle surface has a deep impact on the transfection efficiency of the inorganic carrier. Our data suggest that this impact is related to both PEI conformation and stability of the silica-PEI interface in the intracellular medium. We have also shown that silica-PEI particles have the ability to transfect human cells, although to a lower extent than immortalized fibroblasts. This difference in transfection efficiency was attributed to the lower proliferation rate of the primary cells.

From a fundamental point of view, these studies have brought novel and important information about the mechanisms of gene delivery mediated by PEI-silica nanoparticles. From an application point of view, these results are rather disappointing as these carriers are significantly less effective than pure PEI_{25} in most situations. It is therefore important at this point to remind the advantages of the composite approach: (i) the SiO_2@PEI particles are less cytotoxic than PEI alone at high doses, (ii) once immobilized within the collagen gels, they do not release complexed plasmids outside the material, (iii) silica particles may be loaded with an additional drug, allowing the design of medicated dressings delivering two bioactive molecules.

On this basis, we decided to go a step further towards the design of a biofunctional nanocomposite material by evaluating the possibility to use silica-PEI particles as vectors for the delivery of a plasmid inducing the expression of IL-10, a protein relevant for our targeted application in chronic wound healing.

REFERENCES

(1) Aimé, C.; Mosser, G.; Pembouong, G.; Bouteiller, L.; Coradin, T. Controlling the nano–bio interface to build collagen–silica self-assembled networks. *Nanoscale* **2012,** *4*, 7127-7134.

(2) Ellman G.L. Tissue sulfhydryl groups. *Arch. Biochem. Biophys.* **1959**, *82* 70–73

(3) Bonhomme, C.; Coelho, C.; Baccile, N.; Gervais, C.; Azaïs, T.; Babonneau, F. Advanced solid state NMR techniques for the characterization of sol-gel derived materials. *Acc. Chem. Res.* **2007**, *40*, 738-746.

(4) De Monredon-Senani S., Bonhomme C., Ribot F., Babonneau F. Covalent grafting of organoalkoxysilanes on silica surfaces in water-rich medium as evidenced by ^{29}SiNMR. *J. Sol-Gel Sci. Technol.* **2009**, 50, 152-157

(5) Louette, P.; Bodino, F.; PIreaux, J.-J. Poly-ethylene imine **(**PEI) XPS Reference Core Level and Energy Loss Spectra. *Surface Sci. Spectra*, **2005**, *12*, 54-58

(6) Shchukarev, A.; Rosenqvist, J.; Sjöberg, S. XPS study of the silica–water interface. *J. Electron Spectr. Related Phenom*. **2004**, *137-140*, 171-176

(7) Islam, Md. S.; Choi, W. S.; Lee, H.-J. Controlled Etching of Internal and External Structures of SiO2 Nanoparticles Using Hydrogen Bond of Polyelectrolyte. *ACS Appl. Mater. Interfaces* **2014**, *6*, 9563–9571

(8) Nasef, N.N.; Saidi, H.; Nor, H.M.; Yarmo, M.A. XPS Studies of Radiation Grafted PTFE-g-polystyrene Sulfonic Acid Membranes. *J. Appl. Polym. Sci*. **2000**, *76*, 336–349

(9) Tsiourvas, D.; Tsetsekou, A.; Arkas, M.; Diplas, S.; Mastrogianni, E. Covalent attachment of a bioactive hyperbranched polymeric layer to titanium surface for the biomimetic growth of calcium phosphates. *J. Mater. Sci. Mater. Med*. **2011**, *22*, 85-96.

(10) Cory, D.G.; Ritchey, W.M. Inversion recovery cross-polarization NMR in solid semicrystalline polymer. *Macromolecules*, **1989**, *22*, 1611–1615

(11) Nagaya, J.; Homma, M.; Tanioka, A.; Minakata, A. Relationship between protonation and ion condensation for branched poly(ethylenimine). *Biophys. Chem.* **1996,** *60*, 45-51.

(12) Leung, K.; Nielsen, I. M. B.; Criscenti, L. J. Elucidating the Bimodal Acid−Base Behavior of the Water−Silica Interface from First Principles. *J. Am. Chem. Soc.* **2009,** *131*, 18358-18365.

(13) Godbey, W. T.; Wu, K. K.; Mikos, A. G. Poly(ethylenimine) and Its Role in Gene Delivery. *J. Controlled Release* **1999**, *60*, 149-160.

(14) Wightman, L.; Kircheis, R.; Rossler, V.; Carotta, S.; Ruzicka, R.; Kursa, M.; Wagner, E. Different Behavior of Branched and Linear Polyethylenimine for Gene Delivery In vitro and In vivo. *J. Gene Med.* **2001**, *3*, 362-372.

(15) Won, Y.-Y.; Sharma, R.; Konieczny, S. F. Missing pieces in understanding the intracellular trafficking of polycation/DNA complexes. *J. Controlled Release* **2009,** *139*, 88-93.

(16) Wang, Z. J.; Tiruppathi, C.; Minshall, R. D; Malik, A., B. Size and dynamics of caveolae studied using nanoparticles in living endothelial cells. *ACS Nano.* **2009**, *3*, 4110-4116.

(17) Mao, Z., Zhou, X.; Gao, C. Influence of structure and properties of colloidal biomaterials on cellular uptake and cell functions. *Biomater Sci* **.2013**, *1*, 896-911.

(18) Buchman, Y. K.; Lellouche, E.; Zigdon, S.; Bechor, M.; Michaeli, S.; Lellouche, J.-P. Silica Nanoparticles and Polyethyleneimine (PEI)-Mediated Functionalization: A New Method of PEI Covalent Attachment for siRNA Delivery Applications. *Bioconjugate Chem.* **2013,** *24*, 2076-2087.

(19) Park, I.Y.; Kim, I.Y.; Yoo, M.K.; Choi,Y.J.; Cho, M.H.; Cho, C.S. Mannosylated polyethylenimine coupled mesoporous silica nanoparticles for receptor-mediated gene delivery. *Int. J. Pharm.* **2008**, *359*, 280-287.

(20) Jiang, G.; Park, K.; Kim, J.; Oh, E.J.; Kang, H.; Han, S.-E.; Oh Y.-K; Park, T. G; Hahn, S., K. Hyaluronic acid-polyethyleneimine conjugate for target specific intracellular delivery of siRNA. *Biopolymers* **2008**, *89*, 635-642.

(21) Huang, Y.C.; Connell, M.; Park, Y. ; Mooney, D.J.; Rice, K.G. Fabrication and in vitro testing of polymeric delivery system for condensed DNA. *J. Biomed Mater. Res. A.* **2003**, *67*, 1384-1392.

(22) Fischer, D.; Bieber, T.; Li, Y. X.; , Elsasser, H. P.; Kissel, T. A novel non-viral vector for DNA delivery based on low molecular weight, branched polyethylenimine: Effect of

molecular weight on transfection efficiency and cytotoxicity. *Pharmaceut Res.* **1999**, *16*, 1273-9.

(23) Rejman, J.; Oberle, V.; Zuhorn, I. S.; Hoekstra, D. Size-dependent Internalization of Particles via the Pathways of Clathrin- and Caveolae-mediated Endocytosis. *Biochem. J.* **2004**, *377*, 159-169.

(24) Didenko, V.V DNA Probes using Fluorescence Resonance Energy Transfer (FRET): designs and applications. *Biotechniques* **2001**, *31*, 1106–1121.

(25) Fontana, G.; Srivastava, A.; Thomas, D.; Lalor, P.; Dockery, P.; Pandit, A. Three-Dimensional Microgel Platform for the Production of Cell Factories Tailored for the Nucleus Pulposus, *Bioconjug. Chem*. **DOI:** 10.1021/bc5004247

(26) Grinnell, F. Fibroblast Biology in Three-Dimensional Collagen Matrices. *Trends Cell Biol.* **2003**, *13*, 264-269.

(27) Grinnell, F.; Petroll, W. M. Cell Motility and Mechanics in Three-Dimensional Collagen Matrices. *Annu. Rev. Cell Dev. Biol.* **2010**, *26*, 335-361.

(28) Sarber, R.; Hull, B.; Merrill, C.; Soranno, T., Bell, E. Regulation of proliferation of fibroblasts of low and high population doubling levels grown in collagen lattices. *Mech Ageing Dev.* **1981**, *17*, 107-117

(29) Nabeshi, H.; Yoshikawa, T.; Matsuyama, K.; Nakazato, Y.; Tochigi, S.; Kondoh, S.; Hirai, T.; Akase, T.; Nagano, K.; Abe, Y.; Yoshioka, Y.; Kamada, H.; Itoh, N.; Tsunoda, S., Tsutsumi, Y. Amorphous nanosilica induce endocytosis-dependent ROS generation and DNA damage in human keratinocytes. *Part Fibre Toxicol.* **2011**, *8*, DOI 10.1186/1743-8977-8-1

(30) Wilkins, L.M.; Watson, S.R.; Prosky, S.J.; Meunier, S.F.; , Parenteau, N.L. Development of a bilayered living skin construct for clinical applications. *Biotechnol Bioeng*. **1994**, *43*, 747-756

Annex: Detailed XPS spectra

PEI

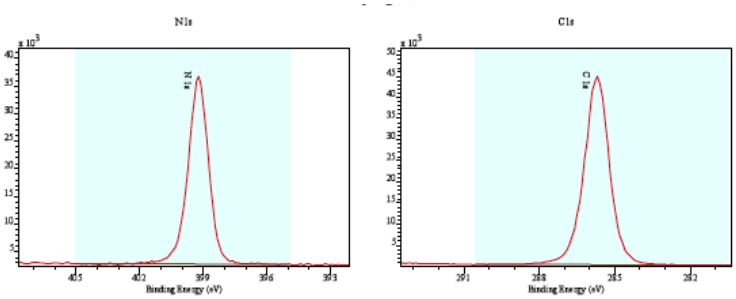

SiO_2

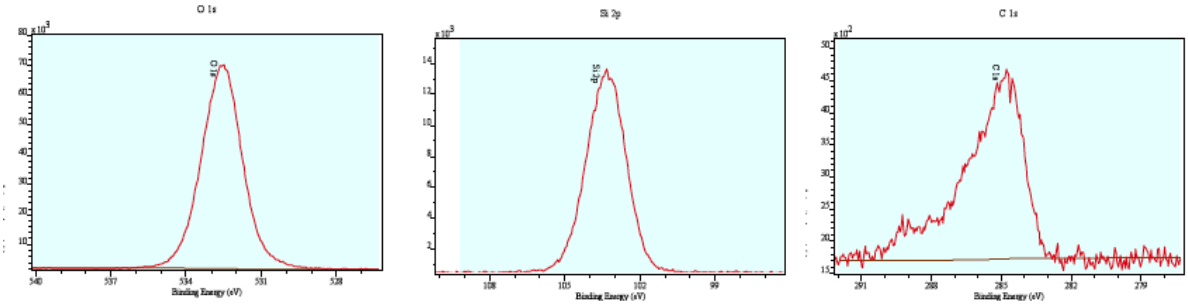

SiO_2@PEI

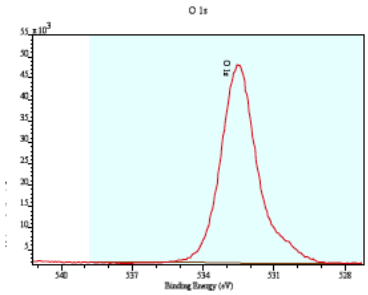

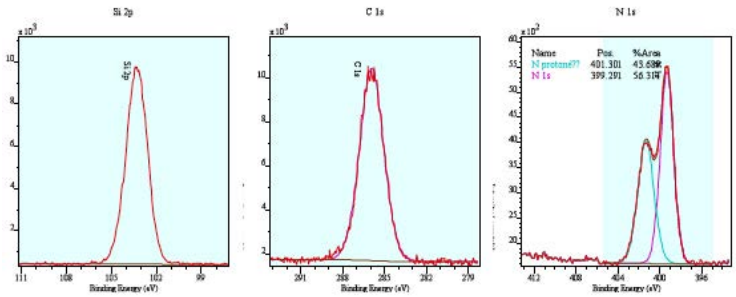

SiO_2-SO_3

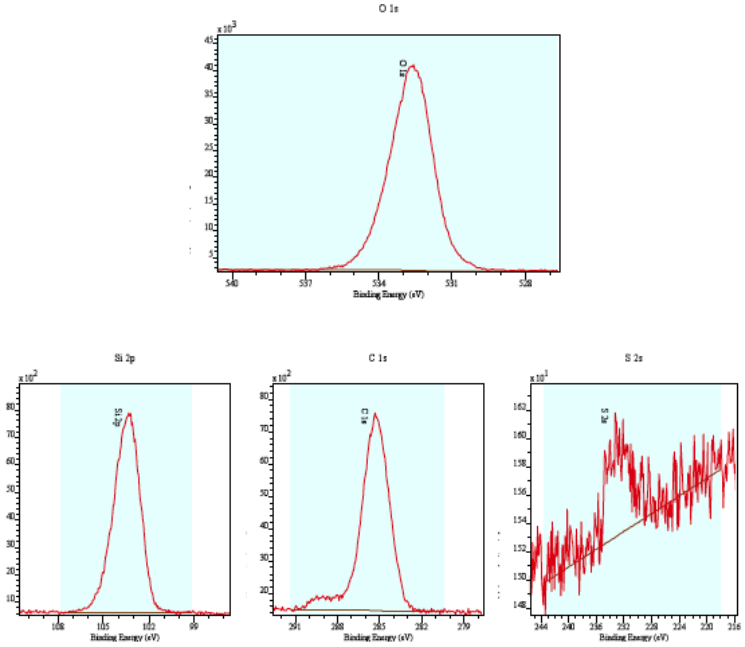

SiO_2-SO_3@PEI

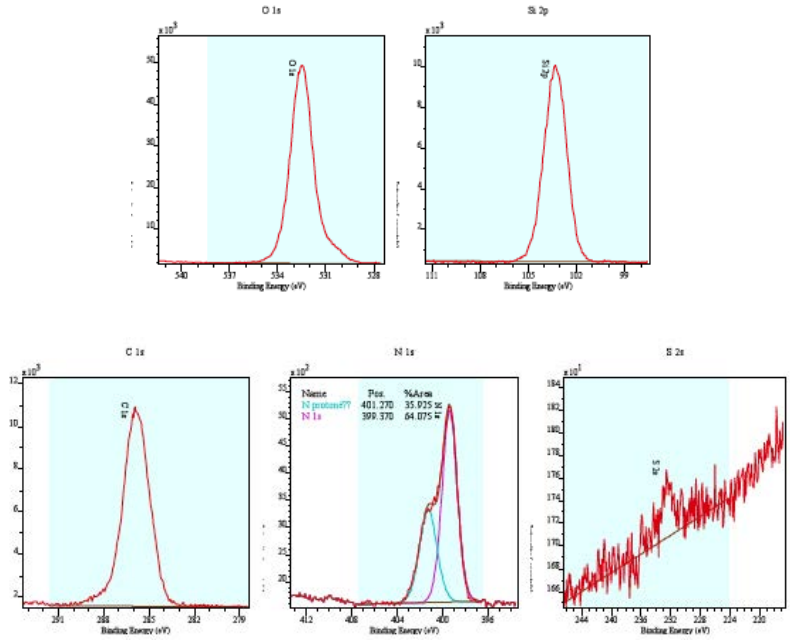

SiO_2-Cl

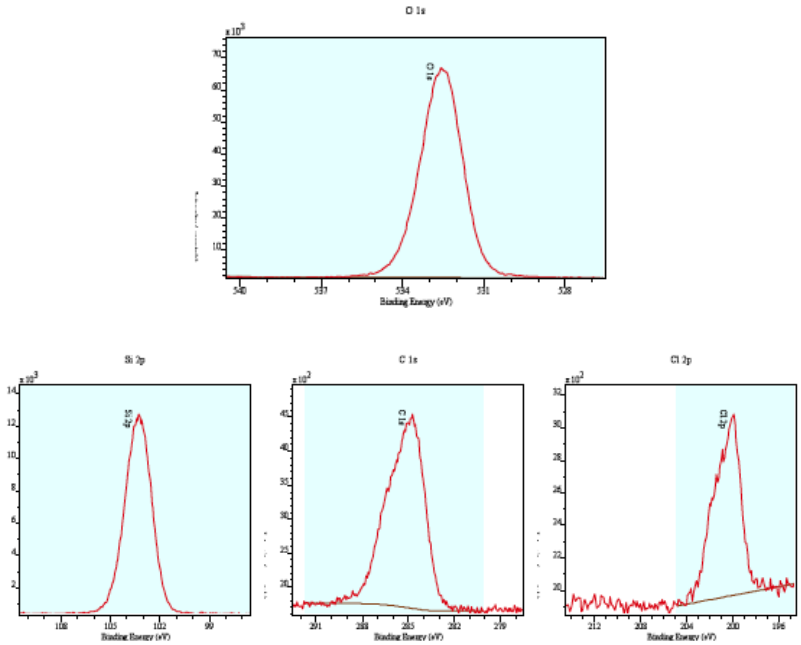

SiO_2-Cl@PEI

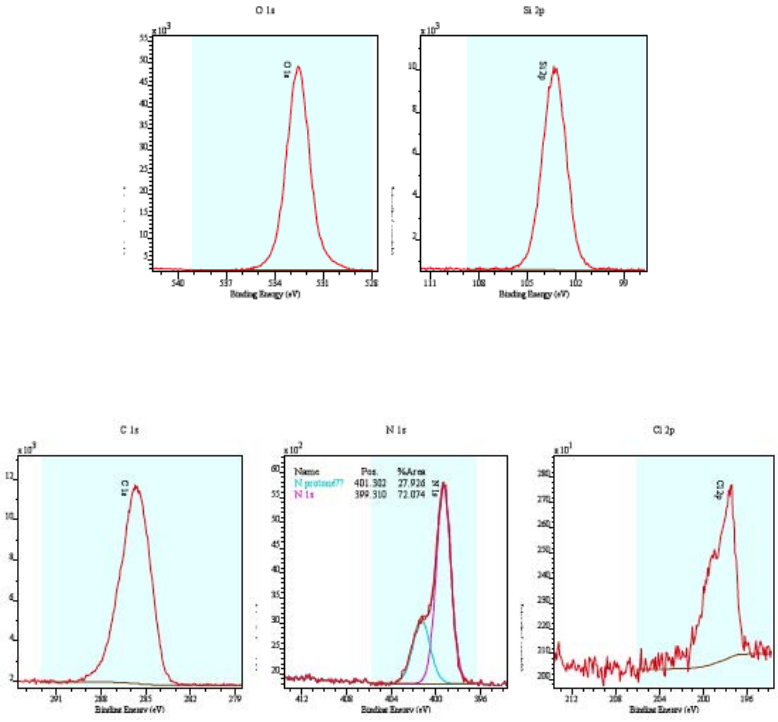

CHAPITRE IV

Modulation de l’inflammation par des nanocomposites silice-collagène

CHAPITRE IV

Modulation de l'inflammation par des nanocomposites silice-collagène

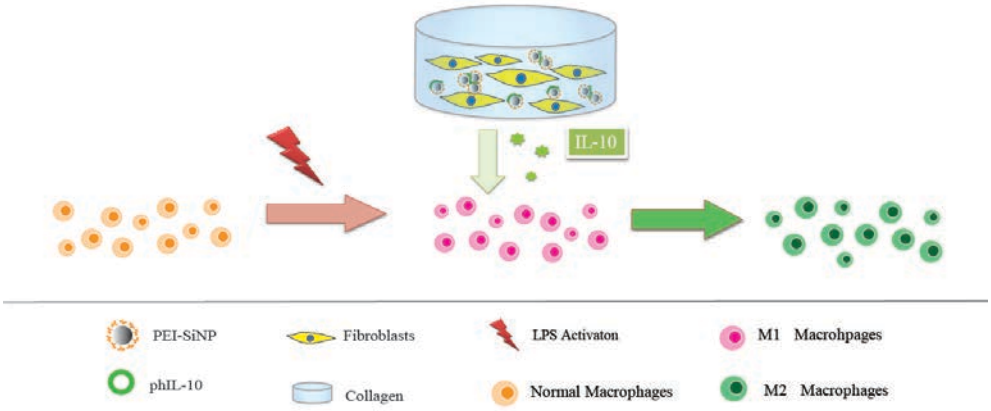

Résumé

Dans ce dernier chapitre, nous avons exploré la capacité des nanocomposites à réguler l'inflammation en utilisant les particules de silice modifiées par le PEI comme vecteur d'un plasmide permettant l'expression de l'Interleukin-10 (IL-10). Dans un premier temps, la production d'IL-10 par des cellules 3T3 en culture 2D après transfection a été démontrée. Un modèle de macrophages activés par les LPS (lipopolysaccharides) a ensuite été mis au point. La réponse de ces cellules à l'IL-10 produites par les fibroblastes a été démontrée par la mesure par PCR quantitative de la décroissance du niveau d'expression du facteur TNF-α. Dans un deuxième temps, la production de l'IL-10 par les cellules 3T3 co-immobilisées avec les complexes au sein des hydrogels de collagène a été démontrée. Malgré les quantités élevées d'IL-10 produites au sein des nanocomposites, il n'a pas été possible d'observer l'impact de cette protéine sur les macrophages activés. Ce résultat nécessitera néanmoins d'être vérifié et l'expérience devra être étendue à des macrophages immobilisés dans les matrices de collagène.

IV-I INTRODUCTION

Wound healing is a multi-cellular process which occurs after an injury, with the aim of restoring the integrity of skin. The phases of normal wound healing involve a range of growth factors and cytokines which act at different stages of tissue repair. Consequently, many of these bioactive proteins such as VEGF[1], PDGF-BB[2], TGF-β[3] and IL-10 have been studied as therapeutic drugs to promote the healing process. Among them, IL-10 has received a particular attention as potent anti-inflammatory biomolecule. This cytokine can inhibit the action of NO and the synthesis of a variety of inflammatory cytokines including IL-1β and TNF-α. More generally, IL-10 allows for the repolarization of pro-inflammatory macrophages into regulatory macrophages. These cells have a crucial role in the modulation of inflammation, thereby promoting cutaneous wound healing. IL-10 is also a product of glia (astrocytes and microglia) and leukocytes such as macrophages and dendritic cells, which express IL-10 receptors. Therefore, IL-10 delivery have been widely investigated to treat inflammation in central nervous system[4], lung (e.g. pneumonia[5]), joint (arthritis[6]), heart fibrosis, liver[7], colon [8] and even cancer[9].

Several trials of protein therapy have been attempted by injection of cytokine in the cutaneous wound bed. Unfortunately, these strategies have failed because of the rapid diffusion and their short half-life due to their degradation[19]. Hence, gene therapy represents an interesting alternative. Current strategies for IL-10 gene delivery rely on the systematic delivery or the local injection. Moreover, this was predominantly achieved by viral vectors such as (adeno-associated virus) AAV[5, 10], (adenovirus) AV[11] and (lentivirus) LV[12] . A few attempts have been carried out with non-viral vector such as dendrimer[13], PEI, alginate nanoparticles[6], PAGA[14] and PLGA microparticles[15]. For example, Jain et al. have developed a gene delivery system for the treatment of rheumatoid arthritis. In this study, pDNA encoding for IL-10 (pIL-10) was immobilized within alginate nanoparticles. Subsequently, particles were modified with tufstin peptide in order to target macrophages.[6] This targeting system was found to be capable of repolarizing macrophages from inflammatory M1 phenotype to anti-inflammatory M2 phenotype. Moreover, animals treated with the particles retained their mobility as a result of IL-10 expression.

Scaffold-based delivery systems create a space for tissue growth and provide a support for cell adhesion and migration. More importantly, spatio-temporal control over bioactive molecules release can achieve the optimal efficacy while averting side effects. Gower *et al.* loaded Lentivirus carrying pIL-10 in porous PLGA scaffold. The main advantage observed

was a decreased inflammation following the scaffold implant. IL-10 delivery was found to decrease leucocyte infiltration in the implanted scaffold by 50%. Thus, this system has the potential to improve the therapeutic effect with minimal inflammatory response. Combination of gene and cell delivery is a promising approach to achieve optimal therapeutic efficacy. On the one hand, implanted cells can replace the damaged tissues and produce growth factors to favor tissue repair. On the other hand, the transfected cells can act as bioreactors to produce therapeutic proteins to promote tissue regeneration. However, few attempts have been made for the co-delivery of cells and genes. Holladay *et al* co-delivered stem cells and plasmid IL-10 (pIL-10) in collagen sponges for the treatment of myocardial infarction.[13] The complexed plasmids were adsorbed within the pre-formed collagen scaffold and stem cells were seeded on top of the sponges. The produced IL-10 downregulated the inflammatory response, thereby improving the survival of the transplanted stem cells.

As shown in **Chapter II**, silica-collagen nanocomposties co-encapsulated with fibroblasts and plasmidic DNA gave promise for the local and sustained release of proteins using pGluc as a gene model. Herein, we further explored the possibility for the delivery of plasmid encoding IL-10 and measured the anti-inflammatory effect of IL-10 on LPS activated macrophages. More specifically, we evaluated our model as gene delivery system to down-regulate the expression of pro-inflammatory cytokines such as TNF-α.

IV-2. MATERIALS AND METHODS

IV-2-1. Production of plasmid encoding human IL-10 (phIL-10)

The phIL-10 plasmid purchased from Origene (USA) is obtained from the pCMV6-XL5 plasmid in which the ORF cDNA sequence encoding for Human Interleukin 10 has been inserted. This plasmid was amplified by one shot BL21(DE3) pLysS kit (Invitrogen, Life technologies), extracted by one PureLink HiPure Plasmid kit (Invitrogen, Life technologies), and finally stored in Tris-EDTA buffer at −20 °C.

IV-2-2. phIL-10-PEI and phIL-10-PEI-SiNP Complexation.

The phIL-10-PEI complexes were prepared at weight ratio of 1:2. Silica nanoparticles 200 nm in diameter and coated with PEI 25 kDa or 10 kDa were used as vectors. The phIL-10-SiNP complexes were prepared at various phIL-10:PEI-SiNP weight ratios. Complex formation was examined by agarose gel electrophoresis. Briefly, 2 µL of phIL-10 solution (0.1 µg.µL^{-1}) was mixed homogeneously with a total volume of 8 µL of PEI-SiNP suspension or PEI solution

(PBS 1×) by vortexing in a microcentrifuge tube. The resulting mixtures were left at room temperature for 2 h to achieve complete complexation, before being loaded into a 0.7% agarose gel with ethidium bromide (0.1 µg.mL^{-1}) and running with TAE 1X (Tris acetate EDTA) buffer at 100 V for 40 min. DNA retardation was observed by irradiation with ultraviolet light.

IV-2-3. Mouse fibroblast and macrophage Cell Culture

3T3 mouse fibroblasts were cultured in complete cell culture medium as previously described in **Chapter II**. The mouse macrophage cell line (RAW264.7 cells) was purchased from Sigma Aldrich. The cells were grown and maintained in the same medium as 3T3 cells. These cells were harvested by scratching, centrifugation and suspended in a fresh medium. Cell counts were measured using a standard trypan blue cell counting technique.

IV-2-4. Preparation of Silica-Collagen Nanocomposites

Complexes were formed by adding 5 µg of phIL-10 to 125 µL of a solution containing PEI or PEI-SiNP in order to achieve the optimal phIL-10:PEI (or phIL-10-PEI-SiNP) ratio identified gel electrophoresis. 500 µL of a type I collagen solution was mixed with 245 µL of culture medium and he complexes were added to the mixtures After addition of 30 µL of 0.1 M NaOH and vortexing, 100 µL of the cell suspension at a density of 1.5×10^6 cells.mL^{-1} was added and mixed homogeneously. Last 0.9 mL was sampled from the mixture and deposited onto a 24-well plate. The plate was then incubated at room temperature for 10 min for complete gelling of collagen.

IV-2-5. Cell Transfection and Cell Viability

Transfection efficiency of phIL-10-PEI and phIL-10-PEI-SiNP was evaluated by the titration of the protein hIL-10 secreted in the cell culture medium using an Elisa-kit for hIL-10 (Novex, life technologies).

To perform cell transfection in 2D, 3T3 mouse fibroblasts were plated at a density of 5×10^4 per well in a 24-well plate. phIL-10-PEI or phIL-10-PEI-SiNP complexes (25 µL, prepared as described above) were added to the cell culture medium. After 4 h, the supernatant was removed, the well was refreshed with 1 mL medium, and the cells were then cultured for another 44 h in complete medium for the expression of hIL-10. Last media from each well were collected and frozen until analysis.

For 3D experiments, silica-collagen nanocomposites were incubated with 1 mL of fresh medium. The ability of nanocomposites to produce and secrete hIL-10 was analyzed over one week. At day 2, 5 and 7, 500 µL of the culture medium was collected from the wells, frozen and replaced with an equal volume of fresh medium. Control groups were under the same culture condition as the experiment groups except for the absence of DNA complexes.

Cell viability was monitored using the Alamar Blue test. For the 2D model, cell culture medium was collected after 2 days and replaced by 200 µL of the Alamar Blue solution (10% in cell culture medium). Cell viability was calculated and reported as a percentage of the control group as described in **Chapter II** (n = 3). Cell viability was assessed at day 7 in the 3D models (using the same procedure, except that 800 µL water was first added to the collagen gel for 0.5 h at room temperature to extract the Alamar blue solution trapped in the gel and then collected for the absorbance measurements.

IV-2-6. Macrophage activation with LPS

Mouse macrophages RAW 264.7 were seeded at a density of 10^5 and cultured overnight before activation with LPS (Sigma). A volume of a LPS stock solution (100 µg/mL) in PBS was added to each well to reach the final concentration of 1µg/mL or 0.1 µg/mL. At different incubation time, 1 h, 3 h and 6 h, cells were treated with Trizol (Invitrogen, Carlsbad, CA, USA) and then stored at -80 ^{o}C before RNA extraction.

IV-2-7. Total RNA extraction and RT-PCR

All studies were carried out in a designated PCR clean area. RNAs were extracted using RNeasy mini-kit (Qiagen, France) according to the manufacturer's recommendations. To eliminate the contamination with genomic DNA, a DNase digestion was performed for 15 min. First-strand cDNA was synthesized at 37°C by M-MLV reverse transcriptase (Invitrogen, France). With the aim of testing the primers, PCR amplification reactions of TNF-α, 18S and GAPDH were carried out using a pool of cDNA (see the primers sequences below). Cycling conditions were: initial denaturation at 94°C for 5 min, followed by 50 cycles consisting of a 30 s denaturation at 94°C, a 30 s annealing at 59°C and a 45 s elongation at 72◦C. PCR products were analyzed after migration in a 1% agarose gel with 0.01 µg/ml ethidium bromide using the Gel Doc analyzer (Biorad, France).

<u>TNF-α C1 (couple 1)</u>

F1 : AAG CCT GTA GCC CAC GTC G TA GCA,

R1: GCA GCC TTG TCC CTT GAA GAG AAC CT)

TNF-α C2 (couple 2)

F2: CGG GGT GAT CGG TCC CCA AAG

R2: GGA GGG CGT TGG CGC GCT GG

18S

F: GTG GAG CGA TTT GTC TGG TTA,

R: CGG ACA TCT AAG GGC ATCA

GAPDH

F: CTT CAC CAC CAT GGA GAA GGC

R: GGC ATG GAC TGT GGT CAT GAG.

IV-2-8. Measurement of gene expression by real time PCR (Q-PCR)

Real-time quantitative PCR amplifications were carried out in a Light Cycler 480 detection system (Roche, France), using the Light Cycler Fast Start DNA Master plus SYBR Green I kit (Roche). The mRNA transcript level of TNF-α was normalized with the housekeeping gene GAPDH because its expression is not modified in our conditions. Gene expressions of TNF-α were quantified using the absolute quantification method (n= 4). Cycling conditions were: initial denaturation at 94 °C for 5 min, followed by 50 cycles consisting of a 10 s denaturation at 94 °C, a 15 s annealing at 59 °C and a 15 s elongation at 72 °C. Then, a melting curve was obtained for each sample by increasing the temperature from 59 °C to 97 °C at a rate of 0.11 °C /s. The results were analyzed using the absolute quantification with arbitrary values. For this purpose, a standard curve was carried out for each target and reference gene. Primer efficiencies were calculated in each experiment from the standard curve carried out in the same plate as the quantified samples. For each sample, a ratio target gene/reference gene was calculated and compared with a calibrator point. This calibrator point was the cDNA obtained from the control samples at day 2 (without Il-10 treatment). The value 1 was given to the mean of ratios for the control samples (n= 4). Arbitrary values were then calculated for each condition by comparison with the value 1, using the ratios.

IV-2-9. Effect of IL-10 on activated macrophages

IV-2-9-1. Dose and time dependent effect of IL-10 on mRNA levels of TNF-α

IL-10 quantities produced by 3T3 fibroblasts during the 2D cell transfection experiments were diluted to a final IL-10 concentration of 0.1, 0.5 and 1.0 ng/mL in cell culture medium. Macrophages were seeded on plastic as introduced in **IV-2-6**. Control group was macrophages only treated with the LPS solutions at 0.1 or 1 $\mu g.\mu L^{-1}$. The IL-10 solutions were added 1 h before or together with LPS. Then, TNF-α expression was quantified 1 h or 3 h after LPS activation by real time PCR to determine the anti-inflammatory effect of IL-10.

IV-2-9-2. Modulatory effect of IL-10 produced from nanocomposites on mRNA level of TNF-α

Supernatants containing IL-10 produced from 3D nanocomposites (after cell transfection by free or SiNP associated PEI) were collected at day 2, 5 and 7. These supernatant were incubated with macrophages under the optimal condition determined in section IV-2-9-1.

IV-2-10. Statistical Analysis.

Results are presented as mean ± SD (standard deviation). Statistical significance was assessed using one way analysis of variance (ANOVA) followed by Tukey (compare all pairs of groups) or Dunnett (compare a control group with other groups) posthoc test. The level of significance in all statistical analyses was set at a probability of $P < 0.05$. Prism (Grahpad) software was used for all data analysis.

IV-3 RESULTS AND DISCUSSION

IV-3-1. Gel electrophoresis

With a phIL-10:SiNP ratio of 1:30 (w/w), full inhibition of the plasmid migration was achieved for both PEI_{25}-SiNP and PEI_{10}-SiNP (**Figure IV-1**) The phIL-10 complexation abilities of the particles were similar to those observed for pGLuc, as expected from the similarity of their size (ca. 5 Kbp).

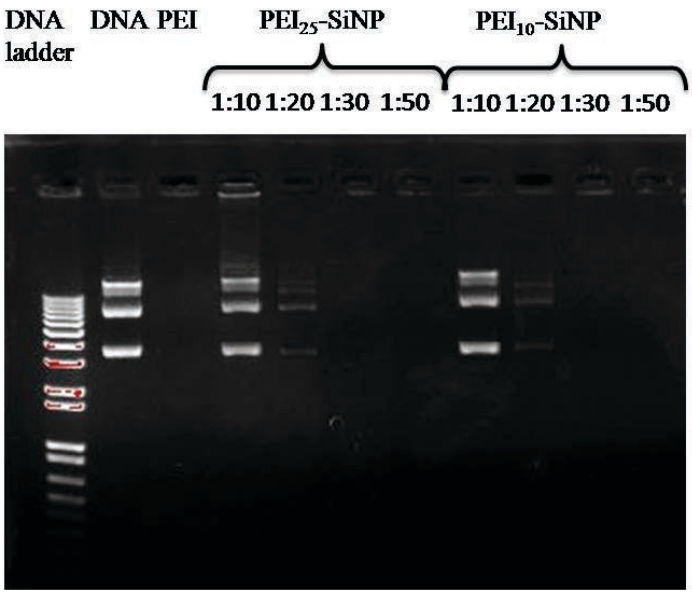

Figure IV-1. Agarose gel electrophoresis of phIL-10 complexation by PEI_{25}-SiNP and PEI_{10}-SiNP. A constant amount of DNA was complexed with silica particles at different weight ratios 1:10, 1:20, 1:30 and 1:50.

IV-3-2. Production of hIL-10 by 3T3 fibroblasts transfected in 2D

The quantification of hIL-10 in the culture media evidenced that the PEI-loaded silica nanoparticles complexed with phIL-10 were able to transfect 3T3 fibroblasts (**Figure IV-2**). These systems permitted a sustained expression of the phIL-10, the synthesis and the secretion of the associated cytokine. The profile of transfection resembled that observed for pGLuc, *i.e.* the free form of PEI_{25} exhibited the best abilities to induce IL-10 expression. However, compared to pGLuc, the variations between the different systems were smaller. The production of IL-10 after transfection with PEI_{10}-SiNP represented 40 % of the quantity produced by 3T3 cells after transfection with free PEI_{25}. However, such a comparison should be taken with care as luciferase quantification is based on the monitoring of its enzymatic activity via the generation of luminescent molecules. Since one enzyme can degrade several substrates, the resulting signal is amplified compared to the direct quantification of IL-10 proteins.

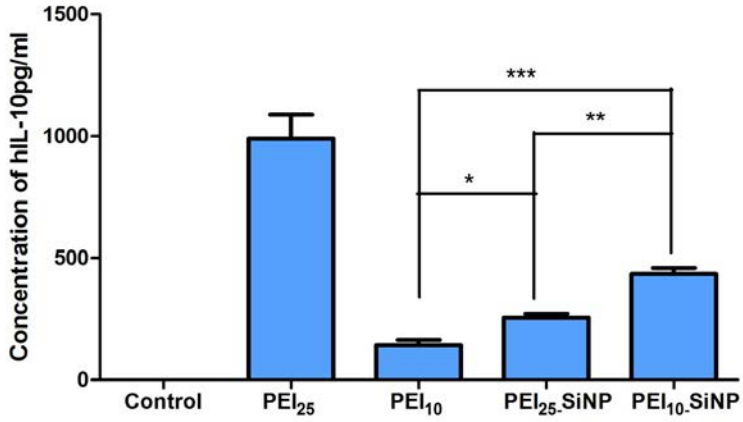

Figure IV-2 Transfection of 3T3 mouse fibroblasts after 4 h incubation with free or PEI_x-SiNP complexed with phIL-10 (n = 3). Variance of the hIL-10 expression among groups PEI_{10}, PEI_{25}-SiNP, PEI_{10}-SiNP was determined by one-way ANOVA with Tukey posthoc test (*P < 0.05, ** P < 0.01, ** P < 0.001).

Therefore, the results obtained with phIL-10 provide a more realistic view of the transfection capabilities of the vectors. Interestingly, the IL-10 production obtained with PEI_{10}-SiNP is 2 and 3 times higher than that with PEI_{25}-SiNP and free PEI_{10}, respectively. Once again the cell transfection and the biomolecule synthesis were not associated with any cytotoxicity (**Figure IV-3**). It has been shown in **Chapter II** that PEI_{25} was toxic for doses equal or higher than 5-10 $\mu g.mL^{-1}$ on 3T3 cells. In contrast, PEI_{25} and PEI_{10} were not toxic at 100 $\mu g.mL^{-1}$ when they were associated with SiNPs. Hence, it should be possible to counterbalance the lower ability of PEI_{10}-SiNP to produce IL-10 by using higher doses than PEI_{25}

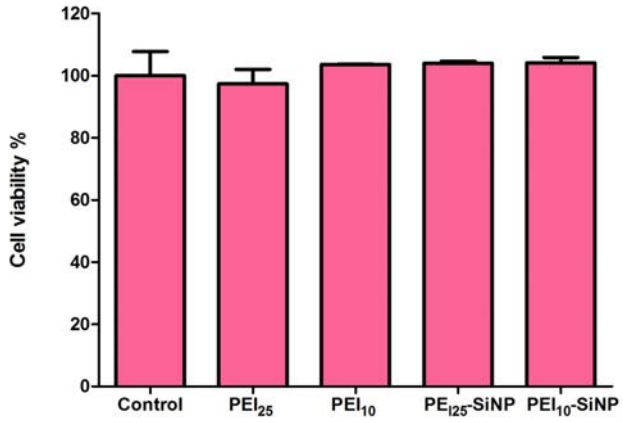

Figure IV-3 Cell viability of 3T3T mouse fibroblasts after 4 h incubation and 44 h transfection as evaluated with Alamar Blue test and calculated as the percentage of the control (n=3).

IV-3-3.Production of hIL-10 from SiNP-Collagen Nanocomposites

The ability of 3T3 cells to produce IL-10 was evaluated in a 3D context after cell encapsulation within a collagen hydrogel to form nanocomposites. Unlike the nanocomposites made with pGLuc, the synthesis of IL-10 was already detectable from day 2 regardless of the transfection system used (**Figure IV-4**). The cell transfection was not associated with any toxicity for the fibroblasts (**Figure IV-5**). The IL-10 synthesis reached a maximum at day 5 with concentrations comparable to those obtained in 2D conditions. This delay of synthesis could be attributed to the time for 3T3 cells to migrate within the collagen network and encounter transfection systems. The slight decrease of IL-10 concentration at day 7 could be due to the IL -10 instability in culture medium [17].

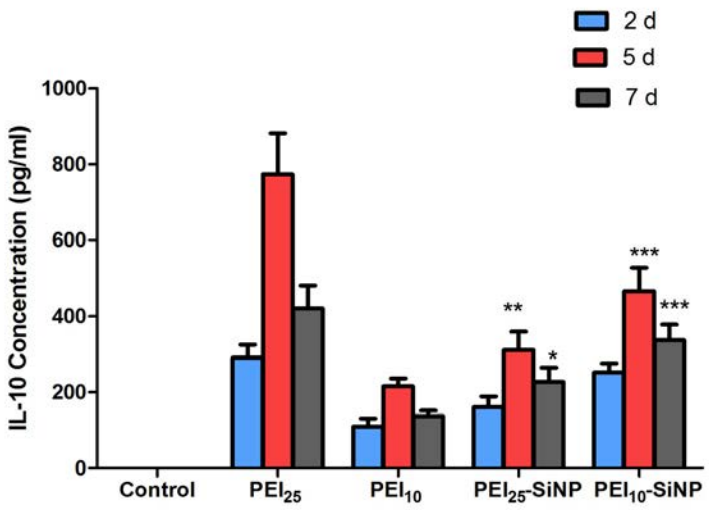

Figure IV-4. Production of hIL-10 by 3T3 mouse fibroblasts encapsulated within silica-collagen nanocomposites (n = 3). Variance of the IL-10 expression among groups PEI_{25}−SiNP, PEI_{10}−SiNP was determined by one-way ANOVA with Tukey posthoc test (*P < 0.05, ** P < 0.01).

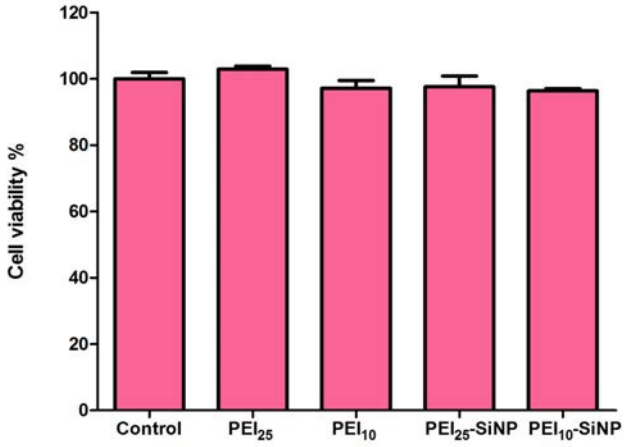

Figure IV-5. Cell viability of 3T3 fibroblasts co-immobilized with phIL-10 complexes in collagen hydrogels after 7 days, as evaluated with Alamar Blue test and calculated as the percentage of the control (n=3).

IV-3-4. Test of Primers

The electrophoresis of the PCR products revealed the presence of intense bands for all the couples of primers tested (**Figure IV-6**). The PCR products had the appropriate size evidencing the efficiency and the specificity of the reaction. However, this specificity will be checked with the melting curve at the end of the real time PCR. For the further experiments, we decided to select TNF-α C1 and GAPDH as housekeeping gene.

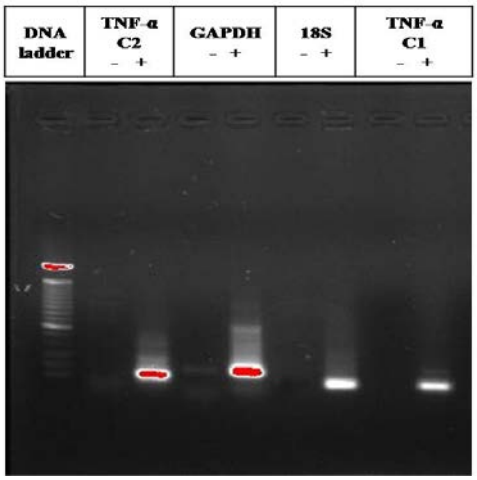

Figure IV-6 Agarose gel electrophoresis for cDNA after reverse transcription for TNF-α C2, GAPDH, 18 S and TNF-α C1.

IV-3-5. Activation of macrophages by LPS

The ability of LPS to activate macrophages was evaluated by measuring the expression level of TNF-α, a marker of inflammation. In contact with a component of the bacterial outer membrane (LPS), macrophages adopt a pro-inflammatory phenotype called M1. Irrespective of the dose of LPS used in this experiment, the macrophage activation was maximal one hour after LPS addition (**Figure IV-7**). Then, the TNF-α amount decreased to reach a level closed to the basal value of control samples (without activation by LPS) after 6 hours. The value 1 (one) was given to control samples and the expression of TNF-α was calculated by comparison with this basal level.

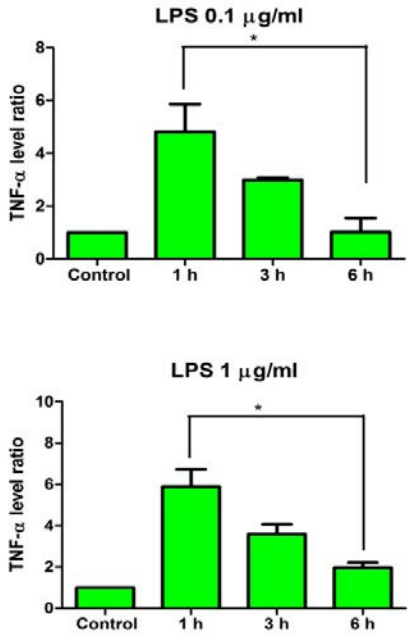

Figure IV-7 The mRNA level of TNF-α at different time points, determined by qPCR and showed in the ratio compared with that of control group (n=2). Variance of the TNF-α expression among 1, 3 and 6 h was determined by one-way ANOVA with Tukey posthoc test. *P<0.05

IV-3-6. Anti-inflammatory effect of the synthesized IL-10 in 2D

Several doses of hIL-10 and different conditions were tested to analyze the effect of this cytokine on the TNF-α expression. hIL-10 was used to modulate inflammation because its sequence is close to that of mouse IL-10. In addition, it has been shown hIL-10 had an activity on mouse cells. The pre-treatment of macrophages with hIL-10 one hour before the

addition of LPS clearly impacted the effect of the biomolecule (**Figure IV-8**). The highest degrees of TNF-α downregulation were reached with the hIL-10 pre-treatment. In addition, the downregulation was dose-dependent regardless of the delay after LPS activation (1 or 3 hours). The best results were obtained with an analysis one hour after activation and with IL-10 pretreatment. The concentration of IL-10 at 0.1 ng.mL^{-1} inhibited the expression of the TNF-α gene by 25%. This inhibition reached 75% when a concentration of 1 ng.mL^{-1} was used. Therefore we decided to select these conditions for the further experiments in 3D with nanocomposites; i.e the IL-10 pre-treatment, LPS activation and analysis after 1 h.

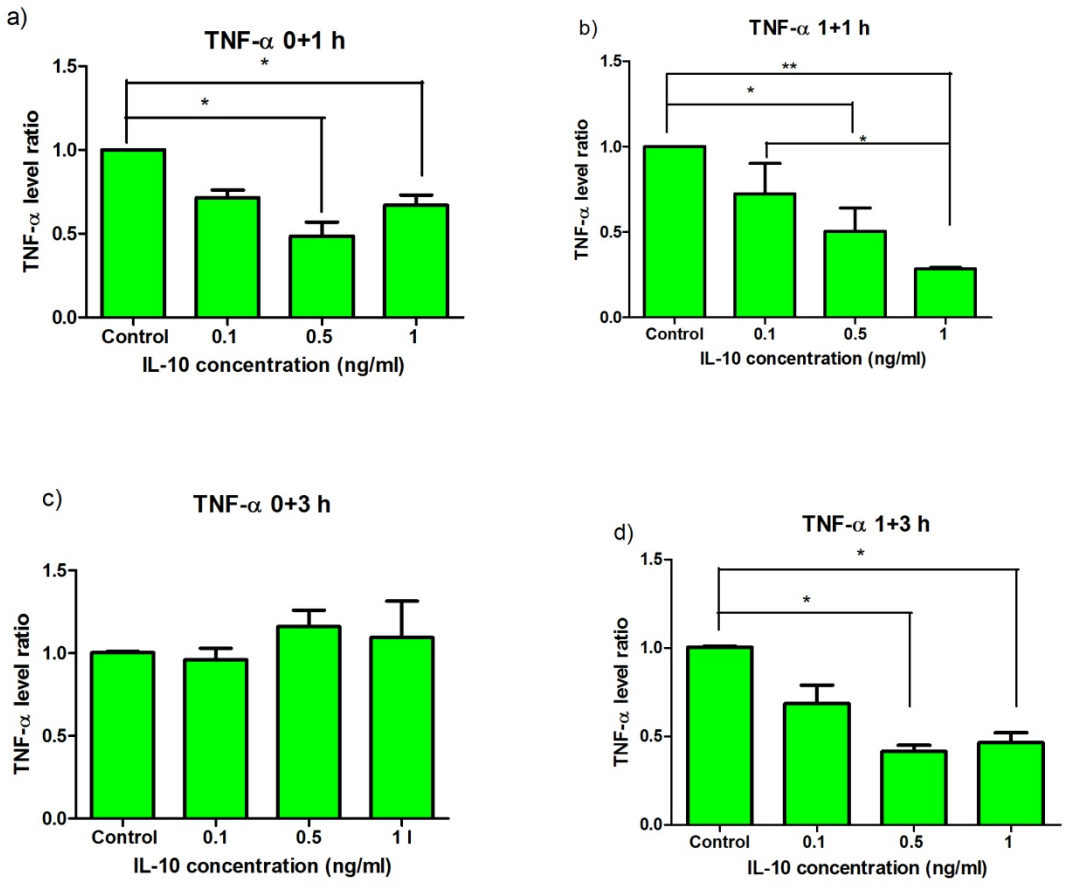

Figure IV-8 The mRNA level of TNF-α at different time points, determined by qPCR and showed in the ratio compared with that of control group. The number before "+" indicates the time (0 or 1 h) for pretreatment with IL-10 while the number after indicates incubation time for IL-10+LPS (n=3). Variance of the TNF-α expression among all the groups was determined by one-way ANOVA with Tukey posthoc test (*P < 0.05, ** P < 0.01, ** P < 0.001).

IV-3-7. Effect of IL-10 produced from silica-collagen nanocomposites on activated macrophages

Supernatants collected from nanocomposites were tested on activated macrophages seeded on plastic. The control used in this experiment was the activated macrophages, with the aim of analyzing the modulation of their activation. Taking into account the doses of IL-10 released from nanocomposites, the downregulation of the TNF-α gene was expected in every condition. Indeed, the concentrations of IL-10 produced by nanocomposites were always higher than 0.1 $ng.mL^{-1}$ regardless of the type of transfection systems and the time point considered (day 2, 5 and 7). Surprisingly, the inhibition of the TNF-α expression was only observed with the PEI_{10}-SiNP systems (**Figure IV-9**).

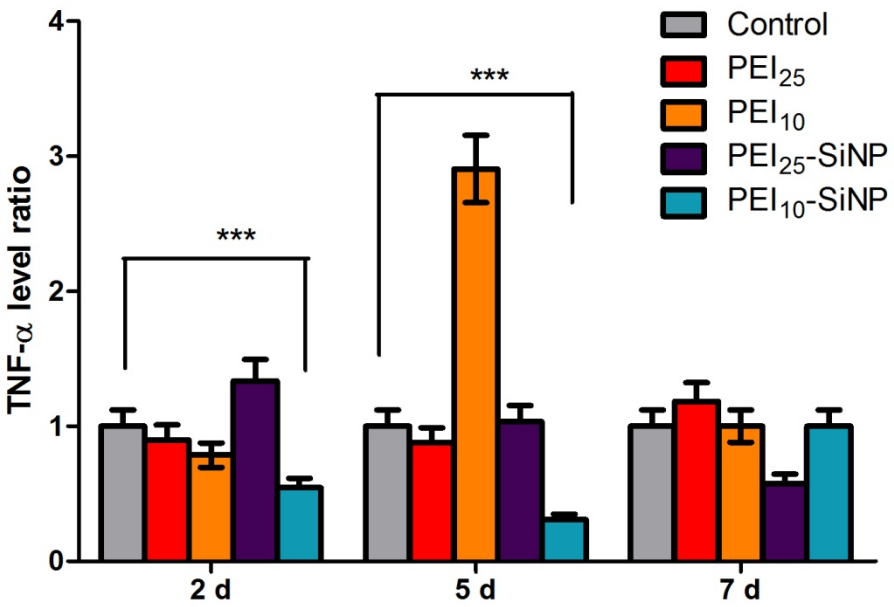

Figure IV-9. The mRNA level of TNF-α at different time points, determined by qPCR and showed in the ratio compared with that of control group. Variance of the TNF-α expression level between control and PEI10-SiNP on 2, 5 and 7 d was determined by non-paired two tailed t test, ****P*<0.001.

These results are not logical in regards with our previous data. For instance, the high quantity of IL-10 produced with the free form of PEI_{25} should have dramatically downregulated the expression of pro-inflammatory molecules such as TNF-α. This shades

serious doubt about the validity of these experiments that will need. These results may be explained by the weak activation of macrophages. To verify this point, unactivated macrophages should be used as negative controls. Another possibility would lie in the unstability of IL-10 in the culture medium. The apparent *in vivo* half-life of i.p. injected IL-10 was approximately 2 h in mice.[16] Kenis et al studied stability of IL-10 in human serum, and the degradation of IL-10 was found both concentration and temperature dependant[17]. The serum concentration of IL-10 samples at 40°C was decreased to 70 % after 1 day's storage. Therefore this point will need to be studied further.

IV-4 CONCLUSIONS AND PERSPECTIVES

In this study we have shown that collagen-silica nanocomposites are able to produce effective doses of IL-10 which inhibit the synthesis of pro-inflammatory cytokines. The system in which PEI_{10}-SiNP:DNA complexes are immobilized give the best performance. As the secretion of Il-10 increases until day 5, the modulation of inflammation is time lapse dependent. As a consequence, nanocomposites could act as spatio-temporal gene delivery systems. The nanocomposites could slightly modulate the inflammation to permit the wound debridement by macrophages during the first days after the injury. In a second time, the inhibition would be more effective to switch towards the proliferative phase of tissue repair. Beyond its anti-inflammatory, the delivery of IL-10 is crucial for wound healing as this cytokine as an effect on the organization of the extracellular matrix (ECM). Indeed it has been shown that transgenic mice exhibited impaired scaring with fragile ECM **[18].**

One possible step further in this study would rely on the design of a more complex fully 3D *in vitro* model. As a model of a chronic wound environment, macrophages may be encapsulated within a collagen gel and activated by LPS. Collagen-based nanocomposites incorporating fibroblasts and phIL-10-PEI-SiNP complexes can be applied onto this gel and their effect analyzed over one week. After transfection, fibroblasts would work as a bioreactor for the production of IL-10, that can act on macrophages to downregulate the expression of pro-inflammatory cytokines. As a consequence, pro-inflammatory macrophages may be differentiated into wound healing macrophages (**Figure IV-10**).

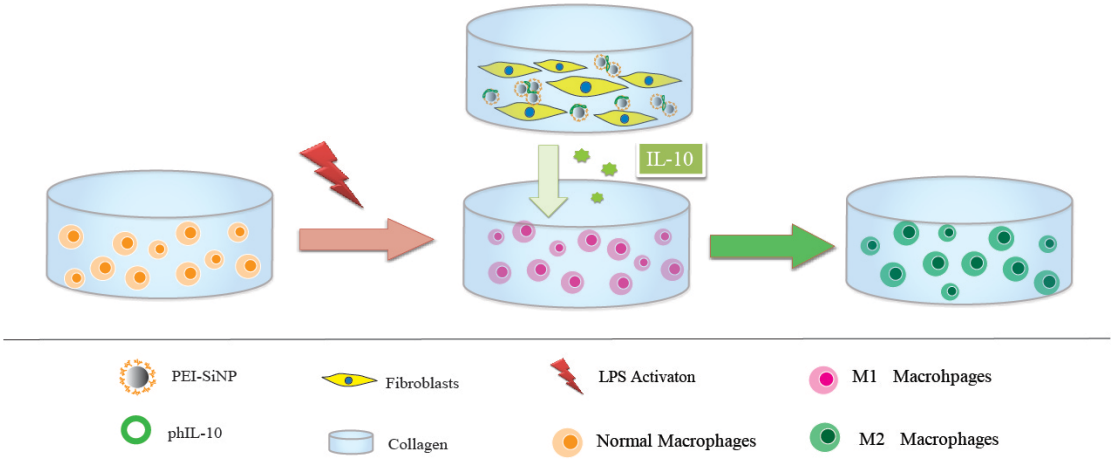

Figure IV-10. Towards a fully 3D model to study the ability of silica-collagen nanocomposites to modulate inflammation in a model of chronic wound.

REFERENCES

(1) Deodato, B.; Arsic, N.; Zentilin, L.; Galeano, M.; Santoro, D.; Torre, V.; Altavilla, D.; Valdembri, D.; Bussolino, F.; Squadrito, F., Recombinant AAV vector encoding human VEGF165 enhances wound healing. *Gene Ther.* **2002,** *9* (12), 777-785.

(2) Suwalski, A.; Dabboue, H.; Delalande, A.; Bensamoun, S. F.; Canon, F.; Midoux, P.; Saillant, G.; Klatzmann, D.; Salvetat, J.-P.; Pichon, C., Accelerated Achilles tendon healing by PDGF gene delivery with mesoporous silica nanoparticles. *Biomaterials* **2010,** *31* (19), 5237-5245.

(3) Lee, P.-Y.; Chesnoy, S.; Huang, L., Electroporatic delivery of TGF-β1 gene works synergistically with electric therapy to enhance diabetic wound healing in db/db mice. *J. Invest. Dermatol.* **2004,** *123* (4), 791-798.

(4) (a) Dengler, E. C.; Alberti, L. A.; Bowman, B. N.; Kerwin, A. A.; Wilkerson, J. L.; Moezzi, D. R.; Limanovich, E.; Wallace, J. A.; Milligan, E. D., Improvement of spinal non-viral IL-10 gene delivery by D-mannose as a transgene adjuvant to control chronic neuropathic pain. *Journal of Neuroinflammation* **2014,** *11*; (b) Jackson, C. A.; Messinger, J.; Peduzzi, J. D.; Ansardi, D. C.; Morrow, C. D., Enhanced functional recovery from spinal cord injury following intrathecal or intramuscular administration of poliovirus replicons encoding IL-10. *Virology* **2005,** *336* (2), 173-183.

(5) Buff, S. M.; Yu, H.; McCall, J. N.; Caldwell, S. M.; Ferkol, T. W.; Flotte, T. R.; Virella-Lowell, I. L., IL-10 delivery by AAV5 vector attenuates inflammation in mice with pseudomonas pneumonia. *Gene Ther.* **2010,** *17* (5), 567-576.

(6) Jain, S.; Tran, T.-H.; Amiji, M., Macrophage repolarization with targeted alginate nanoparticles containing IL-10 plasmid DNA for the treatment of experimental arthritis. *Biomaterials* **2015,** *61*, 162-77.

(7) Oberholzer, C.; Oberholzer, A.; Tschoeke, S. K.; Minter, R. M.; Bahjat, F. R.; LaFace, D.; Hutchins, B.; Moldawer, L. L., Influence of recombinant adenovirus on liver injury in endotoxicosis and its modulation by IL-10 expression. *J. Endotoxin Res.* **2004,** *10* (6), 393-401.

(8) Hsu, E.; Ruffner, M.; Luu, Y.; Gao, J.; Fleet, C.; Jacobson, K.; Mumper, R.; Plevy, S.; Cheung, A., Successful treatment of experimental colitis by a nanoparticle gene delivery system that localizes expression of interleukin-10 (IL-10) to the colon. *Inflamm. Bowel Dis.* **2011,** *17*, S3-S3.

(9) Book, A. A.; Fielding, K. E.; Kundu, N.; Wilson, M. A.; Fulton, A. M.; Laterra, J., IL-10 gene transfer to intracranial 9L glioma: tumor inhibition and cooperation with IL-2. *J. Neuroimmunol.* **1998,** *92* (1-2), 50-59.

(10) Cao, M.; Khan, J. A.; Kang, B.-Y.; Mehta, J. L.; Hermonat, P. L., Dual AAV/IL-10 Plus STAT3 Anti-Inflammatory Gene Delivery Lowers Atherosclerosis in LDLR KO Mice, but without Increased Benefit. *International journal of vascular medicine* **2012,** *2012*, 524235-524235.

(11)Fu, C.-L.; Chuang, Y.-H.; Chau, L.-Y.; Chiang, B.-L., Effects of adenovirus-expressing IL-10 in alleviating airway inflammation in asthma. *J. Gene Med.* **2006,** *8* (12), 1393-1399.

(12). Boehler, R. M.; Kuo, R.; Shin, S.; Goodman, A. G.; Pilecki, M. A.; Leonard, J. N.; Shea, L. D., Lentivirus Delivery of IL-10 to Promote and Sustain Macrophage Polarization Towards an Anti-Inflammatory Phenotype. *Biotechnol. Bioeng.* **2014,** *111* (6), 1210-1221.

(13) Holladay, C. A.; Duffy, A. M.; Chen, X.; Sefton, M. V.; O'Brien, T. D.; Pandit, A. S., Recovery of cardiac function mediated by MSC and interleukin-10 plasmid functionalised scaffold. *Biomaterials* **2012,** *33* (5), 1303-1314.

(14) Koh, J. J.; Ko, K. S.; Lee, M.; Han, S.; Park, J. S.; Kim, S. W., Degradable polymeric carrier for the delivery of IL-10 plasmid DNA to prevent autoimmune insulitis of NOD mice. *Gene Ther.* **2000,** *7* (24), 2099-2104.

(15) Milligan, E. D.; Langer, S. J.; Hughes, T. S.; Sloane, E. M.; Mahoney, J. H.; Jekich, B. M.; Maier, S. F.; Leinwand, L. A.; Watkins, L. R., Plasmid DNA Encoding the Anti-Inflammatory Cytokine Gene, Interleukin-10 (IL-10) for Chronic Pain Control: Taking Advantage of Nuclear Scaffold/Matrix Attachment Regions. *Mol. Ther.* **2006,** *13*, S99-S99.

(16) Li, L.; Elliott, J. F.; Mosmann, T. R., IL-10 inhibits cytokine production, vascular leakage, and swelling during T helper 1 cell-induced delayed-type hypersensitivity. *The Journal of Immunology* **1994,** *153* (9), 3967-3978.

(17) Kenis, G.; Teunissen, C.; De Jongh, R.; Bosmans, E.; Steinbusch, H.; Maes, M., Stability of interleukin 6, soluble interleukin 6 receptor, interleukin 10 and CC16 in human serum. *Cytokine* **2002,** *19* (5), 228-235.

(18). King, A.; Balaji, S.; Le, D.L., Crombleholme, T.M.; Keswani, S.G. Regenerative wound healing: the role of Interleukin-10. *Advanced in Wound Care* **2014**, *3,* 315-322

(19) Eming, S.A.; Kaufmann, J.; Lohrer, R.; Krieg, T. Chronic wounds: Novel approaches in research and therapy. *Hautarzt* **2007**, *58* (11):939–944.

CONCLUSIONS AND PERSPECTIVES

The objective of this thesis was to develop a wound dressing made of collagen type I hydrogel and achieve co-delivery of cells and therapeutic genes to promote healing processes in chronic wounds.

To this end, we first developed a non-viral gene delivery system based on silica nanoparticles (SiNP) by optimizing particle size, PEI molecular weight as well as PEI conjugation method to achieve a high transfection efficiency while reducing the cytotoxicity of PEI. Then, by co-encapsulating mouse fibroblasts and pDNA-PEI-SiNP complexes during gelation of collagen hydrogel, a cell factory was constructed for the sustained and localized gene delivery over one week.

By carrying out experiments both in 2D and 3D configurations, we obtained some interesting findings for gene delivery systems with or without scaffold:

1. Surface modification plays a more important role than size variation for efficient gene delivery by silica nanoparticles

Particle size is an important parameter for cellular uptake and generally the ease for cellular internalization decrease with the increase of particles size. However, PEI-coated silica particles with size from 50 nm to 200 nm showed no significant variation in terms of cell tranfection. Furthermore, when 200 nm SiNP were modified with PEI of different MWs, different transfection efficiencies were obtained. Surpringly, SiNP coated with intermediate size polymers (10 kDa) achieved the highest transfection efficiency Moreover, when we modified particles of same size with -SO_3 or -Cl before the introduction of PEI, significant difference in cell transfection were also observed. More specifically, the transfection of SiO_2-SO_3@PEI particles was on order lower than that of SiO_2@PEI while no protein expression was observed with the SiO_2-Cl@PEI system.

2. Conjugation mode of PEI on silica surface has noticeable impact on cell transfection

Three methods, i.e. direct adsorption, adsorption mediated by–SO_3, and covalent bonding were adopted to graft PEI on silica nanoparticles. These particles showed differences in particle distribution, PEI content, PEI conformation while sharing similar surface charge and closeDNA binding capacity. More importantly, significantly different transfection efficiency was obtained in the trend of SiNP@PEI > SiNP–SO_3@PEI > SiNP–SO_3@PEI. We have

proposed that the persistence of significant interactions between the silica surface and PEI in the acidic conditions of the endosomes can be detrimental to the intracellular trafficking of the plasmid, considering that PEI-DNA should be released from the particle for translocation into nucleus.

3. Silica nanoparticles can alleviate cytotoxicity originating from PEI

During this work, cytotoxicity studies were performed on mouse fibroblasts with different PEIs associated to several types of particles, in a wide range of doses. There is clear trend that cytotoxicity increases with the increase of PEI molecular weight, with PEI 25 kDa becoming detrimental at 10 µg/ml, PEI 10 kDa at 50 µg/ml while no toxic effect was found for PEI 1.8 kDa even at 100 µg/ml. Meanwhile, pure particles and particles modified with $–SO_3$ or –Cl exhibited no toxicity in the testing range. More interestingly, for all PEI-coated particles, cell viability was above 80% throughout all the tests. In conclusion, the association of PEI with silica nanoparticles can significantly reduce its cytotoxicity, allowing the increase of the doses that can be used for transfection experiments.

4. Transfection efficiency and cytotoxicity differ among cell lines

PEI-SiNP particles also showed the ability to transfect human cells, fibroblasts and keratinocytes, although to a lower extent than mouse fibroblasts. This difference in transfection efficiency was attributed to the lower proliferation rate of the primary cells. Furthermore, keratinocytes were more sensitive to PEI-coated particles, requiring to decrease the plasmid :particle weight ratio and therefore lowering the maximal transfection efficiency

5. Silica-collagen nanocomposites can achieve localized and sustained gene delivery

We have built three 3 D models to better understand the release mechanism from or within silica-collagen nanocomposites. Our results indicated that, once immobilized within the collagen gels, particles do not release complexed plasmids outside the material. Moreover, sustained gene delivery can also be achieved by adding complexes to pre-formed cellularized hydrogels. This illustrates that the method used to associate the complexes with the 3D matrix is a key factor for scaffold-based gene delivery system. In particular, the migration and proliferation of cells within the gel seem to be crucial to obtain an effective transfection.

In addition, sustained expression of proteins from silica-collagen nanocomposites was detected for two plasmids, pGluc and phIL-10, over one week. Noticeably, in the case of pGluc, accumulative release of luciferase was presented as luciferase is a very stable protein

that can stand a relatively high temperature (37°C) over this period. For IL-10, only temporal concentration was shown as it undergoes rapid degradation in experimental conditions.

6. Silica-collagen nanocomposites have the potential to co-deliver cells and therapeutic genes

It was possible to achieve high levels of production of IL-10 by fibroblasts transfected by phIL-10-PEI-SiNP nanoparticles in 2D culture. The expressed protein showed a significant ability to reduce TNF-α mRNA levels in LPS-activated macrophages. The sustained release of IL-10 from the nanocomposites was also observed. Unfortunately our first evaluation of the anti-inflammatory effect of the released proteins was not conclusive and should be reproduced. In parallel, developing more realistic 3D models of wound tissues would allow to improve the relevance of our in vitro studies.

Perspectives

Although silica-nanocomposites exhibited desirable sustained gene delivery in preliminary studies, many challenges remain for clinical applications: First, a more efficient non-viral gene delivery system should be developed as our particles still exhibited lower transfection efficiency than free PEI 25 kDa. Therefore it would be interesting to change the nature of the grafted moiety, for instance introducing carboxylic acid groups, for more efficient cell transfection. Secondly, our hypothesis concerning PEI-DNA detachment from the particle surface has to be supported by further experiments. Mimicking the acidic environment of endosomes and neutral cytoplasm could allow to investigate the effect of pH variations on the intracellular fate of the vectors.

From the point of view of applications, a more robust collagen hydrogel must be developed. In our study, the used collagen concentration was low, leading to materials that can be difficult to handle by surgeons. Increasing collagen concentration or introducing another biocompatible polymer could be further explored. However, it will be important to keep in mind that cellular proliferation and migration are key phenomena in the transfection process. As matrix stiffness is a stimulus for cell proliferation, designing dense matrices could favor the transfection

Last but not least, the anti-inflammation properties of silica-collagen nanocomposites are still to be confirmed. The incorporation of other bioactive molecules, such as antibiotics, within the hydrogel and/or the silica particles may also be envisioned. This would allow to progress further towards a medicated dressing capable of delivering multiple therapeutical

agents, and therefore to address the many challenges currently faced to efficiently favor tissue repair.

Annex: List of abbreviations

AAV	Adeno-associated virus
AV	Adenovirus
AS-ODN	Anti-sense oligonucleotides
Bcl-2	B cell lymphoma-2
β-CD	β-cyclodextrin
CSF	Colony-stimulating factor
Cl-PTES	Chloropropyltriethoxysilane
CRISPR	Clustered regularly interspaced short palindromic repeat
DAPI	4’,6-diamidino-2-phenylindole dihydrochloride
DC-cholesterol	3β-[N-(N',N'-dimethylaminoethane)-caramoyl] chelesterol
DLS	Dynamic light scattering
DOGS	Dioctadecylamidoglycylspermine
DMEM	Dulbecco’s Modified Eagle’s Medium
DOPE	Dioleoylphosphatidylethanolamine
DOTAP	1,2-dioleoyl-3-trimethylammonium-propane
DOTMA	N-[1-(2,3-dioleyloxy)propyl]-N,N,N-trimethylammonium chloride
DOX	Doxorubicin
ELISA	Enzyme-linked immunosorbent assay
ECM	Extracellular matrix
EGF	Epidermal growth factor
FGF	Fibroblast growth factor
FITC	Fluorescein isothiocyanate
GAM	Gene activated matrix
GM-CSF	Granulocyte/macrophage colony-stimulating factor
HIF-1α	Hypoxia-inducible factor alpha
IL	Interleukin
IGF-I	Insulin-like growth factor-I
KGF	Keratinocyte growth factor
LPS	Lipopolysaccharides
LPMSN	Large pored mesoporous silica nanoparticle
LV	Lentivirus
miRNA	microRNA
mRNA	Messenger RNA
MSN	Mesoporous silica nanoparticle
MPTMS	3-mercaptopropyltrimethoxysilane
NF-κB	Nuclear factor-κB
NSN	Nonporous silica nanoparticle
nDNA	Compacted DNA
NMR	Nuclear magnetic resonance
NO	Nitric oxide
PAGA	Poly [-(4-aminobutyl)-L-glycolic acid]
PAMAM	Polyamidoamine
PCL	Polycaprolactone
PCR	Polymerase chain reaction

PDGF	Platelet-derived growth factor
pDNA	Plasmid DNA
PEI	Polyethylenimine
PEG	Polyethylene glycol
PFA	Paraformaldehyde
pGluc	Plasmid encoding secreted Gaussia luciferase
PHEMA	Poly(2-hydroxyethyl methacrylate)
phIL-10	Plasmid encoding human interleukin-10
PLGA	poly(lactic-co-glycolic acid)
PLL	Poly-L-lysine
PU	Polyurethane
PVA	Poly(vinyl alcohol)
PVP	Polyvinylpyrrolidone
rhPDGF	Recombinant human platelet-derived growth factor
RLU	Relative lighte unit
ROS	Reactive oxygen species
RV	Retroviral
SEM	Scanning electron microscopy
SiNP	Silica nanoparticle
siRNA	Small interfering RNA
TALEs	Transcription activator-like effector nuclease
TEM	Transmission electron microscopy
TEOS	Tetraethyl orthosilicate
TGA	Thermogravimetric analysis
TNF	Tumor necrosis factor
Tris-HCl	Tris(hydroxymethyl)aminomethane hydrochloride
VEGF	Vascular endothelial growth factor
XPS	X-ray photoelectron spectroscopy
ZFN	Zinc-finger nuclease

Résumé. Ce travail concerne l'évaluation de nanoparticules de silice associées à la poly-ethylèneimine (PEI) comme vecteurs de délivrance de gène pour le traitement des plaies chroniques de la peau. Des matériaux nanocomposites associant des complexes formés par l'association de ces particules hybrides et d'ADN avec des hydrogels de collagène colonisés par des fibroblastes 3T3 ont été élaborés. Grâce à la modulation de la taille de la particule et de la masse moléculaire du polymère, il a été possible de réaliser la transfection des fibroblastes au sein du gel, permettant l'expression génique pendant une semaine. Ces études montrent le rôle clé joué par la prolifération et la migration cellulaire sur l'efficacité de la transfection. L'efficacité de la transfection a ensuite été modulée en modifiant les interactions silice-PEI. Les résultats obtenus suggèrent que le détachement du complexe de la particule dans les endosomes est une étape clé de ce processus. La transfection de cellules humaines primaires a aussi été étudiée en vue d'applications in vivo. La transfection a été observée avec des fibroblastes et des keratinocytes humains en culture et avec les fibroblastes au sein des gels, mais avec des efficacités moindres que pour les cellules 3T3. Ceci est attribué au plus faible taux de prolifération des cellules primaires. Enfin la capacité des nanocomposites à moduler l'inflammation a été testée sur des macrophages humains activés. Ces systèmes permettent la synthèse soutenue d'IL-10 par les fibroblastes et l'inhibition de l'expression de TNF-alpha chez les macrophages.

Abstract. This work is devoted to the evaluation of silica nanoparticles associated to poly-ethyleneimine (PEI) as vectors for gene therapy in the context of skin chronic wounds repair. Nanocomposite materials associating complexes formed by the association of these hybrid particles and DNA with collagen hydrogels cellularized with 3T3 fibroblasts have been prepared. Thank sto the modulation of particle size and polymer molecular weight, it has been possible to achieve fibroblast transfection within the gel, allowing for sustained protein expression over one week. These studies evidence the key role of cell proliferation and migration on transfection efficiency. The transfection process has been further modulated by modification of the silica-PEI interactions. The results suggest that the complex detachment from the particles within the endosomes is a key step in this process. The transfection of human primary cells has also been studied foreseeing in vivo applications. Human fibroblasts and keratinocytes have been successfully transfected in culture and, in the case of fibroblasts, within collagen hydrogels, but with lower efficiency than with 3T3 cells. This has been attributed to the lower proliferation rate of primary cells. Finally the ability of nanocomposites to modulate inflammation has been evaluated on activated human macrophages. These systems have allowed for the sustained production of IL-10 by fibroblasts and the inhibition of TNF-alpha expression by macrophages.